Biomaterials with pro-osteogenic and antibacterial functionalization for oral bone tissue engineering Yiwen Dong

Biomaterials with pro-osteogenic and antibacterial functionalization for oral bone tissue engineering

Yiwen Dong

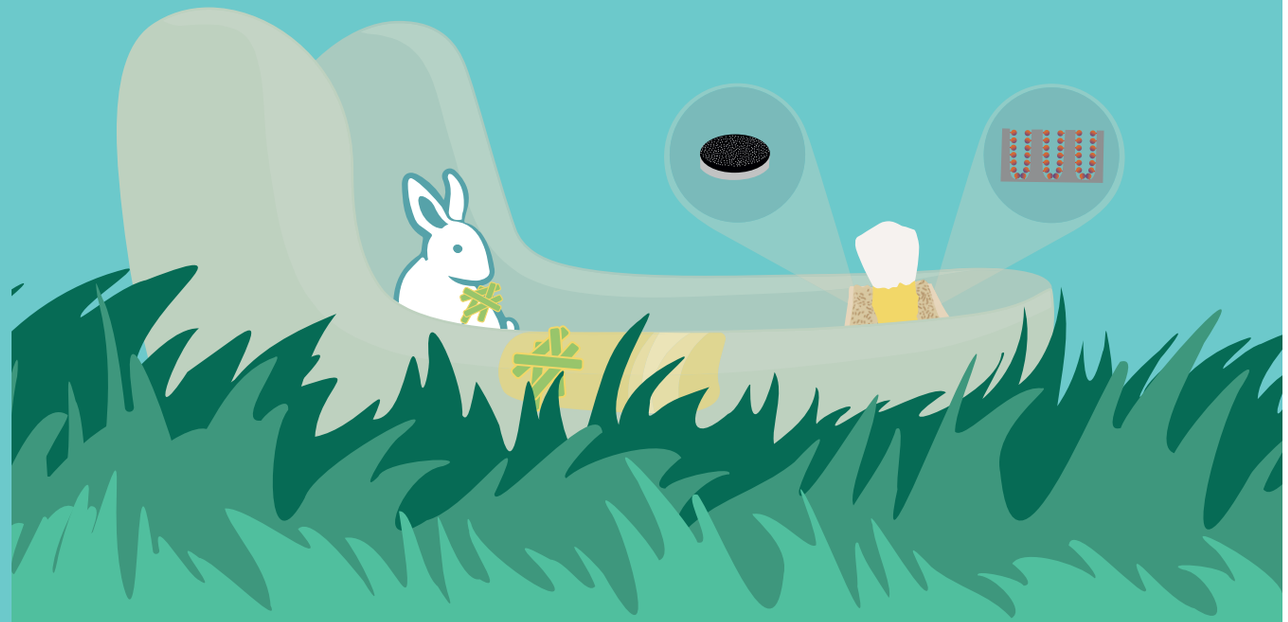

Biomaterials with Pro-Osteogenic and Antibacterial Functionalization for Oral Bone Tissue Engineering

Yiwen Dong

Biomaterials with Pro-Osteogenic and Antibacterial Functionalization for Oral Bone Tissue Engineering
ISBN/EAN: 978-94-93315-98-3
Cover design: Yiwen Dong, Shuyi Li and Guntra | Proefschrift-AIO.nl
Layout & Printing: Proefschrift-AIO.nl
The printing of this bookwas kindly supported by:
Academisch Centrum Tandheelkunde Amsterdam (ACTA), Vrije Universiteit Amsterdam

VRIJE UNIVERSITEIT

Biomaterials with Pro-Osteogenic and Antibacterial Functionalization for Oral Bone Tissue Engineering

ACADEMISCH PROEFSCHRIFT

ter verkrijging van de graad Doctor of Philosophy aan
de Vrije Universiteit Amsterdam,
op gezag van de rector magnificus
prof.dr. J.J.G. Geurts,
in het openbaar te verdedigen
ten overstaan van de promotiecommissie
van de Faculteit der Tandheelkunde
op dinsdag 26 september 2023 om 9.45 uur
in een bijeenkomst van de universiteit,
De Boelelaan 1105

door

Yiwen Dong

geboren te Zhejiang, China

promotor:	prof.dr. T. Forouzanfar
copromotoren:	dr. G. Wu dr. J. Liu
promotiecommissie:	dr. M.N. Helder prof.dr. J. Klein Nulend prof.dr. R.T. Jaspers dr. Q. Wang dr. J. van den Beucken

CONTENTS

CHAPTER ONE

General introduction

Dental implants and osteointegration

Dental implants are medical devices that are surgically anchored in the maxillofacial bone and mechanically support a dental prosthesis, for instance, crowns, bridges, overdenture, and/or facial prostheses [1,2]. Compared with other conventional methods, for example, fixed prosthesis, and removable partial and/or full dentures, dental implants are superior not only in aesthetics, and comfort but also in natural teeth and bone tissue preservation [3]. Hence, dental implantation is more and more widely applied for partially or completely edentulous patients in the past several decades. In the European Union, over 1.8 million dental implants are implanted per year [4]. In the 1960s, Branemark and colleagues first describe the relationship between implants and bone and define the term osteointegration [5]. Osteointegration is the biological basis for the anchorage of dental implants in bone tissue — the formation of a direct interface between an implant and bone that is not intervened by soft tissue [6]. Sufficient osteointegration is essential for the proper functionality and long-term survival of implants [7]. Sufficient bone volume and adequate bone quality are of paramount importance to achieve sufficient osteointegration [8]. A larger and denser bone mass peri-implant significantly enlarges the surface of bone-to-implant contact, thereby enhancing the osteointegration of dental implants [8]. Implantations with titanium (Ti) and its alloys are considered a predictable and reliable therapy with 10-year survival rates are over 95% in normal bone conditions [9]. However, various adverse bone abnormalities such as low bone density, periimplantitis, and large-volume bone defects can dramatically impair new bone regeneration and implant osteointegration, eventually delaying implant loading and potentially resulting in implant failure. [10,11].

Adverse bone abnormalities

Low bone density

Low bone density is a widespread problem: Every year over 1.5 million people suffer a fracture due to this bone disease [12]. Low bone density commonly occurs in patients with osteoporosis or bad habits (such as smoking and alcoholism) [12]. Osteoporosis is defined as a systemic degenerative disease

with dysregulation of bone formation and progressive bone micro-architectural deterioration [13]. With the prolongation of life span and the aging of the population, the number of patients with osteoporosis is increasing rapidly. There are millions of people diagnosed with osteoporosis worldwide annually [14]. The diagnosis of osteoporosis depends on the assessment of bone mineral density [15,16]. Since Godfrey Hounsfield presented computerized axial transverse scanning in 1972, computed tomography (CT) is the only diagnostically justified imaging technology that can at least approximate conclusions about maxillofacial bone structure and density [17]. It is considered a valuable method for evaluating the relative distribution of compact and cancellous bone. Bone mineral density can be assessed by Hounsfield units (HU), which are directly related to tissue attenuation coefficients. Bone tissues are classified into three categories based on their HU values: highly dense cortical bone (> 600 HU), dense cortical-spongy bone (between 400 and 600 HU), and cortical-spongy bone of low density (< 200 HU) [17]. Patients with osteoporosis are commonly presented with low-density cortical spongy bone [12]. Busenlechner *et al*. demonstrate that the implant survival rate is significantly decreased to as low as 84.8% with low-density bone, which is induced by insufficient osteointegration [12].

One clinical technique to enhance osteointegration of implants is the adoption of more bone-implant healing time, in which the implants have to be left in the bone at least 6 months post-surgery [18,19]. Such a method significantly prolongs the waiting period before functional loading. Another potential solution is the adoption of a SLActive Ti implant [20]. The Ti implants with higher surface energy and hydrophilicity (for example, Straumann® SLActive) are suggested to apply in low-density bone. The surface of the SLActive implant is produced with the same sandblasting and acid-etching technique but rinsed under nitrogen protection and stored in sealed glass tubes containing isotonic NaCl solution to avoid oxygen exposure [21]. However, the SLActive implant survival rate in low-density bone is still below 90%, which is far from satisfactory [22]. In addition, for patients with high smile lines, thin gingival biotypes, and gingival recession, the esthetic risk posed by Ti implants has necessitated the exploration of alternative materials with better esthetic

performance. In this regard, zirconia (Zr) has emerged as a promising option, due to its opaque white color, corrosion resistance, and low affinity for bacterial plaque [23,24], making it suitable for dental implants in the anterior aesthetic zone or for patients with metal allergies or bacterial susceptible diseases, such as diabetes [24]. On the other hand, the biological inertness of Zr may reduce osteointegration and lead to a lower clinical survival rate than Ti implants even in normal bone conditions. This disadvantage of Zr implants may be further exacerbated for the patients with low bone densities [25].

Periimplantitis

Periimplantitis is a destructive inflammatory process surrounding artificial implants, which results in the loss of supporting bone through a bacterial etiology [26,27]. The incidence rate of “moderate to severe periimplantitis” (bleeding on probing/suppuration and bone loss > 2 mm) after 10 to 15 years are as high as 14.5% [28]. Periimplantitis exhibits pronounced inflammatory progress in the mucosa at first, extends rapidly into bone marrow afterward, and finally progresses to a great extent of bone loss [29–31]. Periimplantitis can induce the failure of implants and impose financial and health burdens on both patients and healthcare providers. In 2016, the cost of therapies for periimplantitis is almost 2.91 billion dollars in the US [32]. The pathological bacteria associated with periimplantitis are clusters of bacteria including *T. forsythia* and *S. aureus* [33]. The conventional therapeutic approaches for periimplantitis include the removal of necrotic bone fragments, local, and/or systemic administration of antibiotics, and bone restoration process for the bone defects. However, these therapies are time-consuming (usually taking months to years) and may not always yield satisfactory results. This situation is largely attributed to the difficulties in infection control. The residual bacteria in peri-implant tissues and/or on the surface of implants that escape from the chemical and mechanical elimination procedures may rapidly proliferate and form biofilms, resulting in a series of complications, such as post-operative infection, bone graft exposure, and impeded bone regeneration [34]. Consequently, an efficient strategy for eradicating infection and promoting new bone production is desperately needed.

Large-volume bone defects

Severe periimplantitis often accompany with large-volume bone defects. According to recent reports of Bone Grafts and Substitutes, large-volume bone defects affect almost two million individuals globally with an economic burden of $3 billion per year [35]. Large-volume bone defects may largely surpass the spontaneous healing ability of bone tissue and will be healed only by connective tissues [36]. One approach for restoring large-volume bone defects is the adoption of autologous bone chips, whose use is, whereas, associated with limited availability, donor site pain, and morbidity [37]. In clinic, guided bone regeneration (GBR) technique is the most widely used surgical procedure for large-volume bone defects, that adopts barrier membranes and particulate bone-defect-filling materials to restore peri-implant bone tissues both in volume and dimensions [38]. In the classic GBR concept, barrier membranes mainly function to prevent the invasion of surrounding connective tissues to provide a favorable microenvironment to facilitate osteoblast proliferation, migration, differentiation, and finally bone tissue regeneration [38]. However, the efficacy of GBR may be greatly challenged by inflammation. Periimplantitis-derived inflammation may further compromise the healing capacity of bone tissue [39,40]. In clinic, systemic administration of antibiotics is conventionally applied to combat these complications. Whereas, its application is also associated with certain concerns, such as dysbacteriosis, poor biodistribution, toxicity, and bacterial resistance [41,42]. Continuous efforts should be made to promote the osteointegration of implants in such adverse conditions. The current trend is to modify the surfaces of implants and synthesize GBR membranes with pro-osteogenic and antibacterial functionalization to cope with these complicated adverse conditions. The pro-osteogenic property of the biomaterials generally functions as the improvements of pre-osteoblast cell proliferation, osteogenic differentiation, and so on [43].

Surface modifications of implants

The designs of dental implants are crucial determinants for sufficient osteointegration. Hitherto, dental implants have experienced rapidly

progressing with frequent production of new designs, such as materials, shapes, and surface treatments to enhance their osteointegration [44]. Surface topography and chemical composition of implant materials affect the pro-osteogenic cells adhesion, osteogenic differentiation and eventually modulate the osteointegration efficacy of dental implants [45,46]. Furthermore, surface modifications are also flexible strategies for endowing multifunctionality on implant materials, such as antibacterial and pro-osteogenic functions.

Electrochemical anodization

Titanium nanotube arrays (TNTs) that have special tunable pore structures and large surface area, are commonly applied as reservoirs for loading high amounts of bioactive agents [47,48]. Electrochemical anodization is routinely adopted in the fabrication of nanotube arrays, which involves the immersion of a target metal implant material (anode) and a counter electrode (cathode) in an organic electrolyte (with acid and water) with a voltage/current supply [49]. By adjusting various parameters, such as the composition of the organic electrolyte, voltage, reaction time, and temperature, nanotubes or nanopores with desired diameter and depths form on the implant surfaces [49]. The incorporation of antibacterial agents into these nanotube arrays has been proposed as a strategy for sustained local delivery of these agents, thereby providing a continuous protection against bacteria adhesion, proliferation, and biofilm formation [50]. However, implants are at constant risk of infection by a variety of bacterial species from early days to years later after implantation [51,52]. Antimicrobials applied locally (in the nanotube or nanoporous) or adsorbed on the implant surface cannot sustain for such a long period [53,54]. Therefore, approaches of loading antimicrobial agents on implant surface that can store antimicrobial agents for long periods and release only during the infection are desperately needed.

Zirconia (Zr) has been reported as an alternative implant material to avoid the disadvantages associated with titanium (Ti) implants, such as titanium allergy, dark color, and corrosion [23,24]. However, it has been observed that the biological inertness of Zr impedes its osteointegration capacity, even in normal bone conditions, when compared with Ti [25]. The fibrous tissue tends

to grow into the interface between bio-inertia Zr implants and bone tissue in the early stage of osteointegration, which results in loosening and micro-motion [25]. Fortunately, surface modification techniques are valid for Zr implants as well. The modification of surface topography — nanostructures such as nanotubes, nanopores, nanodots, nanogrooves can improve osteointegration by affecting bio-molecular interaction and chemical reactivity between the implants and bone tissue [55,56]. Particularly, the nanoporous array can modulate cell behavior and enhance osteointegration by providing a framework for synthesizing new bone tissue [57,58]. The dimension of nanopores, especially diameter, has been considered a crucial role in affecting cellular behavior. In comparison with nanoporous diameters in the range of 15 to 100 nm, nanopores with a diameter of about 30 nm significantly enhance osteogenic differentiation of cells, ultimately promoting osteointegration of implants [59]. Electrochemical anodization is a simple and commonly used method to fabricate nanopores with uniform and ordered structures [49]. The fabrication of diameter-controllable nanoporous arrays via electrochemical anodization on Zr implant surface may be a promising way to enhance its osteointegration.

Antibacterial and pro-osteogenic functionalized Guided bone regeneration membranes

Biodegradable synthetic polymers

A commonly used approach to synthesize a multi-functionalized membrane is coaxial electrospinning. It involves the arrangement of multiple solution feed systems to simultaneously electrospun two or more polymer solutions to form core-shell structured nanofibers. This technique allows for the encapsulation of two different bioactive agents respectively into core and shell layers, enabling their sustained releases [60]. Due to the complexity of the oral flora, broad-spectrum antibiotics are frequently applied in membranes [61]. Compared with clinically available antibiotics, antibacterial metallic nanoparticles are a promising alternative due to their significantly broader antimicrobial spectrum while lowering the risk of bacterial resistance [60,61]. Silver-based nanoparticles, a frequently used antibacterial metallic nanoparticle, are associated with several concerns, such as local accumulation of heavy metal

elements causing cytotoxicity [62]. To counter these issues, antibacterial metallic nanoparticles with lower toxicity are desired.

Biodegradable magnesium alloy

The resorbable membranes, which are made of natural or synthetic polymers (such as collagen and polylactic acid) are usually associated with suboptimal mechanical stiffness, which can not sufficiently shield exogenous forces, leading to membrane collapse and compromised osteogenesis [63,64]. Consequently, a resorbable membrane with sufficient stiffness, antibacterial property, and pro-osteogenic capacity will be more favorable to achieve desirable osteogenic efficacy in clinic. One of the promising materials to fabricate such a membrane is magnesium (Mg) alloys. Mg alloys are of sufficient mechanical strength, biodegradable, and biocompatible [65]. However, the naked Mg alloys degrade too fast *in-vivo* [66], therefore continuous efforts should be made to reduce their degradation rates to ensure adequate functional duration [67].

Scope of the thesis:

The primary objective of the studies presented in this thesis was to confer antibacterial and pro-osteogenic properties to implant materials, thereby lowering down implant infection risk, enhancing the efficacy of bone regeneration and improving the osteointegration of the implants. To investigate this further, the following scientific questions were addressed in this thesis:

1) Is it possible to make a diameter-controllable nanoporous arrays on Zr implant surface through electrochemical anodization? How do the nanoporous arrays affect the osteointegration of zirconia implant (**Chapter 2**)?
2) Is it possible to load antimicrobial agents in the nanotube arrays, which can store antimicrobial agents for long periods and release only during the infection (**Chapter 3**)?
3) Can the coaxial electrospinning allow for the encapsulation of two different bioactive agents into the nanofibers membrane? Can the membrane enable

these two bioactive agents sustained release and achieve antibacterial and pro-osteogenic functions with lower toxicity (**Chapter 4**)?

4) Is it possible to reduce the degradation rate of Mg alloys through surface modifications? How do these modified Mg alloys affect the bacteria viability and osteogenesis (**Chapter 5**)?

The surface chemical composition of Zr implant affects the pro-osteogenic cells adhesion, osteogenic differentiation and eventually affects osteointegration as well [45,46]. Tantalum (Ta) coatings have emerged as promising candidates due to their excellent biocompatibility, anticorrosion, and osteogenesis [68]. Compared with Ta coatings, diameter-controllable Ta nanoporous arrays (TaNS) further enhance the osteointegration of artificial joints and implants [69,70]. In addition, the color of the Ta coating presents an unsightly grey hue, which is undesirable for implantation in the aesthetic zone. On the contrary, the transparent nanoporous Ta coating (TaNS) prepared by electrochemical anodization can obtain a similar color to the substrate. In **Chapter 2**, we first deposit a thin Ta film on the zirconia surface by magnetron sputtering. Afterward, Ta coating is anodized in the electrolyte to prepare TaNS coating to promote osteointegration of zirconia implant and simultaneously sustained its opaque white color of zirconia. We evaluated the surface topography, chemical composition, bond strength, hydrophilicity, and roughness of TaNS coating to confirm its successful fabrication and physiochemical properties. *In-vitro* and *in-vivo* tests were performed to assess the pro-osteogenic property and osteointegration of TaNS coated Zr implants.

Implant infection occurs from early days to years later after implantation [51,52]. It calls for approaches of loading antimicrobial agents on implant surfaces that can store antimicrobial agents for long periods and release them only during the infection. Utilizing the difference of pH in the microenvironment between infection and normal conditions, a low pH-liable acetal linker (AL) was introduced to store the antibacterial drugs under normal conditions and release them adequately and timely under infection [71,72]. In **Chapter 3**, we designed a low pH-triggered silver-releasing TNT-AL-AgNPs implant to control peri-implant infection. We characterized the physicochemical properties of TNT-AL-AgNPs, analyzed a pH-dependent release of AgNPs from TNT-AL-AgNPs, and tested its antibacterial efficacy *in-vitro*. Furthermore, we evaluated the

biocompatibility of TNT-AL-AgNPs, as well as its effects on pre-osteoblast morphology and differentiation *in-vitro*.

Magnesium oxide nanoparticles (MgONPs) are metallic nanoparticles, which possess biodegradability and lower toxicity [73]. The benefits of MgONPs, which include pro-osteogenic properties [74] and significant inhibition of biofilm formation and maturation, have attracted increasing interest in membrane applications [73]. Parathyroid hormone (PTH) is a commonly used drug for bone regeneration. PTH promotes osteogenesis by activating osteoblast cells and the secretion of SOST through the receptor PTHr1 [75,76]. Therefore, the new composite membrane loading with MgONPs and PTH may be a promising approach to enhance bone regeneration in periodontitis or peri-implantitis patients with large-volume bone defects. In **Chapter 4**, we synthesized a sustained released antibacterial and pro-osteogenic coaxially-electrospun GBR membrane by encapsulating different concentrations of PTH in the core layer and MgONPs in the shell layer (MgONPs-PCL/PTHn-PCL). We characterized the physicochemical properties of MgONPs-PCL/PTHn-PCL, evaluated release profiles of MgONPs and PTH, and assessed the antibacterial efficiency of the new membrane *in-vitro*. Furthermore, the pre-osteogenesis property of the membrane was evaluated both *in-vitro* and *in-vivo.*

The high purity, excellent uniformity, and high bond strength of the gallium (Ga) coatings generated via magnetron sputtering have been shown to significantly reduce the corrosion and degradation of Mg alloys [77]. In the meanwhile, the chemical properties of Ga are very similar to iron (Fe) so that it can replace Fe^{3+} in ribonucleotide reductase, thereby impairing bacterial DNA synthesis and causing their death [78,79]. Ga^{3+} ions are also shown to increase alkaline phosphatase (ALP) activity, accelerate calcium nodule formation, and upregulate expression levels of osteogenic proteins in osteoblasts through activating transient receptor potential melastatin 7/Akt signaling pathway [80]. The Ga-coated membranes may be potential materials with antibacterial and pro-osteogenic properties for enhancing the efficacy of bone regeneration applied for GBR process. In **Chapter 5**, we aimed to synthesize a properly biodegradable, antibacterial, and pro-osteogenic Ga-coated Mg alloy (Ga/AZ31) membrane through magnetron sputtering for GBR. The bond strength of the Ga coatings, the antibacterial ability of the Ga-coated Mg alloy (Ga/AZ31)

membrane, and cell proliferation and osteogenic differentiation of MC3T3-E1 were tested to assess the biocompatibility and osteogenesis of Ga/AZ31 membrane.

References

[1] Nct, Comparison of short and standard dental implants. (2020). https://clinicaltrials.gov/show/NCT04475406.

[2] F. Accioni, J. Vázquez, M. Merinero, B. Begines, A. Alcudia, Latest trends in surface modification for dental implantology: Innovative developments and analytical applications. Pharmaceutics. 14 (2022) 455. https://doi.org/10.3390/pharmaceutics14020455.

[3] Y. Liu, C. Bao, D. Wismeijer, G. Wu, The physicochemical/biological properties of porous tantalum and the potential surface modification techniques to improve its clinical application in dental implantology. Materials Science and Engineering: C. 49 (2015) 323–329. https://doi.org/10.1016/J.MSEC.2015.01.007.

[4] M.A. Saghiri, P. Freag, A. Fakhrzadeh, A.M. Saghiri, J. Eid, Current technology for identifying dental implants: A narrative review. Bulletin of the National Research Centre. 45 (2021) 1–11. https://doi.org/10.1186/s42269-020-00471-0.

[5] P.I. Brånemark, B.O. Hansson, R. Adell, U. Breine, J. Lindström, O. Hallén, A. Ohman, Osseointegrated implants in the treatment of the edentulous jaw. Experience from a 10-year period. Scandinavian Journal of Plastic and Reconstructive Surgery. Supplementum. 16 (1977) 16.

[6] B. Hanes, S. Feitosa, K. Phasuk, J.A. Levon, D. Morton, W.S. Lin, Fracture resistance behaviors of titanium-zirconium and zirconia implants. Journal of Prosthodontics. 31 (2021) 441–446. https://doi.org/10.1111/jopr.13440.

[7] K.P. Nobles, A.V. Janorkar, R.S. Williamson, Surface modifications to enhance osseointegration–resulting material properties and biological responses. Journal of Biomedical Materials Research-Part B Applied Biomaterials. 109 (2021) 1909–1923. https://doi.org/10.1002/jbm.b.34835.

[8] M.R. Wood, S.G. Vermilyea, A review of selected dental literature on evidence-based treatment planning for dental implants: Report of the Committee on Research in Fixed Prosthodontics of the Academy of Fixed Prosthodontics. Journal of Prosthetic Dentistry. 92 (2004) 447–462. https://doi.org/10.1016/j.prosdent.2004.08.003.

[9] P. Rafael, E. Fernandes, A. Isis, P. Otero, J. Campos, H. Fernandes, L.M. Nassani, R.M. Castilho, G. Vicentis, O. Fernandes, Clinical performance comparing titanium and titanium-zirconium or zirconia dental implants: A systematic review of randomized controlled trials. Dentistry Journal. 10 (2022) 83. https://doi.org/10.3390/dj10050083.

[10] S. Raikar, P. Talukdar, S. Kumari, S.K. Panda, V.M. Oommen, A. Prasad, Factors affecting the survival rate of dental implants: A retrospective study. Journal of International Society of Preventive and Community Dentistry. 7 (2017) 351. https://doi.org/10.4103/jispcd.JISPCD_380_17.

[11] P. Dhatrak, U. Shirsat, S. Sumanth, V. Deshmukh, Finite element analysis and experimental investigations on stress distribution of dental implants around implant-bone interface. Materials Today: Proceedings. 5 (2018) 5641–5648. https://doi.org/10.1016/j.matpr.2017.12.157.

[12] D. Busenlechner, R. Fürhauser, R. Haas, G. Watzek, G. Mailath, B. Pommer, Long-term implant success at the academy for oral implantology: 8-year follow-up and risk factor analysis. Journal of Periodontal and Implant Science. 44 (2014) 102–108. https://doi.org/10.5051/jpis.2014.44.3.102.

[13] N. Ayub, M. Faraj, S. Ghatan, J.A.A. Reijers, N. Napoli, L. Oei, V. Valderrabano, The treatment gap in osteoporosis. Journal of Clinical Medicine. 10 (2021) 3002. https://doi.org/10.3390/jcm10133002.

[14] S. Khosla, L.C. Hofbauer, Osteoporosis treatment: Recent developments and ongoing challenges. The Lancet Diabetes and Endocrinology. 5 (2017). https://doi.org/10.1016/S2213-8587(17)30188-2.

[15] J.A. Kanis, Osteoporosis III: Diagnosis of osteoporosis and assessment of fracture risk. Lancet. 359 (2002) 1929–1936. https://doi.org/10.1016/S0140-6736(02)08761-5.

[16] World Health Organization, WHO scientific group on the assessment of osteoporosis at primary health care level. in: Summary meeting report. (2004) pp. 5–7. https://doi.org/10.1016/S0140-6736(02)08761-5.

[17] G.N. Hounsfield, Computerized transverse axial scanning (tomography): I. Description of system. British Journal of Radiology. 46 (1973) 1016–1022. https://doi.org/10.1259/0007-1285-46-552-1016.

[18] S. Nimbalkar, P. Dhatrak, C. Gherde, S. Joshi, A review article on factors affecting bone loss in dental implants. Materials Today: Proceedings. 43 (2021) 970–976. https://doi.org/10.1016/j.matpr.2020.07.428.

[19] T.T.T. Dao, J.D. Anderson, G.A. Zarb, Is osteoporosis a risk factor for osseointegration of dental implants? Implant Dentistry. 3 (1994) 56. https://doi.org/10.1097/00008505-199404000-00014.

[20] L.W. Lindquist, G.E. Carlsson, T. Jemt, A prospective 15-year follow-up study of mandibular fixed prostheses supported by osseointegrated implants. Clinical results and marginal bone loss. Clinical Oral Implants Research. 7 (1996) 329–336. https://doi.org/10.1034/j.1600-0501.1996.070405.x.

[21] G.L. Stafford, L. Chambrone, J.A. Shibli, C.E. Mercúrio, B. Cardoso, P.M. Preshaw, Review found little difference between sandblasted and acid-etched (SLA) dental implants and modified surface (SLActive) implants. Evidence-Based Dentistry. 15 (2014) 87–88. https://doi.org/10.1038/sj.ebd.6401047.

[22] T.A.L. Hassan, H.B. Mohammed, Effect of implant surface modification on bone mineral density and survival rate in the maxilla after a short period using cone beam computed tomography. Journal of Craniofacial Surgery. 33 (2022) e49–e52. https://doi.org/10.1097/SCS.0000000000007908.

[23] L. Wu, Y. Dong, L. Yao, C. Liu, A.M. Al-Bishari, K.H. Ru Yie, H. Zhang, J. Liu, G. Wu, Nanoporous tantalum coated zirconia implant improves osseointegration. Ceramics International. 46 (2020) 17437–17448. https://doi.org/10.1016/j.ceramint.2020.04.038.

[24] J. Han, J. Zhao, Z. Shen, Zirconia ceramics in metal-free implant dentistry. Advances in Applied Ceramics. 116 (2017) 138–150. https://doi.org/10.1080/17436753.2016.1264537.

[25] S. Roehling, K.A. Schlegel, H. Woelfler, M. Gahlert, Zirconia compared to titanium dental implants in preclinical studies—a systematic review and meta-analysis. Clinical Oral Implants Research. 30 (2019) 365–395. https://doi.org/10.1111/clr.13425.

[26] J. Lindhe, J. Meyle, Peri-implant diseases: Consensus Report of the Sixth European Workshop on Periodontology. in: Workshop on Periodontology. (2008) pp. 282–285. https://doi.org/10.1111/j.1600-051X.2008.01283.x.

[27] S. Bauer, P. Schmuki, K. von der Mark, J. Park, Engineering biocompatible implant surfaces Part I: materials and surfaces. Progress in Materials Science. 58 (2013) 261–326. https://doi.org/10.1016/j.pmatsci.2012.09.001.

[28] C. Fransson, U. Lekholm, T. Jemt, T. Berglundh, Prevalence of subjects with progressive bone loss at implants. Clinical Oral Implants Research. 16 (2005) 440–446. https://doi.org/10.1111/j.1600-0501.2005.01137.x.

[29] S. Schou, P. Holmstrup, K. Stoltze, E. Hjørting-hansen, K.S. Kornman, Ligature-induced marginal inflammation around osseointegrated implants and ankylosed teeth. Clinical and radiographic observations in cynomolgus monkeys (Macaca fascicularis). Clinical Oral Implants Research. 4 (1993) 12–22. https://doi.org/10.1034/j.1600-0501.1993.040102.x.

[30] I. Ericsson, T. Berglundh, C. Marinello, B. Liljenberg, J. Lindhe, Long-standing plaque and gingivitis at implants and teeth in the dog. Clinical Oral Implants Research. 3 (1992) 99–103. https://doi.org/10.1034/j.1600-0501.1992.030301.x.

[31] P.E. Petersen, H. Ogawa, The global burden of periodontal disease: Towards integration with chronic disease prevention and control. Periodontology 2000. 60 (2012) 15–39. https://doi.org/10.1111/j.1600-0757.2011.00425.x.

[32] I. Fragkioudakis, G. Tseleki, A.-E. Doufexi, D. Sakellari, Current concepts on the pathogenesis of peri-implantitis: A narrative review. European Journal of Dentistry. 15 (2021) 379–387. https://doi.org/10.1055/s-0040-1721903.

[33] G.R. Persson, S. Renvert, Cluster of bacteria associated with peri-implantitis. Clinical Implant Dentistry and Related Research. (2014) 783–793. https://doi.org/10.1111/CID.12052.

[34] S. Calamak, R. Shahbazi, I. Eroglu, M. Gultekinoglu, K. Ulubayram, An overview of nanofiber-based antibacterial drug design. Expert Opinion on Drug Discovery. 12 (2017) 391-406. https://doi.org/10.1080/17460441.2017.1290603.

[35] J.L. Golubovsky, T. Ejikeme, R. Winkelman, M.P. Steinmetz, Osteobiologics. Operative Neurosurgery. 21 (2021) S2–S9. https://doi.org/10.1093/ons/opaa383.

[36] J.P. Schmitz, J.O. Hollinger, The critical size defect as an experimental model for craniomandibulofacial nonunions. Clinical Orthopaedics and Related Research. 205 (1986) 299–308. https://doi.org/10.1097/00003086-198604000-00036.

[37] A. Stahl, Y.P. Yang, Regenerative approaches for the treatment of large bone defects. Tissue Engineering-Part B: Reviews. 27 (2021) 539–547. https://doi.org/10.1089/ten.teb.2020.0281.

[38] M.C. Bottino, V. Thomas, G. Schmidt, Y.K. Vohra, T.M.G. Chu, M.J. Kowolik, G.M. Janowski, Recent advances in the development of GTR/GBR membranes for periodontal regeneration-a materials

perspective. Dental Materials. 28 (2012) 703–721. https://doi.org/10.1016/j.dental.2012.04.022.

[39] E. Shoba, R. Lakra, M.S. Kiran, P.S. Korrapati, 3D nano bilayered spatially and functionally graded scaffold impregnated bromelain conjugated magnesium doped hydroxyapatite nanoparticle for periodontal regeneration. Journal of the Mechanical Behavior of Biomedical Materials. 109 (2020) 103822. https://doi.org/10.1016/j.jmbbm.2020.103822.

[40] R. Zhang, J. Yang, J. Wu, L. Xiao, L. Miao, X. Qi, Y. Li, W. Sun, Berberine promotes osteogenic differentiation of mesenchymal stem cells with therapeutic potential in periodontal regeneration. European Journal of Pharmacology. 851 (2019) 144–150. https://doi.org/10.1016/j.ejphar.2019.02.026.

[41] G. Isola, A. Polizzi, S. Santonocito, D. Dalessandri, M. Migliorati, F. Indelicato, New frontiers on adjuvants drug strategies and treatments in periodontitis. Scientia Pharmaceutica. 89 (2021) 46. https://doi.org/10.3390/scipharm89040046.

[42] P. Makvandi, U. Josic, M. Delfi, F. Pinelli, V. Jahed, E. Kaya, M. Ashrafizadeh, A. Zarepour, F. Rossi, A. Zarrabi, T. Agarwal, E.N. Zare, M. Ghomi, T. Kumar Maiti, L. Breschi, F.R. Tay, Drug delivery (nano)platforms for oral and dental applications: Tissue regeneration, infection control, and cancer management. Advanced Science. 8 (2021) 2004014. https://doi.org/10.1002/advs.202004014.

[43] M. Eischen-Loges, K.M.C. Oliveira, M.B. Bhavsar, J.H. Barker, L. Leppik, Pretreating mesenchymal stem cells with electrical stimulation causes sustained long-lasting pro-osteogenic effects. PeerJ. 6 (2018) e4959. https://doi.org/10.7717/peerj.4959.

[44] H. Huang, Z. Xu, X. Shao, D. Wismeijer, P. Sun, J. Wang, G. Wu, J. Leicester Williams, Multivariate linear regression analysis to identify general factors for quantitative predictions of implant stability quotient values. PLoS ONE. 12 (2017) e0187010. https://doi.org/10.1371/journal.pone.0187010.

[45] J. Moritz, A. Abram, M. Čekada, U. Gabor, M. Garvas, I. Zdovc, A. Dakskobler, J. Cotič, K. Ivičak-Kocjan, A. Kocjan, Nanoroughening of sandblasted 3Y-TZP surface by alumina coating deposition for improved osseointegration and bacteria reduction. Journal of the European Ceramic Society. 39 (2019) 4347-4357. https://doi.org/10.1016/j.jeurceramsoc.2019.05.051.

[46] G. Soon, B. Pingguan-Murphy, K.W. Lai, S.A. Akbar, Review of zirconia-based bioceramic: Surface modification and cellular response. Ceramics International. 42 (2016) 12543–12555. https://doi.org/10.1016/j.ceramint.2016.05.077.

[47] N. Wang, H. Li, W. Lü, J. Li, J. Wang, Z. Zhang, Y. Liu, Effects of TiO2 nanotubes with different diameters on gene expression and osseointegration of implants in minipigs. Biomaterials. 32 (2011) 6900–6911. https://doi.org/10.1016/j.biomaterials.2011.06.023.

[48] L. Zhao, H. Wang, K. Huo, L. Cui, W. Zhang, H. Ni, Y. Zhang, Z. Wu, P.K. Chu, Antibacterial nano-structured titania coating incorporated with silver nanoparticles. Biomaterials. 32 (2011) 5706–5716. https://doi.org/10.1016/j.biomaterials.2011.04.040.

[49] P. Roy, S. Berger, P. Schmuki, TiO2 nanotubes: Synthesis and applications. Angewandte Chemie International Edition. 50 (2011) 2904–2939. https://doi.org/10.1002/anie.201001374.

[50] K. Gulati, M. Kogawa, S. Maher, G. Atkins, D. Findlay, D. Losic, Titania nanotubes for local drug delivery from implant surfaces. Springer Series in Materials Science. 220 (2015) 307–355. https://doi.org/10.1007/978-3-319-20346-1_10.

[51] D. Neut, O.S. Kluin, B.J. Crielaard, H.C. van der Mei, H.J. Busscher, D.W. Grijpma, A biodegradable antibiotic delivery system based on poly-(trimethylene carbonate) for the treatment of osteomyelitis. Acta

Orthopaedica. 80 (2009) 514–519. https://doi.org/10.3109/17453670903350040.

[52] A. Mombelli, N.P. Lang, The diagnosis and treatment of peri-implantitis. Periodontology 2000. 17 (1998) 63–76. https://doi.org/10.1111/j.1600-0757.1998.tb00124.x.

[53] H.I. Chang, Y. Perrie, A.G.A. Coombes, Delivery of the antibiotic gentamicin sulphate from precipitation cast matrices of polycaprolactone. Journal of Controlled Release. 110 (2006) 414–421. https://doi.org/10.1016/j.jconrel.2005.10.028.

[54] D. Campoccia, L. Montanaro, P. Speziale, C.R. Arciola, Antibiotic-loaded biomaterials and the risks for the spread of antibiotic resistance following their prophylactic and therapeutic clinical use. Biomaterials. 31 (2010) 6363–6377. https://doi.org/10.1016/j.biomaterials.2010.05.005.

[55] V.V. Divya Rani, L. Vinoth-Kumar, V.C. Anitha, K. Manzoor, M. Deepthy, V.N. Shantikumar, Osteointegration of titanium implant is sensitive to specific nanostructure morphology. Acta Biomaterialia. 8 (2012) 1976–1989. https://doi.org/10.1016/j.actbio.2012.01.021.

[56] J. Liu, J.L. Pathak, X. Hu, Y. Jin, Z. Wu, M.A. Al-Baadani, S. Wu, H. Zhang, S. Farkasdi, Y. Liu, J. Ma, G. Wu, Sustained release of zoledronic acid from mesoporous TiO2-layered implant enhances implant osseointegration in osteoporotic condition. Journal of Biomedical Nanotechnology. 14 (2018) 1965–1978. https://doi.org/10.1166/jbn.2018.2635.

[57] M. Heiden, S. Huang, E. Nauman, D. Johnson, L. Stanciu, Nanoporous metals for biodegradable implants: Initial bone mesenchymal stem cell adhesion and degradation behavior. Journal of Biomedical Materials Research-Part A. 104 (2016) 1747–1758. https://doi.org/10.1002/jbm.a.35707.

[58] M.N. Aboushelib, E. Osman, I. Jansen, V. Everts, A.J. Feilzer, Influence of a nanoporous zirconia implant surface of on cell viability of human osteoblasts. Journal of Prosthodontics. 22 (2013) 190–195. https://doi.org/10.1111/j.1532-849X.2012.00920.x.

[59] J. Park, S. Bauer, K.A. Schlegel, F.W. Neukam, K. der von Mark, P. Schmuki, TiO2 nanotube surfaces: 15 nm-an optimal length scale of surface topography for cell adhesion and differentiation. Small. 5 (2009) 666–671. https://doi.org/10.1002/smll.200801476.

[60] K. Blecher, A. Nasir, A. Friedman, The growing role of nanotechnology in combating infectious disease. Virulence. 2 (2011) 395–401. https://doi.org/10.4161/viru.2.5.17035.

[61] J. Hornak, Synthesis, properties and selected technical applications of magnesium oxide nanoparticles: A review. International Journal of Molecular Sciences. 22 (2021) 12752. https://doi.org/10.3390/ijms222312752.

[62] R. Eivazzadeh-Keihan, E. Bahojb Noruzi, K. Khanmohammadi Chenab, A. Jafari, F. Radinekiyan, S.M. Hashemi, F. Ahmadpour, A. Behboudi, J. Mosafer, A. Mokhtarzadeh, A. Maleki, M.R. Hamblin, Metal-based nanoparticles for bone tissue engineering. Journal of Tissue Engineering and Regenerative Medicine. 14 (2020) 1687–1714. https://doi.org/10.1002/term.3131.

[63] M.A. McGinnis, P. Larsen, M. Miloro, F.M. Beck, Comparison of resorbable and nonresorbable guided bone regeneration material. British Journal of Oral and Maxillofacial Surgery. 35 (1997) 445–446. https://doi.org/10.1016/s0266-4356(97)90742-7.

[64] Y.Y. Jo, J.H. Oh, New resorbable membrane materials for guided bone regeneration. Applied Sciences (Switzerland). 8 (2018) 2157. https://doi.org/10.3390/app8112157.

[65] X.N. Gu, Y.F. Zheng, A review on magnesium alloys as biodegradable materials. Frontiers of Materials Science in China. 4 (2010) 111–115. https://doi.org/10.1007/s11706-010-0024-1.

[66] E. Marukawa, M. Tamai, Y. Takahashi, I. Hatakeyama, M. Sato, Y. Higuchi, H. Kakidachi, H. Taniguchi, T. Sakamoto, J. Honda, K. Omura, H. Harada, Comparison of magnesium alloys and poly-l-lactide screws as degradable implants in a canine fracture model. Journal of Biomedical Materials Research-Part B Applied Biomaterials. 104 (2016) 1282–1289. https://doi.org/10.1002/jbm.b.33470.

[67] H. Hornberger, S. Virtanen, A.R. Boccaccini, Biomedical coatings on magnesium alloys — a review. Acta Biomaterialia. 8 (2012) 2442–2455. https://doi.org/10.1016/j.actbio.2012.04.012.

[68] Y. Liu, C. Bao, D. Wismeijer, G. Wu, The physicochemical/biological properties of porous tantalum and the potential surface modification techniques to improve its clinical application in dental implantology. Materials Science and Engineering C. 49 (2015) 323–329. https://doi.org/10.1016/j.msec.2015.01.007.

[69] Q. Wang, H. Zhang, H. Gan, H. Wang, Q. Li, Z. Wang, Application of combined porous tantalum scaffolds loaded with bone morphogenetic protein 7 to repair of osteochondral defect in rabbits. International Orthopaedics. 42 (2018) 1437–1448. https://doi.org/10.1007/s00264-018-3800-7.

[70] D. Fraser, G. Mendonca, E. Sartori, P. Funkenbusch, C. Ercoli, L. Meirelles, Bone response to porous tantalum implants in a gap-healing model. Clinical Oral Implants Research. 30 (2019) 156–168. https://doi.org/10.1111/clr.13402.

[71] R. Liu, Y. Zhang, X. Zhao, A. Agarwal, L.J. Mueller, P. Feng, pH-responsive nanogated ensemble based on gold-capped mesoporous silica through an acid-labile acetal linker. Journal of the American Chemical Society. 132 (2010) 1500–1501. https://doi.org/10.1021/ja907838s.

[72] N. Murthy, Y.X. Thng, S. Schuck, M.C. Xu, J.M.J. Fréchet, A novel strategy for encapsulation and release of proteins: Hydrogels and microgels with acid-labile acetal cross-linkers. Journal of the American Chemical Society. 124 (2002) 12398–12399. https://doi.org/10.1021/ja026925r.

[73] S. Hayat, S. Muzammil, M.H. Rasool, Z. Nisar, S.Z. Hussain, A.N. Sabri, S. Jamil, In vitro antibiofilm and anti-adhesion effects of magnesium oxide nanoparticles against antibiotic resistant bacteria. Microbiology and Immunology. 62 (2018) 211–220. https://doi.org/10.1111/1348-0421.12580.

[74] G.K. Meenashisundaram, N. Wang, S. Maskomani, S. Lu, S.K. Anantharajan, S.T. Dheen, S.M.L. Nai, J.Y.H. Fuh, J. Wei, Fabrication of Ti + Mg composites by three-dimensional printing of porous Ti and subsequent pressureless infiltration of biodegradable Mg. Materials Science and Engineering C. 108 (2020) 110478. https://doi.org/10.1016/j.msec.2019.110478.

[75] B. Safari, S. Davaran, A. Aghanejad, Osteogenic potential of the growth factors and bioactive molecules in bone regeneration. International Journal of Biological Macromolecules. 175 (2021) 544–557. https://doi.org/10.1016/j.ijbiomac.2021.02.052.

[76] J.B. Cannata-andía, N. Carrillo-lópez, O.D. Messina, N.A.T. Hamdy, S. Panizo, S.L. Ferrari, Pathophysiology of vascular calcification and bone loss: Linked disorders of ageing? Nutrients. 13 (2021) 3835. https://doi.org/10.3390/nu13113835.

[77] I.V. Tudose, F. Comanescu, P. Pascariu, S. Bucur, L. Rusen, F. Iacomi, E. Koudoumas, M.P. Suchea, Chemical and physical methods for multifunctional nanostructured interface fabrication. Functional Nanostructured Interfaces for Environmental and Biomedical Applications. (2019) 15–26. https://doi.org/10.1016/B978-0-12-814401-5.00002-5.

[78] C.R. Chitambar, W.G. Matthaeus, W.E. Antholine, K. Graff, W.J. O'Brien, Inhibition of leukemic HL60 cell growth by transferrin-gallium: Effects of

ribonucleotide reductase and demonstration of drug synergy with hydroxyurea. Blood. 72 (1988) 1930–1936. https://doi.org/10.1182/blood.v72.6.1930.1930.

[79] D.W. Hedley, E.H. Tripp, P. Slowiaczek, G.J. Mann, Effect of gallium on DNA synthesis by human T-cell lymphoblasts. Cancer Research. 48 (1988) 3014–3018.

[80] M. Yu, Y. Wang, Y. Zhang, D. Cui, G. Gu, D. Zhao, Gallium ions promote osteoinduction of human and mouse osteoblasts via the TRPM7/Akt signaling pathway. Molecular Medicine Reports. 22 (2020) 2741–2752. https://doi.org/10.3892/mmr.2020.11346.

CHAPTER TWO

Nanoporous tantalum coated zirconia implant improves osteointegration

Lianjun Wu[1, *], Yiwen Dong[2, *], Litao Yao[1], Chuantong Liu[1], Abdullrahman M Al-Bishari[1], Kendrick Hii Ru Yie[1], Hualin Zhang[3, 4], Jinsong Liu[1], Gang Wu[2].

[1] School and Hospital of Stomatology, Wenzhou Medical University, Wenzhou, China

[2] Department of Oral Implantology and Prosthetic Dentistry, Academic Centre for Dentistry Amsterdam (ACTA), University of Amsterdam and Vrije Universiteit Amsterdam, Amsterdam Movement Sciences, Amsterdam, The Netherlands

[3] College of Stomatology, Ningxia Medical University, Yinchuan, China

[4] General Hospital of Ningxia Medical University, Yinchuan, China

[*] Shared first authorship

Ceramics International. 46 (2020) 17437–17448.

Abstract

Zirconia (Zr) is nowadays a versatile dental implant material due to its opaque white color, corrosion resistance and low affinity for bacterial plaque. Unfortunately, the biological inertness of zirconia surface results in weak integration with bone tissue in the early stage of osteointegration. To enhance the early osteointegration of zirconia implant, a homogeneous nanoporous tantalum (TaNS) coating (~ 30 nm in diameter and 1 μm in length) with appropriate adhesion strength was prepared on zirconia surface via magnetron sputtering combined with anodization. ZrO_2/TaNS significantly improved the roughness and hydrophilicity compared with ZrO_2/TaNS and ZrO_2. The protein adsorption, initial adhesion, spreading, and proliferation of MC3T3-E1 cells were significantly enhanced in ZrO_2/TaNS group as compared to ZrO_2 and ZrO_2/Ta groups. Moreover, the osteogenic differentiation of MC3T3-E1 cells was significantly improved in ZrO_2/TaNS groups than in other groups by up-regulating the expression of the osteogenic-related genes (RUNX2, ALP, COL-1, OSX, OCN, and OPG). Histological analysis displayed that more newly regenerated bone was deposited around ZrO_2/TaNS group than in other groups, and the bone-implant contact in ZrO_2/TaNS group was enhanced correspondingly. In conclusion, the TaNS coating with good adhesion strength can be successfully prepared on zirconia surface by magnetron sputtering combined with anodization. This novel coating will be a promising clinical application in improving osteointegration of the zirconia implant.

Keywords: Zirconia; Nanoporous tantalum coating; Magnetron sputtering; Anodization; Osteointegration

1. Introduction

Titanium (Ti) has been the mainstream material of dental implants. However, an unaesthetic metallic hue in the anterior area and hypersensitivity reaction in some cases caused by released Ti ion has led to the increasing demand for new biomaterials [1,2]. In recent years, zirconia ceramic has become a viable option for dental implant material due to its excellent aesthetic, chemical stability, and biocompatibility [3]. Different from Ti implants, the “tooth-like” color appearance of zirconia implants without toxic ion release makes them suitable for patients with metal ion allergy and thin gingival biotype. Nowadays, some commercial zirconia implants such as CeraRoot, Nobel Biocare, and Senden have been already applied in clinic.

However, the clinical failure of zirconia implants still occurs due to the biological inertness of zirconia surface. Studies have reported that the clinical success rate of zirconia dental implants is lower than titanium dental implants [4,5]. The fibrous tissue tends to grow into the interface between bio-inertia zirconia implants and bone tissue in the early stage of osteointegration, which will result in loosening and micro-motion [6]. Therefore, how to improve the early osteointegration of zirconia surface has been a vital issue. Osteointegration is the direct interaction between the implant surface and bone tissue. Studies have shown that surface properties like topography and chemical composition play a fundamental role in osteointegration, which affects the adsorption of proteins and cellular behavior [7,8]. Therefore, numerous surface modifications such as abrasive blasting, acid-etching, laser, coating, etc. are adopted to improve the bioactivity of zirconia surface. However, current surface treatments have some disadvantages, such as surface contamination, coating separation, and undesirable osteointegration. Recently, studies have reported that the nanostructures such as nanotubes, nanopores, nanodots, nanogrooves, *etc.* can improve osteointegration by affecting bio-molecular interaction and chemical reactivity between the implants and bone tissue [9,10]. Particularly, the nanoporous array can modulate cell behavior and enhance osteointegration by providing a framework for synthesizing new bone tissue [11,12]. The dimension of nanostructure, especially diameter, has been considered a crucial role in cellular behavior. The study by Park *et al*. has shown

that the diameter of nanostructure about 30 nm is beneficial for cell behavior and osteointegration [13]. Modifying the chemical composition of zirconia surface is also a feasible strategy to promote osteointegration [14]. Tantalum (Ta) and its oxides have emerged as an essential biomaterial due to their excellent biocompatibility, anticorrosion, and osteoinductivity [15]. Whereas, a high modulus of elasticity results in the mismatch between Ta-based biomaterials and bone tissue, which will lead to the failure of implants. Therefore, Ta and its oxides are often modified into porous coatings on substrates [16,17]. Recently, studies have demonstrated that micro-porous Ta coating presents enhanced osteointegration in artificial joints and implants [18,19]. For instance, a study has shown that Ta nanotube can improve the proliferation and differentiation of osteoblasts [15]. Thus, nanoporous Ta coating will be a successful strategy for improving osteointegration [20–22]. So far, most studies have only focused on the modification of TiO_2 and ZrO_2 nanostructure, whereas few studies are performed to prepare and analyze the osteoinductivity of TaNS coating on the zirconia substrates. Based on the above information, we combined the advantage of the nanoporous array with Ta coating on zirconia to improve osteointegration. Therefore, we first deposit a thin Ta film on zirconia surface by magnetron sputtering. Afterward, Ta coating is anodized in the electrolyte to prepare TaNS coating. Surface topography, chemical composition, bond strength, hydrophilicity, and roughness of TaNS coating are evaluated. *In vitro* and *vivo* tests are performed to assess the bioactivity and osteointegration of the TaNS-coated zirconia implant surface. Fig.1 presents the schematic illustration of our study.

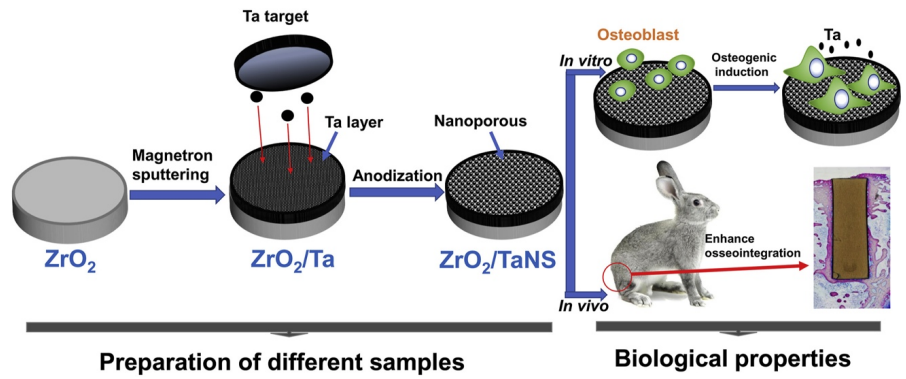

Figure 1. Schematic diagram of the preparation of TaNS coating on zirconia surface and the evaluation of biological effect *in vitro* and *in vivo*.

2. Materials and methods

2.1 Sample preparation

Briefly, the 3% yttria-stabilized zirconia ceramics (99.6% purity, UPCERA, Shenyang, China) were cut into ZrO_2 discs (10 mm in diameter, 1.5 mm in thickness) and cylindrical ZrO_2 implants (4 mm in diameter, 10 mm in length) for cellular and animal test, respectively. Then the samples were sintered at 1500°C for 2 h and cleaned by sequential ultrasonic in acetone (AR, Aladdin, Shanghai, China), ethanol (AR, Aladdin, Shanghai, China), and deionized water for 10 min, respectively. The control group was designated as ZrO_2. Then, Ta coating was deposited onto zirconia surface via DC magnetron sputtering machine (VTC-600-2HD, KEJING AUTO-INSTRUMENT CO., Shenyang, China). ZrO_2 substrates were displayed on a rotating sample stage and a sputtering target consisting of 99.9% high purity Ta (ZhongNuo Advanced Material Technology Co., Beijing, China) was applied to sputter Ta film. Pre-sputtering was performed in an argon (Ar_2) atmosphere to remove the oxide layer of the substrate. To prepare desirable Ta coating, magnetron sputtering was performed with different power (25 W, 50 W, 75 W, 100 W) and time (0.5 h, 1 h, 1.5 h, 2 h). The desirable condition of sputtering was as follows: the power was 100W with 0.5 Pa Ar_2 pressure and 10 cm target-substrate distance. The time of sputtering was 2 h. The parameters were summarized in Table 1. Ta deposited samples were designated as ZrO_2/Ta. The ZrO_2/Ta samples were then cleaned by ultrasonic in acetone and ethanol for 10 min, respectively. Afterward, ZrO_2/Ta was anodized in an electrolyte comprised of 98% sulfuric acid mixed with hydrofluoric acid (v/v = 9:1) in deionized water. All electrolytes were prepared using reagent-grade chemistry (AR, Aladdin, Shanghai, China). The anode and cathode were ZrO_2/Ta and Pt foil, respectively. The distance between electrodes was about 10 mm. The condition of anodization was a constant voltage of 15 V for 5 min at 0°C. The preparation of TaNS coating in our study was adopted according to the study by Masoud Sarraf *et al*. [23]. Finally, the samples were cleaned by ultrasonic in ethanol and deionized water for 10 min to remove surface contaminants, and the anodized samples were designated as ZrO_2/TaNS. A total of three groups were involved in our study: ZrO_2, ZrO_2/Ta, and ZrO_2/TaNS.

Variable factors	Quantity
Power (Watt)	100
Sputtering rate (nm/s)	1
Base pressure (Pa)	5×10^{-4}
Working pressure (Pa)	0.5
Time (h)	2
Temperature (°C)	37

Table 1. The parameters of magnetron sputtering for the deposition of Ta layer.

2.2 Bond strength of the coating

The bond strength of Ta coating with different power (25 W, 50 W, 75 W, 100 W) and time (0.5 h, 1 h, 1.5 h, 2 h), and TaNS coating were detected by scratch test using nanoindentation instrument (WS-2005, Lanzhou Zhongke Kaihua Technology Development Co., Ltd, China). A rockwell head with a curvature radius of 200 μm was applied at a loading rate of 30 N/min, and the terminal load was about 40 N. When the coating was scratched or peeled by the rockwell head, a weak sound signal would be sent out by the acoustic emission measurement, and the critical load (Lc) of coating can be obtained. Meantime, FESEM was used to observe the topography of scratches on the surface of samples to determine the Lc values.

2.3 Surface characterization

The color appearance of different samples was observed under white light condition and the optimal images of different samples were captured by a camera (Canon EOS 800D, Japan). Field emission scanning electron microscopy was used to observe the surface topography of different samples (FESEM, Nova NanoSEM200, FEI Co., USA). The chemical composition of ZrO_2/Ta and ZrO_2/TaNS were detected via X-ray photoelectron spectroscopy (XPS, K-alpha, Thermo, USA), and the amount of Ta element was measured by XPS quantitative analysis. 3D topographic images and the average roughness (Ra) were obtained by atomic force microscopy (AFM, Veeco Co.,

USA). The hydrophilicity of different samples was detected by a water contact angle system (data physics OCA20, Germany).

2.4 Protein adsorption

The fluorescein isothiocyanate-bovine serum albumin (FITC-BSA, AR, Aladdin, Shanghai, China) was used to evaluate the concentration of FITC-BSA protein adsorbed on samples (c_1). All steps were performed in the dark. The standard curve of FITC-BSA protein concentration was acquired by adding the gradient concentration of FITC-BSA protein into a 96-well plate. Then, the different samples were separately soaked into 1 μg/ml (c) FITC-BSA protein and incubated in the shaking table with constant temperature and speed (37°C, 100 r/min) for 30 min, 60 min, and 120 min, respectively. At each time point, 100 μl soaking solution was collected to measure the concentration of residual FITC-BSA protein (c_2) at 490 nm wavelength via a fluorescence spectrometer (SpectraMax M5 Molecular Devices, Sunnyvale, USA). The c_1 value can be calculated as the following formula: $c_1 = (c - c_2)$. After incubation of 120 min, the samples were transferred to a new plate and rinsed with phosphate-buffered saline (PBS, AR, Aladdin, Shanghai, China). Then fluorescence microscopy (FM, OLYMPUS IX71, Japan) was used to observe the fluorescent intensity of FITC-BSA protein adsorbed on samples.

2.5 In vitro evaluation

2.5.1 Cell culture

The mouse embryonic precursor osteoblast cells (MC3T3-E1 cells, ATCC, Chinese Academy of Science, China) were cultured in alpha-minimum essential medium (α-MEM, Gibco, USA) supplemented with 10% fetal bovine serum (FBS, Gibco, USA) under the condition of 5% CO_2 at 37°C. When the density of MC3T3-E1 cells reached to 80–90% confluence, 25% trypsin (Gibco, USA) was added to detach cells, and the medium was centrifuged at 1000 rpm for 5 min. Then, the supernatant liquid was discarded and 1 ml medium was added to resuspend cells. All samples were sterilized in 75% ethanol solution and a density of $10^4/cm^2$ of cells was seeded onto each sample for further cellular tests.

2.5.2 Cell adhesion and morphology

The cell morphology on samples was observed by fluorescence microscopy (FM, OLYMPUS IX71, Japan). After incubation of 6 h, 24 h, and 48 h, the samples with attached MC3T3-E1 cells were fixed with 3.7% formaldehyde, and then the cell cytoplasmic and nucleus were stained with fluorescein isothiocyanate (FITC, Aladdin)-labeled phalloidin and 4', 6-diamidino-2-phenylindole (DAPI, AR Aladdin, China), respectively. Afterwards, the stained cells were observed using fluorescence microscopy. Meanwhile, the number and spreading area of initial adherent cells on samples were calculated by Image J (National Institutes of Health, Bethesda, MD).

2.5.3 Cell proliferation

The proliferation of MC3T3-E1 was detected using 3-(4, 5-dimethylthiazol-2-yl)-2, 5-diphenyltetra-zolium bromide (MTT assay, Invitrogen Corporation, USA) by measuring absorbance after incubation of 1, 3, and 5 days. At each time point, the samples were washed twice with PBS and transferred to a new 24-well plate containing 300 μl medium and 60 μl MTT per well. Then, the samples were incubated for another 4 h to form formazan and then 500 μl dimethyl sulfoxide (DMSO, Sigma) was added to dissolve the formazan crystals. The absorbance was detected at 490 nm wavelength using a fluorescence spectrometer (SptraMax M5 Molecular Devices, USA).

2.5.4 Alkaline phosphatase activity (ALP)

After incubation of 7 days and 14 days, MC3T3-E1 cells on samples were lysed with 1% Triton X-100 at 0°C for 30 min. Then, the lysates were measured via LabAssayTM ALP colorimetric assay kit (Wako Pure Chemicals, Japan), and the total intracellular protein content was detected by BCA Protein Assay Kit (Beyotime, China). The absorbance was subsequently measured at 410 nm wavelength via a spectrophotometer, and the ALP activity was normalized by corresponding protein concentration.

2.5.5 Alizarin red S (ARS) staining

After incubation of 14 days and 21 days, the samples cultured with MC3T3-E1 cells were fixed with 4% paraformaldehyde for 30 min and stained with 40 mM Alizarin Red reagent for 30 min. Then, the samples were washed with DI water until the red color could not be observed. Then, 10% cetylpyridinium chloride (500 ml) in 10 mM sodium phosphate (pH 7.0) was used to elute the bound stain for 2 h and the OD values of absorbance were detected at 540 nm wavelength using the microplate reader.

2.5.6 Osteogenic-related gene expressions

After incubation for 14 days, the total amount of RNA in the lysate was collected and isolated using RNAiso Kit (TaKaRa, Japan). The RNA concentration was determined using a TECAN Infinite® F200 Pro microtiter plate reader (Thermo Fisher Scientific). Then, M-MLV RTase cDNA Synthesis Kit (TaKaRa, Japan) was applied to reverse RNA to cDNA. Osteogenic-related genes (ALP, OSX, RUNX2, COL-1, OCN, and OPG) were programmed by SYBR Premix ExTM Taq-II (TaKaRa, Japan), and the primers of target and housekeeping genes were listed in Table 2. Subsequently, 50 ml PCR mixture (1 ml PCR Forward Primer + 1 ml PCR Reserve Primer + 0.3 ml Taq DNA Polymerase + 2 ml of template cDNA + 25 ml of 2 × SYBR Mix + 20.7 ml double distilled H_2O_2) was added into each well of the PCR array to measure the CT values of the target genes that were normalized to the relative expression of GAPDH gene.

Target genes	Primers
ALP	F:5'-GGCCAGCTACACCACAACA-3' R:5'-CTGAGCGTTGGTGTTATATGTCTT-3'
RUNX2	F:5'-CCCGTGGCCTTCAAGGT-3' R:5'-CGTTACCCGCCATGACAGTA-3'
Osx	F: 5'-ACTACCCACCCTTCCCTCACTC-3' R: 5'-CCACCACCTAGCCAGTTGCC-3'
OCN	F:5'-AGACTCCGGCGCTACCTT-3' R:5'-CTCGTCACAAGCAGGGTTAAG-3'
COL-1	F: 5'-CCTGAGCCAGCAGATTGA-3' R:5'-TCCGCTCTTCCAGTCAG-3'
OPG	F: 5'-GCCCAGACGAGATTGAGAG-3' R:5'-CAGACTGTGGGTGACGGTT-3'
GAPDH	F: 5'-TGGACAGCACTGACTTCCAG-3' R: 5'-CAAAGCATCGACCAGTGCTA-3'

Table.2 Primers of target and housekeeping genes. **Notes:** RUNX2: Runt-related transcription factor 2; Osx: Osterix; ALP: Alkaline phosphatase; COL-1: Collagen-I; OPG: Osteoprotegerin; OCN: Osteocalcin; GAPDH: Glyceraldehyde-3-phosphate dehydrogenase.

2.6 In-vivo experiment

2.6.1 Surgery procedures

The animal experiment agreed with the rules of the Animal Ethics Committee of Wenzhou Medical University (No. wydw201–0955). A total of 18 male Japanese white rabbits (6 months old, 2.5–4.0 kg) were included in our study and all surgical procedures were performed by the same surgeon. All rabbits were bred in individual cages with the temperature maintained at 37°C. A standard diet and water were provided throughout the study. Rabbits were randomly divided into three groups: I) ZrO_2 in the left and ZrO_2/Ta in the right side (n = 6); II) ZrO_2 in the left side and ZrO_2/TaNS in the right side (n = 6); III) ZrO_2/Ta in the left side and ZrO_2/TaNS in the right side (n = 6). All rabbits went through intravenous injections of 3% sodium pentobarbital (35 mg/kg, Merck Drugs and Biotechnology, Germany) and lidocaine hydrochloride for general anesthesia and local anesthesia, respectively. After skin preparation and sterilization, a 2 cm vertical incision was made at the protrusion of the femoral condyle. The femoral condyle was fully exposed by stripping the subcutaneous tissue, muscle, and periosteum. The osteotomy in the femoral condyle was prepared using drills with ascending diameter. Then, different samples (4 mm in diameter, 10 mm in length) were inserted into the implant site immediately, and soft tissue was sutured with 4–0 silk sutures (Fig. 2A, B, C). X-rays were taken immediately to confirm the location of the implants (Fig. 2 D). After surgery, subcutaneous injections with gentamicin and penicillin were performed for 3 days to avoid infection.

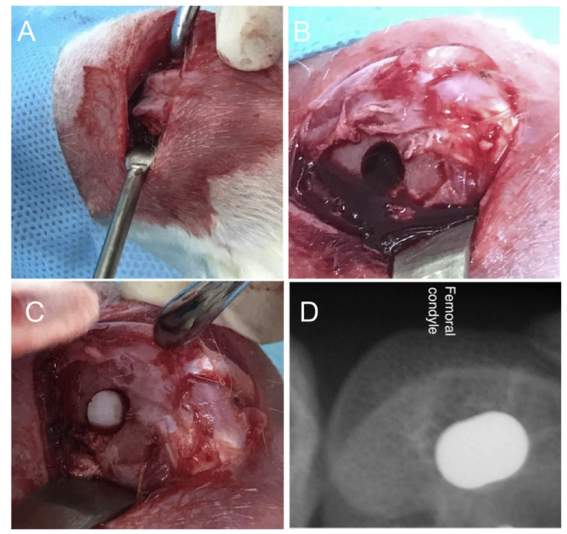

Figure 2. The process of implantation in rabbits. Surgical site with implants inserted (A, B, C). X-ray of the placement location-white image indicates the implant (D).

2.6.2 Histological analysis

4 and 8 weeks after surgery, the rabbits were sacrificed by excessive injection of 3% sodium pentobarbital and bone blocks containing the implants were dissected for histological analysis (n = 6). In brief, the bone blocks were firstly fixed in 4% paraformaldehyde (Yili Fine Chemical Co., Ltd, China) for 48 h, and then soaked in the gradient ethanol solution for dehydration. After being embedded in Technovit 7200 resin liquid (KULZER, Germany), a sliding microtome (EXAKT300CP, Germany) was used to cut the specimens along the long axis to form 200 μm thickness slices. Then, the abrasive papers with a grit size of 320, 800, and 1200 were performed to yield 20 μm thickness slices. Then, a grit size of 4000 was used to polish the slices. The methylene blue and fuchsin staining reagent (SINOPHARM, China) were used to stain the slices for image acquisition via fluorescence microscopy (FM, OLYMPUS IX71, Japan). The percentage of bone-implant contact (BIC %) was measured by image pro plus software.

2.7 Statistical analysis

Data are presented as mean ± standard deviation (SD). Data were analyzed using Graphpad Prism® 7.5 (GraphPad Software Inc., La Jolla, CA, USA). One-way analysis of variance (ANOVA) with Bonferroni's post hoc test was used for multiple comparisons. For the data in Figure 3C, we used independent-sample t-test. For all analysis, p values < 0.05 was considered statistically significant.

3. Results and discussion

3.1 Bond strength of the coating

To prepare desirable Ta coating on ZrO_2, magnetron sputtering with different power and time was performed in our study. Fig. 3A shows that the bond strength of Ta coating on the ZrO_2 substrate was positively correlated with the sputtering power and time. The results were consistent with the study by Masoud Sarraf *et al*. [23]. With the increase of sputtering power and time, the energy of ionized particles increases, which results in the higher available energy for coating growth. As a result, the compaction degree and density of the coating are improved, thus enhancing the adhesion strength [24,25]. The results of the scratch test show that a power of 100 W and a deposited time of 2 h were considered the optimal parameter to achieve the desirable Ta coating. Thus, the parameter (100 W, 2 h) was adopted to prepare Ta coating on ZrO_2 surface in our study for the next step.

The relationship between Lc and sound signal was shown in Fig. 3B. The load was considered as Lc value When the sound signal first appeared. The SEM images of ZrO_2/Ta and ZrO_2/TaNS show that the first semicircular crack appeared with edge cracking when the load reached to ~20 N and ~14 N, respectively. From Fig. 3C, the average Lc values of ZrO_2/Ta and ZrO_2/TaNS were 20.2 ± 0.28 N and 14.25 ± 0.79 N, respectively. There was no significant difference between ZrO_2/Ta and ZrO_2/TaNS (p > 0.05). Compared with other studies, the bond strength of TaNS coating in our study was strong enough to avoid the separation from zirconia during implant surgery [23,24]. The adhesion strength of TaNS coating was mainly influenced by the concentration of HF and anodization time [26]. The TaNS coating will be separated from ZrO_2 due to the anodizing process by HF. Therefore, a lower concentration of HF was used to reduce the degree of detachment between the coating and substrate in our study. Additionally, the lower temperature during anodization will avoid volume expansion and release deformational stress to form tight bond strength between the nanoporous array and ZrO_2 substrate [27].

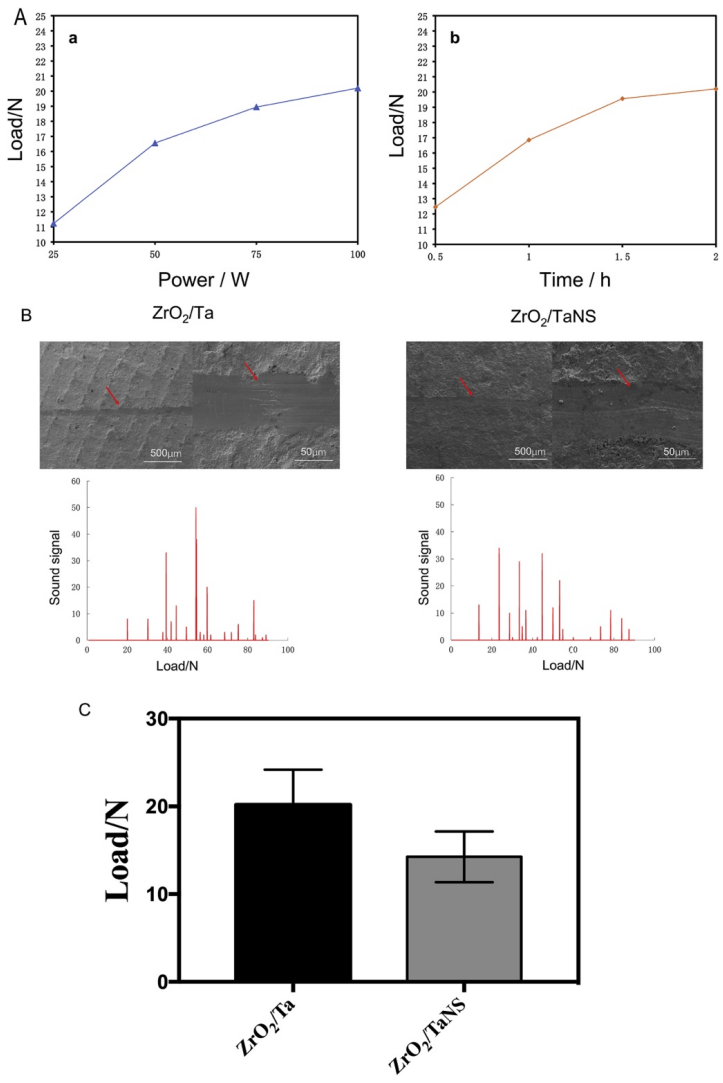

Figure 3. (A) The load response of DC power (a) and time (b) for adhesion strength. (B) The SEM images of scratch topography of ZrO_2/Ta and ZrO_2/TaNS, and the relationship between sound signal and load of Ta and TaNS coating. (C) The load values of ZrO_2/Ta and ZrO_2/TaNS. There is no statistically significant difference.

3.2 Surface characterizations

3.2.1 Optical and FESEM observation

Fig. 4 shows that the optical images of ZrO_2 displayed a bright "tooth-like" color appearance. However, the color appearance of ZrO_2/Ta presented a grey hue due to the metal color of the Ta layer on ZrO_2 substrates after magnetron sputtering. Unlike ZrO_2/Ta samples, the optical appearance of ZrO_2/TaNS became similar to that of ZrO_2 samples due to the transparent nanoporous array prepared by anodization. Although the color of ZrO_2/TaNS was not exactly the same as ZrO_2, it presented a similar bright tooth-like color appearance, which indicated that ZrO_2/TaNS coating maintained the aesthetic appearance of ZrO_2 implants [28]. The SEM images show that irregular granules were observed on the surface of ZrO_2. The surface of ZrO_2/Ta was covered with a layer formed by the accumulation of Ta particles after magnetron sputtering. The top view and cross-section of ZrO_2/TaNS exhibited a homogeneously distributed nanoporous array with ~ 30 nm in diameter and 1 μm in length over the entire surface. No cracks or delamination were observed on the surface. From a physical point of view, the mechanism of formation of TaNS can be described as follows [29,30]: (i) The formation of the initial barrier layer. During this phase, the current density of the anode decreases exponentially until it reaches a stable state. (ii) O^{2-} or OH^- transfers through the oxide layer to the metal/oxide and reacts with Ta metal. (iii) Homogeneous nanopores are formed due to the local dissolution of Ta_2O_5. In this phase, the current density gradually becomes stable. The parameters of anodization in our study were determined according to the study by Masoud Sarraf *et al*. [23]. They found that the diameter of nanopores increased slightly from 20–40 nm as the anodization time from 0.5 min to 20 min. Sebastian Bauer *et al*. also reported that smaller nanotube inner diameters (< 50 nm) can improve cell adhesion and spreading [31]. In our study, the diameter of the nanopore was about 30 nm which was claimed to be beneficial for cell activity.

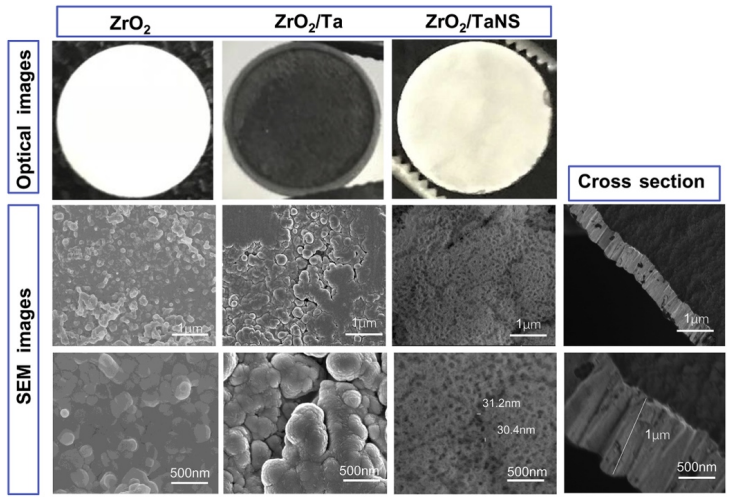

Figure 4. Optical and SEM images of ZrO_2, ZrO_2/Ta, and ZrO_2/TaNS. Cross-sectional SEM images of ZrO_2/TaNS. A homogeneous nanoporous array with ~30 nm in diameter and 1 μm in length was observed in ZrO_2/TaNS.

3.2.2 XPS analysis

The element and chemical bonding state of ZrO_2/Ta and ZrO_2/TaNS were analyzed by XPS. Table .3 shows that ZrO_2 was comprised of Zr3d, C1s and O1s, while Ta4f ($Ta4f_{7/2}$ and $Ta4f_{5/2}$), C1s and O1s existed in ZrO_2/Ta and ZrO_2/TaNS. The atomic percentage of Ta4f in ZrO_2/Ta and ZrO_2/TaNS was 21.15 ± 0.1% and 15.32 ± 0.2%, respectively. The narrow scan spectrums of ZrO_2/Ta and ZrO_2/TaNS were further studied and detailed information about the shape and position of the peaks was obtained (Fig. 5). Four types of Ta chemical states existed in ZrO_2/Ta (Fig. 5A): (1) Ta metallic state (21.40 eV); (2) $Ta4f_{7/2}$ (28.37 eV); (3) $Ta4f_{5/2}$ (26.58 eV); (4) Ta suboxides (23.21 eV). The results of XPS show that Ta metallic was the main state in ZrO_2/Ta, and the Ta_2O_5 state detected from ZrO_2/Ta may be attributed to partially oxidized Ta in the air. Generally, $Ta4f_{7/2}$ and $Ta4f_{5/2}$ were the typical peaks of the Ta chemical bonding states in Ta_2O_5 [32]. As shown in Fig. 5C, $Ta4f_{7/2}$ (28.37 eV), $Ta4f_{5/2}$ (26.58 eV), and a small amount of Ta suboxide (23.21 eV) without Ta metallic state were detected in ZrO_2/TaNS, suggesting that ZrO_2/TaNS coating mainly

consisted of Ta_2O_5 after anodization. The existence of Ta suboxide might be attributed to the n-type semiconductor behavior of Ta electrodes covered by a thin electrogenic oxide film.

In the terms of the O peaks, O1 (530 eV), O2 (531 eV), and O3 (532 eV) were detected in ZrO_2/Ta (Fig. 5B). After anodization, there were four types of O chemical states in ZrO_2/TaNS (Fig. 5D). The O1 peak at ~ 530 eV was related to Ta_2O_5, and the extra peak at the higher binding energy might be due to physical adsorption or retention of water [33]. The ratio of O1s and Ta4f was 2.6 in ZrO_2/Ta, whereas O1s: Ta4f in ZrO_2/TaNS was 4.9. The results show that the content of oxygen element was significantly enhanced in ZrO_2/TaNS after anodization, which was beneficial for cell growth and attachment. The results were consistent with the study by Na Wang *et al* [34].

Samples	Ta4f	Zr3d	C1s	O1s
ZrO_2	-	34.56 ± 0.2	20.36 ± 0.3	43.08 ± 0.1
ZrO_2/Ta	21.15 ± 0.1	-	21.86 ± 0.2	54.99 ± 0.2
ZrO_2/TaNS	15.32 ± 0.2	-	9.15 ± 0.2	75.53 ± 0.2

Table.3 The content of the elements (at%) obtained by XPS

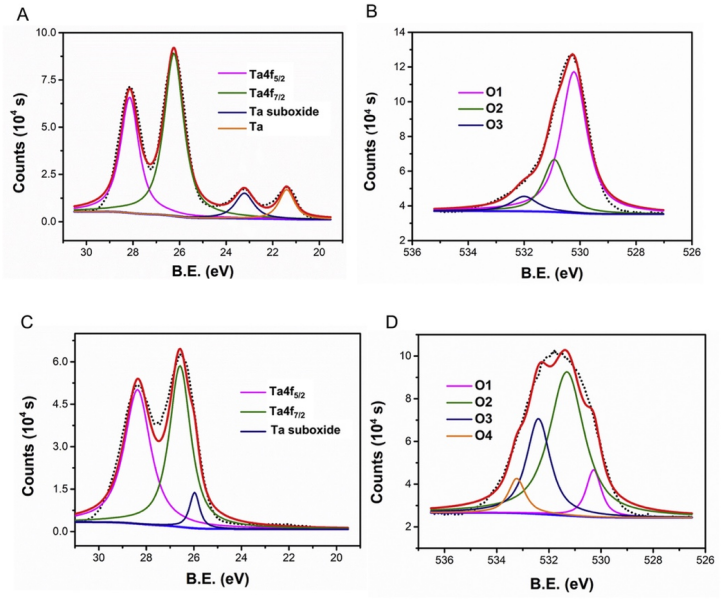

Figure 5. XPS spectra of (A) Ta and (B) O of ZrO_2/Ta. (C) Ta and (D) O of ZrO_2/TaNS. Ta_2O_5 state can be detected in ZrO_2/TaNS.

3.2.3 AFM and water contact angle measurement

The AFM profiles and surface roughness of ZrO_2, ZrO_2/Ta, and ZrO_2/TaNS were shown in Fig. 6A. A rougher surface with pits was observed in ZrO_2/TaNS as compared to ZrO_2 and ZrO_2/Ta. The roughness analysis (Ra) indicates that ZrO_2/TaNS had significantly enhanced average roughness (Ra = 151.0 ± 14.5 nm) than ZrO_2 (Ra = 87.4 ± 12.4 nm) and ZrO_2/Ta (Ra = 107.3 ± 13.3 nm) (Fig. 6C). The graphs of AFM indicate that the roughness of ZrO_2/TaNS was significantly increased compared to ZrO_2 and ZrO_2/Ta because the surface of ZrO_2/TaNS consisted of numerous nanopores, which significantly enhanced the surface area. Nanoscale roughness can enhance protein adsorption and subsequent cell functions, thus improving the BIC% and bond strength with bone [35,36].

Additionally, the water contact angle of ZrO_2/TaNS (16.6 ± 2.65°) was lower than ZrO_2/Ta (44.6 ± 2.12°) and ZrO_2 (67.9 ± 3.22°), which indicated the surface hydrophilicity was increased after anodization (Fig. 6B, D). The possible

reasons for enhanced hydrophilicity of anodized surface have been extensively discussed by previous studies [37,38]. The water contact angle is inversely related to surface free energy and roughness. In the Wenzel model, when the contact angle is between 0° and 90°, the higher the surface roughness is, the higher the wettability will be [37]. The nanoporous structure with a larger surface area and higher roughness improves surface free energy, thus enhancing the hydrophilicity of ZrO_2/TaNS. It is also reported that enhanced hydrophilicity is beneficial for the adsorption of vitronectin and fibronectin, which enables the formation of strong actin between cells and implants [39].

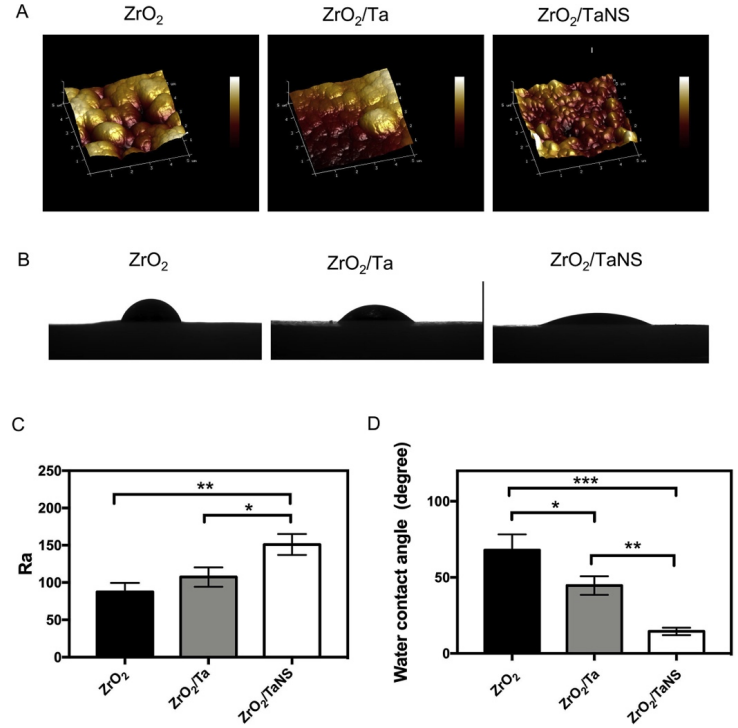

Figure 6. AFM topography images (A, C) and the water contact angle (B, D) of ZrO_2, ZrO_2/Ta, and ZrO_2/TaNS. $^*p < 0.05$, $^{**}p < 0.01$, $^{***}p < 0.001$.

3.3 Biological evaluation

3.3.1 Protein adsorption

The fluorescent intensity of FITC-BSA protein adsorbed on all samples after incubation of 2 h was presented in Fig. 7A. Significantly stronger fluorescent intensity was observed on the surface of ZrO_2/TaNS than the other two groups. Likewise, the concentration of FITC-BSA protein absorbed on ZrO_2/TaNS was significantly higher than that of ZrO_2 and ZrO_2/Ta after 30 min, 60 min, and 120 min ($p < 0.01$), and there was no significant difference between ZrO_2 and ZrO_2/Ta ($p > 0.05$). The adsorption of protein on the surface is the crucial step to induce subsequent cell attachment and spreading [40,41]. The scale of protein is generally within the range of ~10 nm, and the surface with a similar nanoscale is beneficial for protein adsorption [40]. The larger amount of protein adsorbed on ZrO_2/TaNS might be due to its nanoscale structure and enhanced hydrophilicity confirmed by the contact angle test.

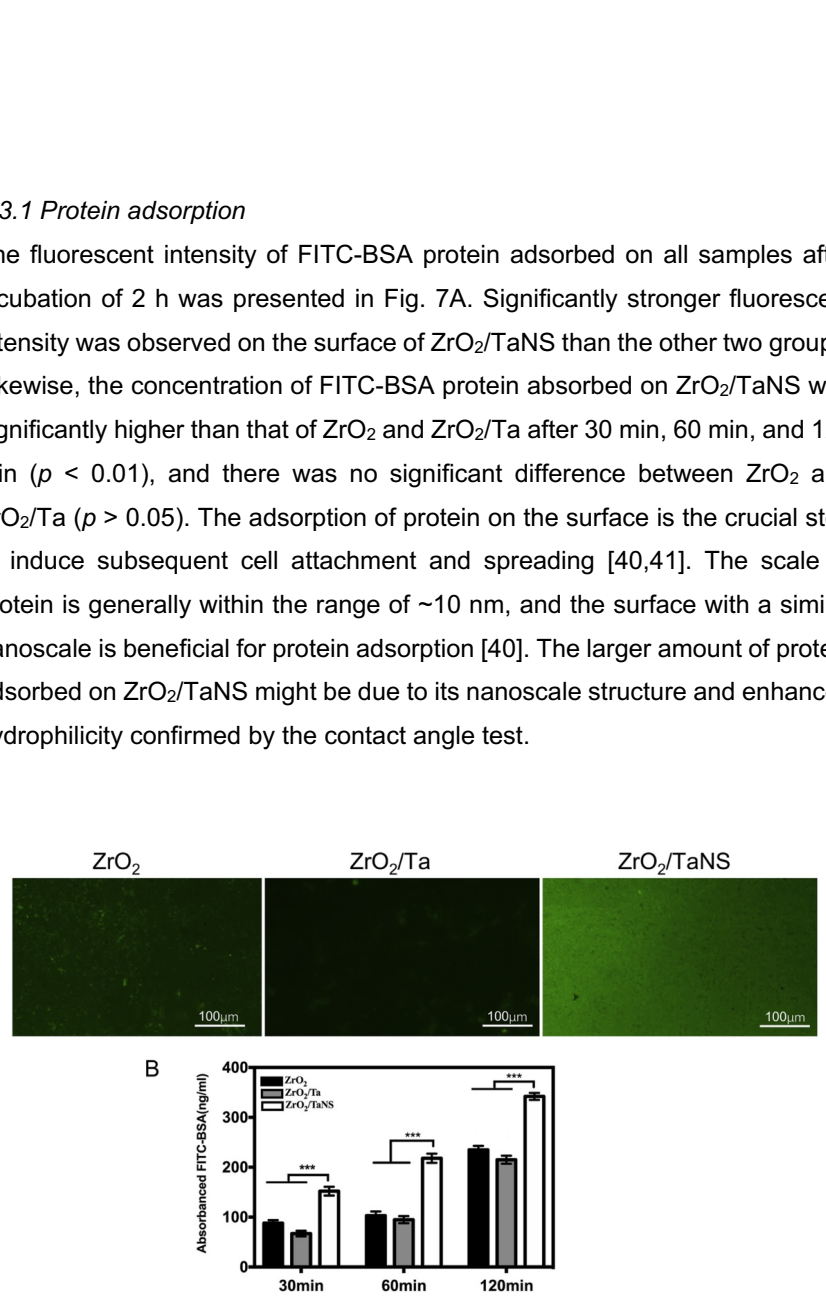

Figure 7. (A) Fluorescent images of FITC-BSA protein in ZrO_2, ZrO_2/Ta, and ZrO_2/TaNS after 120 min. (B) The concentration of FITC-BSA deposited in ZrO_2, ZrO_2/Ta, and ZrO_2/TaNS after 30 min, 60 min, and 120 min. ***$p < 0.001$.

3.3.2 Cell adhesion and morphology

The morphology of adherent MC3T3-E1 cells on different samples after incubation of 6 h, 24 h, and 48 h was shown in Fig. 8A. The cells on ZrO_2 were rounded or oval with fewer filopodia, and appeared to be clumped together, while cells on ZrO_2/Ta spread with more filopodia and cellular junctions. In particular, well-elongated MC3T3-E1 cells with affluent mature filopodia and long pseudopodia were observed on ZrO_2/TaNS, which indicated that TaNS coating can promote MC3T3-E1 cells adhesion and spreading. The initial cell adhesion plays a crucial role in subsequent cell proliferation, differentiation, and mineralization, which profits biomaterials to recruit cells and triggers osteointegration [42]. Well-elongated cells with mature filopodia will lead to cytoskeleton reorganization and changes in nucleus conformation, which induces cell differentiation process by DNA unfolding [43]. Besides, the initial adherent cell number (Fig. 8B) on all samples increased throughout the entire process (6 h, 24 h, and 48 h), the ZrO_2/TaNS had significantly more adherent cells than the other two groups ($p < 0.01$). Similarly, Fig. 8C indicated that the cells spreading area in ZrO_2/TaNS and ZrO_2/Ta was significantly larger compared to that in ZrO_2 (ZrO_2/TaNS > ZrO_2/Ta > ZrO_2) ($p < 0.05$). The explanation might be that the larger surface area and nanoscale features of TaNS coating can induce strong cytoskeletal tension of MC3T3-E1 cells, thus promoting cell spreading and adhesion [44,45]. The study by C.M. Hsu *et al.* reported that the nanoporous structure can enhance intern clustering on the cell membrane, which allows cells to make focal adhesion with the surface of materials [46]. These results above were consistent with the study done by N. Wang *et al*., which reported that small diameters of nanopores can promote osteoblast adhesion [34].

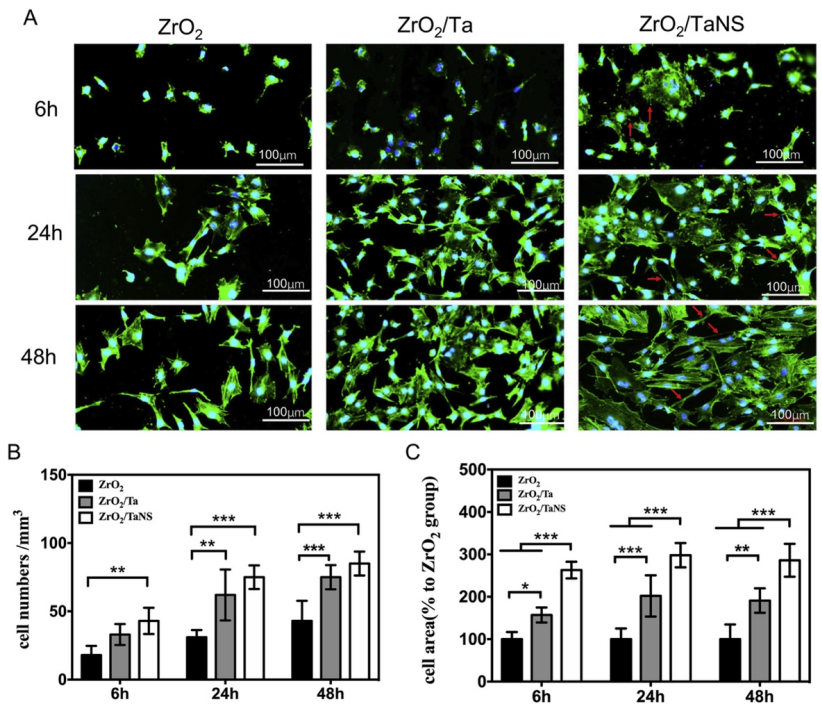

Figure 8. (A) Fluorescent images (phalloidin-FITC in green and DAPI in blue color), and (B, C) Initial adherent number and spreading area of MC3T3-E1 cells in ZrO_2, ZrO_2/Ta and ZrO_2/TaNS after 6 h, 24 h and 48 h. *p < 0.05, **p < 0.01, *** p < 0.001.

3.3.3 Cell proliferation and differentiation

The proliferation of MC3T3-E1 cells cultured on different samples was shown in Fig. 9A, and an increasing tendency was observed over culture time after 1, 3, and 5 days, showing good cell activity on all three groups. The cell proliferation in ZrO_2/Ta and ZrO_2/TaNS was higher than that of ZrO_2, and no significant difference was observed between ZrO_2/Ta and ZrO_2/TaNS at 1, 3, and 5 days. The results indicated that TaNS coating and Ta coating can both prompt MC3T3-E1 cells proliferation, which may be attributed to the effect of Ta. Studies reported that Ta nanotube formed by anodization can improve

osteoblast proliferation and differentiation [47]. Hao Zhu *et al.* also found polyetheretherketone (PEEK) with different content of Ta nanoparticles (1%wt-9%wt) could improve cell proliferation [48]. The ALP is a marker for osteogenic differentiation, which is highly activated in the early stage [49]. Fig. 9B indicated that ZrO_2/TaNS showed considerably higher ALP activity as compared to the other two groups, and there was no significant difference between ZrO_2 and ZrO_2/Ta after 7 days of incubation. After 14 days of culture, cells on ZrO_2/TaNS and ZrO_2/Ta displayed significantly higher ALP activity than that of ZrO_2 (ZrO_2/TaNS > ZrO_2/Ta > ZrO_2) (p < 0.05). The results indicated that TaNS coating and Ta coating can prompt early osteogenic differentiation of MC3T3-E1 cells by improving ALP activity. The mineralization is gradually increased after 14 and 21 days of incubation, which is regarded as a marker of late osteogenic differentiation [50]. Fig. 9C showed that a significantly larger amount of mineralization in ZrO_2/TaNS was detected than that of the other two groups after 14 days and 21 days (ZrO_2/TaNS > ZrO_2/Ta > ZrO_2), which suggested that TaNS coating induces more mineralization. Our results were consistent with previous studies [51,52]. They reported that cells can response to the shape of the surface and the nanoporous array, which might be beneficial for cell differentiation and mineralization.

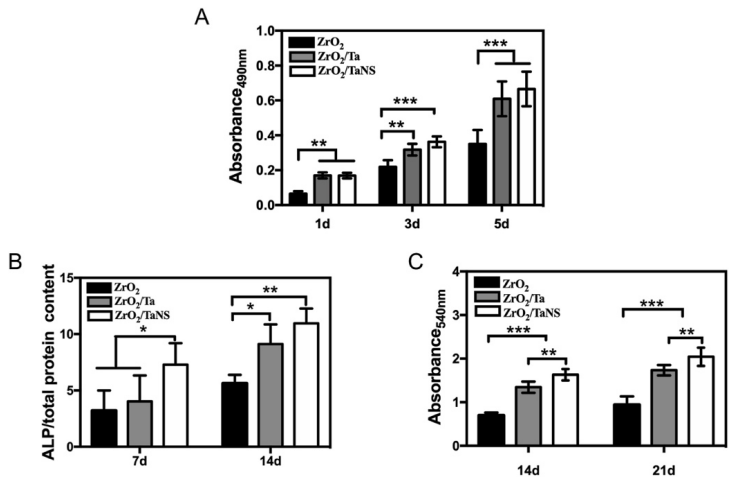

Figure 9. (A) The proliferation of MC3T3-E1 cells after incubation of 1, 3, and 5 days. (B) The ALP activity of MC3T3-E1 cells on various surfaces for 7 and 14 days. (C)The quantitative detection of mineralization in ZrO_2, ZrO_2/Ta, and ZrO_2/TaNS after 14 and 21 days. *$p < 0.05$, **$p < 0.01$, ***$p < 0.001$.

3.3.4 Osteogenic-related gene expressions

The expression of osteogenic-related genes (RUNX2, ALP, COL-1, OSX, OCN, and OPG) in all groups was evaluated by RT-PCR assays at 14 days (Fig. 10). After 14 days of incubation, these osteogenic-related markers were the highest in ZrO_2/TaNS surface among the three groups, followed by ZrO_2/Ta and ZrO_2 in order. RUNX2 is a transcription factor that regulates the expression of other osteogenic-related genes such as ALP, OCL-I, OCN, and OSX [53]. In our study, RUNX2 expressed in ZrO_2/TaNS was 3.6-, and 1.7- fold higher than ZrO_2 and ZrO_2/Ta on day 14, respectively. The expression of ALP in ZrO_2/TaNS was 3.14- and 1.4- fold higher as compared to ZrO_2 and ZrO_2/Ta, respectively. Likewise, COL-1 showed 70% increased expression in ZrO_2/TaNS as compared to ZrO_2, and a similar increase was observed in ZrO_2/Ta, with 1.9-fold higher than ZrO_2. The higher expression of the ALP gene can promote more pre-osteoblasts to differentiate into osteoblast lineage, and COL-I is essential for mineralization [54]. These results indicate that TaNS coating can extensively improve early osteogenic differentiation. OSX is a zinc finger transcription factor that directs pre-osteoblasts to differentiate into mature osteoblasts [55]. OCN is a major non-collagenous protein of extracellular matrix synthesized by mature osteoblasts [56]. The expression of OCN and OSX in ZrO_2/Ta and ZrO_2 had no significant difference, but ZrO_2/TaNS presented the highest expression among the three groups, which means that TaNS coating can enhance early differentiation and matrix protein production. OPG/RANKL/RANK system in osteoclast is a crucial pathway to regulate bone metabolism, and OPG can block bone resorption by inhibiting the maturation of osteoclasts [57]. OPG expression in ZrO_2/TaNS displayed a 71% increase in relation to ZrO_2, which demonstrated that TaNS coating can stimulate the synthesis of bone tissue by inhibiting the activity of osteoclasts. These findings were consistent with the results for ALP activity and ARS staining analysis,

suggesting that the TaNS coating can robustly stimulate MC3T3-E1 cells differentiation and mineralization.

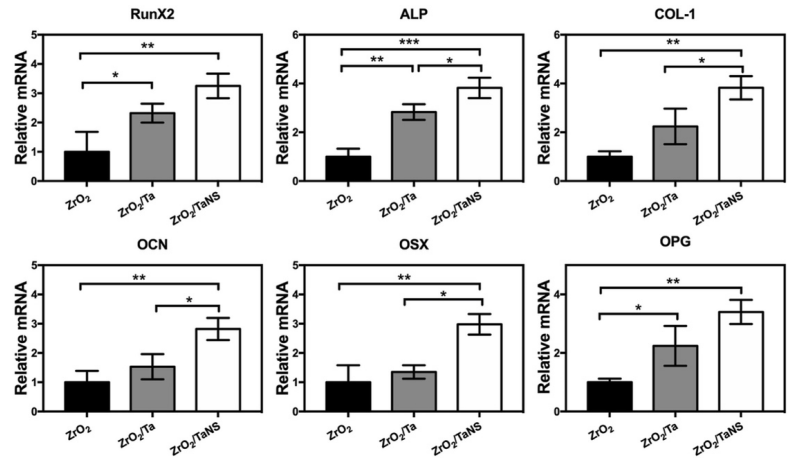

Figure 10. ZrO_2/TaNS enhanced osteogenic-related gene expression. Real-time PCR analysis: The expression of RUNX2, ALP, COL-1, OSX, OCN, and OPG in different surfaces after incubation for 14 days. *$p < 0.05$, **$p < 0.01$, ***$p < 0.001$.

3.3.5 Histological analysis

The histological analysis is the gold standard for the evaluation of implant osteointegration [58]. The histological sections with methylene blue and fuchsin staining for 4 weeks and 8 weeks of all three groups with zoomed images were shown in Fig. 11A, B. The calcified bone was stained with bright pink, and the blue staining represented osteoblast or osteoid tissue. After 4 weeks and 8 weeks, more new bone tissue (red arrow) was observed around the ZrO_2/TaNS implant as compared to ZrO_2/Ta and ZrO_2. Moreover, bright pink staining around ZrO_2/Ta implant was more than that of ZrO_2, and osteoblasts and osteoid attached around most areas of the ZrO_2 implants. Fig. 12 shows the BIC% in ZrO_2/TaNS (38.93% ± 0.78%) was the highest among the three groups, and ZrO_2/Ta (24.83% ± 0.21%) exhibited higher BIC% than ZrO_2 (9.33% ±

0.73%) after 4 weeks. Similarly, BIC% in ZrO_2/TaNS (65.27% ± 3.10%) was 2.29- and 1.32- fold higher compared to ZrO_2 (28.47% ± 1.45%) and ZrO_2/Ta (49.53% ± 1.56%) after 8 weeks. Results from the histological analysis show that more bone tissue and enhanced BIC% were observed around ZrO_2/Ta surface than ZrO_2 at 4 and 8 weeks, suggesting that Ta coating might induce bone formation. The results are similar to the study by Liang-Yu Shi *et al.*, which reported that Ta coating can enhance the osteointegration of Ti implants [59]. In particular, the ZrO_2/TaNS presented the most bone tissue and highest BIC% among the three groups at 4 and 8 weeks. Our *in vivo* results indicated that TaNS coating might robustly enhance the early osteointegration of zirconia implants [60]. However, this conclusion needs to be checked up with a larger sample size *in vivo* test, and the underlying mechanisms responsible for the effect of TaNS coating on osteointegration remain to be further studied.

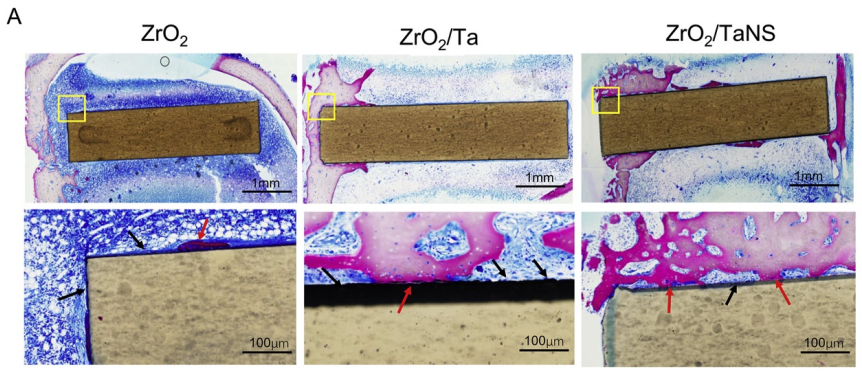

Figure 11. Histological analysis of three different implants after 4 weeks (A) and 8 weeks (B). New bone tissue formation around implant (Red arrows) and osteoblast or osteoid tissue (Black arrows).

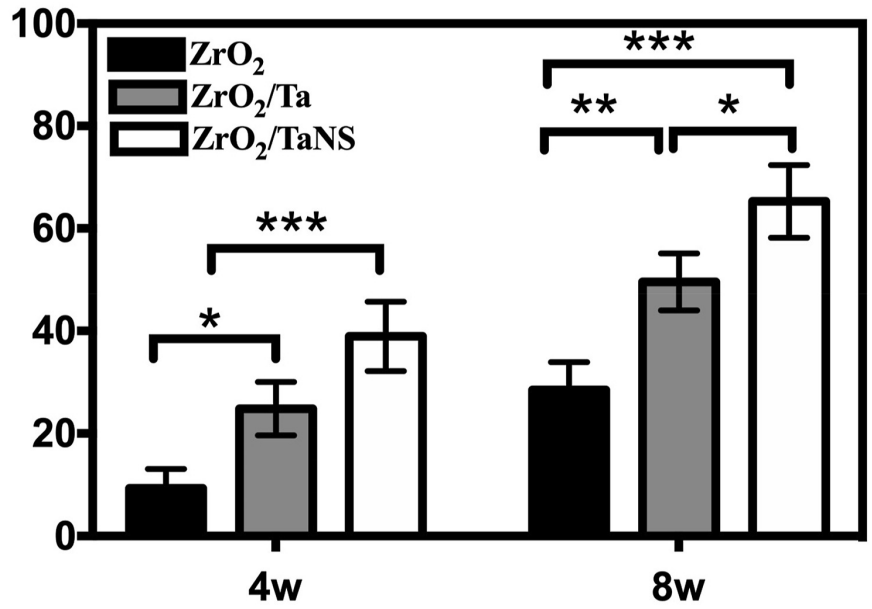

Figure 12. The percentage of the bone-implant contact of ZrO_2, ZrO_2/Ta, and ZrO_2/TaNS after 4 weeks and 8 weeks (n = 6). *p < 0.05, **p < 0.01, ***p < 0.001.

4. Conclusion

In this work, we developed a novel surface coating via magnetron sputtering and anodization to enhance the bioactivity of zirconia surface. Results from our study showed that the TaNS coating can modulate MC3T3-E1 cells attachment, proliferation, osteogenic differentiation, and mineralization by up-regulating osteogenic-related gene expressions. Moreover, the animal experiment also showed that the TaNS coating can induce more bone tissue around zirconia implants. *In vitro* and *vivo* findings in our study indicated the nanoporous Ta-coated zirconia implants can improve early osteointegration of the zirconia implant and will be a promising biomaterial for clinical application.

Declaration of competing interest

The authors declare that they have no known competing financial interests or personal relationships that could have appeared to influence the work reported in this paper.

Acknowledgments

This work was financially supported by National Natural Science Foundation of China (81870810, 31700827, and 81701016), Major Science and Technology Development Program of Wenzhou of China (ZY2019009), Scientific Research of Zhejiang Provincial Education Department (Y201839924), and Wenzhou Municipal Science and Technology Project for Public Welfare (2017Y0308).

References

[1] J. Han, J. Zhao, Z. Shen, Zirconia ceramics in metal-free implant dentistry. Advances in Applied Ceramics. 116 (2017) 138–150. https://doi.org/10.1080/17436753.2016.1264537.

[2] N.P.J. de Graaf, A.J. Feilzer, C.J. Kleverlaan, H. Bontkes, S. Gibbs, T. Rustemeyer, A retrospective study on titanium sensitivity: Patch test materials and manifestations. Contact Dermatitis. 79 (2018) 85–90. https://doi.org/10.1111/cod.13010.

[3] K. Sivaraman, A. Chopra, A.I. Narayan, D. Balakrishnan, Is zirconia a viable alternative to titanium for oral implant? A critical review. Journal of Prosthodontic Research. 62 (2018) 121–133. https://doi.org/10.1016/j.jpor.2017.07.003.

[4] D.D. Bosshardt, V. Chappuis, D. Buser, Osseointegration of titanium, titanium alloy and zirconia dental implants: Current knowledge and open questions. Periodontology 2000. 73 (2017) 22–40. https://doi.org/10.1111/prd.12179.

[5] S. Pieralli, R.J. Kohal, E. Lopez Hernandez, S. Doerken, B.C. Spies, Osseointegration of zirconia dental implants in animal investigations: A systematic review and meta-analysis. Dental Materials. 34 (2018) 171–182. https://doi.org/10.1016/j.dental.2017.10.008.

[6] S. Roehling, K.A. Schlegel, H. Woelfler, M. Gahlert, Zirconia compared to titanium dental implants in preclinical studies—a systematic review and meta-analysis. Clinical Oral Implants Research. 30 (2019) 365–395. https://doi.org/10.1111/clr.13425.

[7] J. Moritz, A. Abram, M. Čekada, U. Gabor, M. Garvas, I. Zdovc, A. Dakskobler, J. Cotič, K. Ivičak-Kocjan, A. Kocjan, Nanoroughening of sandblasted 3Y-TZP surface by alumina coating deposition for improved osseointegration and bacteria reduction. Journal of the European Ceramic Society. 39 (2019) 4347-4357. https://doi.org/10.1016/j.jeurceramsoc.2019.05.051.

[8] G. Soon, B. Pingguan-Murphy, K.W. Lai, S.A. Akbar, Review of zirconia-based bioceramic: Surface modification and cellular response. Ceramics International. 42 (2016) 12543–12555. https://doi.org/10.1016/j.ceramint.2016.05.077.

[9] V.V. Divya Rani, L. Vinoth-Kumar, V.C. Anitha, K. Manzoor, M. Deepthy, V.N. Shantikumar, Osteointegration of titanium implant is sensitive to specific nanostructure morphology. Acta Biomaterialia. 8 (2012) 1976–1989. https://doi.org/10.1016/j.actbio.2012.01.021.

[10] J. Liu, J.L. Pathak, X. Hu, Y. Jin, Z. Wu, M.A. Al-Baadani, S. Wu, H. Zhang, S. Farkasdi, Y. Liu, J. Ma, G. Wu, Sustained release of zoledronic acid from mesoporous TiO2-layered implant enhances implant osseointegration in osteoporotic condition. Journal of Biomedical Nanotechnology. 14 (2018) 1965–1978. https://doi.org/10.1166/jbn.2018.2635.

[11] M. Heiden, S. Huang, E. Nauman, D. Johnson, L. Stanciu, Nanoporous metals for biodegradable implants: Initial bone mesenchymal stem cell adhesion and degradation behavior. Journal of Biomedical Materials Research-Part A. 104 (2016) 1747–1758. https://doi.org/10.1002/jbm.a.35707.

[12] M.N. Aboushelib, E. Osman, I. Jansen, V. Everts, A.J. Feilzer, Influence of a nanoporous zirconia implant surface of on cell viability of human osteoblasts. Journal of Prosthodontics. 22 (2013) 190–195. https://doi.org/10.1111/j.1532-849X.2012.00920.x.

[13] J. Park, S. Bauer, K.A. Schlegel, F.W. Neukam, K. der von Mark, P. Schmuki, TiO2 nanotube surfaces: 15 nm-an optimal length scale of surface topography for cell adhesion and differentiation. Small. 5 (2009) 666–671. https://doi.org/10.1002/smll.200801476.

[14] F.H. Schünemann, M.E. Galárraga-Vinueza, R. Magini, M. Fredel, F. Silva, J.C.M. Souza, Y. Zhang, B. Henriques, Zirconia surface modifications for implant dentistry. Materials Science and Engineering C. 98 (2019) 1294–1305. https://doi.org/10.1016/j.msec.2019.01.062.

[15] Y. Liu, C. Bao, D. Wismeijer, G. Wu, The physicochemical/biological properties of porous tantalum and the potential surface modification techniques to improve its clinical application in dental implantology. Materials Science and Engineering: C. 49 (2015) 323–329. https://doi.org/10.1016/J.MSEC.2015.01.007.

[16] J.W. Lee, H.B. Wen, P. Gubbi, G.E. Romanos, New bone formation and trabecular bone microarchitecture of highly porous tantalum compared to titanium implant threads: A pilot canine study. Clinical Oral Implants Research. 29 (2018) 164–174. https://doi.org/10.1111/clr.13074.

[17] B.R. Levine, S. Sporer, R.A. Poggie, C.J. della Valle, J.J. Jacobs, Experimental and clinical performance of porous tantalum in orthopedic surgery. Biomaterials. 27 (2006) 4671–4681. https://doi.org/10.1016/j.biomaterials.2006.04.041.

[18] Q. Wang, H. Zhang, H. Gan, H. Wang, Q. Li, Z. Wang, Application of combined porous tantalum scaffolds loaded with bone morphogenetic protein 7 to repair of osteochondral defect in rabbits. International Orthopaedics. 42 (2018) 1437–1448. https://doi.org/10.1007/s00264-018-3800-7.

[19] D. Fraser, G. Mendonca, E. Sartori, P. Funkenbusch, C. Ercoli, L. Meirelles, Bone response to porous tantalum implants in a gap-healing model. Clinical Oral Implants Research. 30 (2019) 156–168. https://doi.org/10.1111/clr.13402.

[20] C.J. Frandsen, K.S. Brammer, K. Noh, G. Johnston, S. Jin, Tantalum coating on TiO2 nanotubes induces superior rate of matrix mineralization and osteofunctionality in human osteoblasts. Materials Science and Engineering C. 37 (2014) 332–341. https://doi.org/10.1016/j.msec.2014.01.014.

[21] R. Zhou, D. Wei, J. Cao, W. Feng, S. Cheng, Q. Du, B. Li, Y. Wang, D. Jia, Y. Zhou, Synergistic effects of surface chemistry and topologic structure from modified microarc oxidation coatings on Ti implants for improving osseointegration. ACS Applied Materials and Interfaces. 7 (2015) 8932–8941. https://doi.org/10.1021/acsami.5b02226.

[22] V.K. Balla, S. Bodhak, S. Bose, A. Bandyopadhyay, Porous tantalum structures for bone implants: Fabrication, mechanical and in vitro biological properties. Acta Biomaterialia. 6 (2010) 3349–3359. https://doi.org/10.1016/j.actbio.2010.01.046.

[23] M. Sarraf, B. Abdul Razak, A. Dabbagh, B. Nasiri-Tabrizi, N.H. Abu Kasim, W.J. Basirun, Optimizing PVD conditions for electrochemical anodization growth of well-adherent Ta2O5 nanotubes on Ti-6Al-4V alloy. RSC Advances. 6 (2016) 78999–79015. https://doi.org/10.1039/c6ra11290k.

[24] Z. Ding, Q. He, Z. Ding, C. Liao, D. Chen, L. Ou, Fabrication and performance of ZnO doped tantalum oxide multilayer composite coatings on Ti6Al4V for orthopedic application. Nanomaterials. 9 (2019) 685. https://doi.org/10.3390/nano9050685.

[25] H. Sun, S.S. Lin, K.L. Wang, Q. Shi, S.M. Song, Y.Q. Xin, T.L. Yang, X.Y. Zheng, W.X. Wang, Z.M. Yue, Influence of power frequency on the performance of SiC thin films deposited by pulsed DC magnetron sputtering. Journal of Adhesion Science and Technology. 33 (2019) 2181–2190. https://doi.org/10.1080/01694243.2019.1639885.

[26] H.A. El-Sayed, C.A. Horwood, A.D. Abhayawardhana, V.I. Birss, New insights into the initial stages of Ta oxide nanotube formation on polycrystalline Ta electrodes. Nanoscale. 5 (2013) 1494–1498. https://doi.org/10.1039/c3nr33396e.

[27] S. Minagar, C.C. Berndt, J. Wang, E. Ivanova, C. Wen, A review of the application of anodization for the fabrication of nanotubes on metal implant surfaces. Acta Biomaterialia. 8 (2012) 2875–2888. https://doi.org/10.1016/j.actbio.2012.04.005.

[28] S.B. Patel, N. Baker, I. Marques, A. Hamlekhan, M.T. Mathew, C. Takoudis, C. Friedrich, C. Sukotjo, T. Shokuhfar, Transparent TiO2 nanotubes on zirconia for biomedical applications. RSC Advances. 7 (2017) 30397–30410. https://doi.org/10.1039/c7ra03940a.

[29] H.A. El-Sayed, V.I. Birss, Controlled growth and monitoring of tantalum oxide nanostructures. Nanoscale. 2 (2010) 793–798. https://doi.org/10.1039/c0nr00011f.

[30] C.A. Horwood, H.A. El-Sayed, V.I. Birss, Precise electrochemical prediction of short tantalum oxide nanotube length. Electrochimica Acta. 132 (2014) 91–97. https://doi.org/10.1016/j.electacta.2014.03.128.

[31] J. Ma, Y. Sun, R. Zan, J. Ni, X. Zhang, Cellular different responses to different nanotube inner diameter on surface of pure tantalum. Materials Science and Engineering C. 109 (2020) 110520. https://doi.org/10.1016/j.msec.2019.110520.

[32] C.F. Almeida Alves, V.S. Calderon, P.J. Ferreira, L. Marques, S. Carvalho, Passivation and dissolution mechanisms in ordered anodic tantalum oxide nanostructures. Applied Surface Science. 513 (2020) 145575. https://doi.org/10.1016/j.apsusc.2020.145575.

[33] R.A. Silva, I.P. Silva, B. Rondot, Effect of surface treatments on anodic oxide film growth and electrochemical properties of tantalum used for biomedical applications. Journal of Biomaterials Applications. 21 (2006) 93–103. https://doi.org/10.1177/0885328206056378.

[34] N. Wang, H. Li, J. Wang, S. Chen, Y. Ma, Z. Zhang, Study on the anticorrosion, biocompatibility, and osteoinductivity of tantalum decorated with tantalum oxide nanotube array films. ACS Applied Materials and Interfaces. 4 (2012) 4516–4523. https://doi.org/10.1021/am300727v.

[35] A. Arsiwala, P. Desai, V. Patravale, Recent advances in micro/nanoscale biomedical implants. Journal of Controlled Release. 189 (2014) 25–45. https://doi.org/10.1016/j.jconrel.2014.06.021.

[36] X. Gou, Z. Guo, Surface topographies of biomimetic superamphiphobic materials: design criteria, fabrication and performance. Advances in Colloid and Interface Science. 269 (2019) 87–121. https://doi.org/10.1016/j.cis.2019.04.007.

[37] F. Rupp, L. Scheideier, N. Olshanska, M. de Wild, M. Wieland, J. Geis-Gerstorfer, Enhancing surface free energy and hydrophilicity through chemical modification of microstructured titanium implant surfaces. Journal of Biomedical Materials Research - Part A. 76 (2006) 323–334. https://doi.org/10.1002/jbm.a.30518.

[38] D.H. Shin, T. Shokuhfar, C.K. Choi, S.H. Lee, C. Friedrich, Wettability changes of TiO2 nanotube surfaces. Nanotechnology. 22 (2011) 315704. https://doi.org/10.1088/0957-4484/22/31/315704.

[39] Z. Du, Y. Xiao, S. Hashimi, S.M. Hamlet, S. Ivanovski, The effects of implant topography on osseointegration under estrogen deficiency induced osteoporotic conditions: Histomorphometric, transcriptional and ultrastructural analysis. Acta Biomaterialia. 42 (2016) 351–363. https://doi.org/10.1016/j.actbio.2016.06.035.

[40] O.E. Ogle, Implant surface material, design, and osseointegration. Dental Clinics of North America. 59 (2015) 505–520. https://doi.org/10.1016/j.cden.2014.12.003.

[41] R. Huntley, E. Jensen, R. Gopalakrishnan, K.C. Mansky, Bone morphogenetic proteins: Their role in regulating osteoclast differentiation. Bone Reports. 10 (2019) 100207. https://doi.org/10.1016/j.bonr.2019.100207.

[42] W.M.S. al Qahtani, C. Schille, S. Spintzyk, M.S.A. al Qahtani, E. Engel, J. Geis-Gerstorfer, F. Rupp, L. Scheideler, Effect of surface modification of zirconia on cell adhesion, metabolic activity and proliferation of human osteoblasts. Biomedizinische Technik. 62 (2017) 75–87. https://doi.org/10.1515/bmt-2015-0139.

[43] Y. Li, Y. Qi, Q. Gao, Q. Niu, M. Shen, Q. Fu, K. Hu, L. Kong, Effects of a micro/nano rough strontium-loaded surface on osseointegration. International Journal of Nanomedicine. 10 (2015) 4549–4563. https://doi.org/10.2147/IJN.S84398.

[44] N. Gui, W. Xu, D.E. Myers, R. Shukla, H.P. Tang, M. Qian, The effect of ordered and partially ordered surface topography on bone cell responses: A review. Biomaterials Science. 6 (2018) 250–264. https://doi.org/10.1039/c7bm01016h.

[45] J. Zhou, X. Zhang, J. Sun, Z. Dang, J. Li, X. Li, T. Chen, The effects of surface topography of nanostructure arrays on cell adhesion. Physical Chemistry Chemical Physics. 20 (2018) 22946–22951. https://doi.org/10.1039/C8CP03538E.

[46] D. Guadarrama Bello, A. Fouillen, A. Badia, A. Nanci, A nanoporous titanium surface promotes the maturation of focal adhesions and formation of filopodia with distinctive nanoscale protrusions by osteogenic cells. Acta Biomaterialia. 60 (2017) 339–349. https://doi.org/10.1016/j.actbio.2017.07.022.

[47] K.S. Brammer, S. Oh, C.J. Cobb, L.M. Bjursten, H. van der Heyde, S. Jin, Improved bone-forming functionality on diameter-controlled TiO2 nanotube surface. Acta Biomaterialia. 5 (2009) 3215–3223. https://doi.org/10.1016/j.actbio.2009.05.008.

[48] A. Aminian, B. Shirzadi, Z. Azizi, K. Maedler, E. Volkmann, N. Hildebrand, M. Maas, L. Treccani, K. Rezwan, Enhanced cell adhesion on bioinert ceramics mediated by the osteogenic cell membrane enzyme alkaline phosphatase. Materials Science and Engineering C. 69 (2016) 184–194. https://doi.org/10.1016/j.msec.2016.06.056.

[49] R. Fraioli, K. Dashnyam, J.H. Kim, R.A. Perez, H.W. Kim, J. Gil, M.P. Ginebra, J.M. Manero, C. Mas-Moruno, Surface guidance of stem cell behavior: Chemically tailored co-presentation of integrin-binding peptides stimulates osteogenic differentiation in vitro and bone formation in vivo. Acta Biomaterialia. 43 (2016) 269–281. https://doi.org/10.1016/j.actbio.2016.07.049.

[50] R.P. Ocaña, G.D. Rabelo, L.M. Sassi, V.P. Rodrigues, F.A. Alves, Implant osseointegration in irradiated bone: An experimental study. Journal of Periodontal Research. 52 (2017) 505–511. https://doi.org/10.1111/jre.12416.

[51] M. Lai, K. Cai, Y. Hu, X. Yang, Q. Liu, Regulation of the behaviors of mesenchymal stem cells by surface nanostructured titanium. Colloids and Surfaces B: Biointerfaces. 97 (2012) 211–220. https://doi.org/10.1016/j.colsurfb.2012.04.029.

[52] A.T. Sverzut, G.E. Crippa, M. Morra, P.T. de Oliveira, M.M. Beloti, A.L. Rosa, Effects of type I collagen coating on titanium osseointegration: Histomorphometric, cellular and molecular analyses. Biomedical Materials. 7 (2012) 035007. https://doi.org/10.1088/1748-6041/7/3/035007.

[53] G. Dai, W. Wan, J. Chen, J. Wu, X. Shuai, Y. Wang, Enhanced osteogenic differentiation of MC3T3-E1 on rhBMP-2 immobilized titanium surface through polymer-mediated electrostatic interaction. Applied Surface Science. 471 (2019) 986–998. https://doi.org/10.1016/j.apsusc.2018.11.243.

[54] K. Hata, K. Ikebe, M. Wada, T. Nokubi, Osteoblast response to titanium regulates transcriptional activity of Runx2 through MAPK pathway. Journal of Biomedical Materials Research-Part A. 81 (2007) 446–452. https://doi.org/10.1002/jbm.a.31086.

[55] Y. Liu, J. Hu, B. Liu, X. Jiang, Y. Li, The effect of osteoprotegerin on implant osseointegration in ovariectomized rats. Archives of Medical Science. 13 (2017) 489–495. https://doi.org/10.5114/aoms.2017.65468.

[56] C.M. Stanford, J.C. Keller, The concept of osseointegration and bone matrix expression. Critical Reviews in Oral Biology and Medicine. 2 (1991) 83–101. https://doi.org/10.1177/10454411910020010601.

[57] M. Lennerås, A. Palmquist, B. Norlindh, L. Emanuelsson, P. Thomsen, O. Omar, Oxidized titanium implants enhance osseointegration via mechanisms involving RANK/RANKL/OPG regulation. Clinical Implant Dentistry and Related Research. 17 (2015) e486–e500. https://doi.org/10.1111/cid.12276.

[58] J.L. Calvo-Guirado, M. Satorres-Nieto, A. Aguilar-Salvatierra, R.A. Delgado-Ruiz, J.E. Maté-Sánchez de Val, J. Gargallo-Albiol, G. Gómez-Moreno, G.E. Romanos, Influence of surface treatment on osseointegration of dental implants: histological, histomorphometric and radiological analysis in vivo. Clinical Oral Investigations. 19 (2015) 509–517. https://doi.org/10.1007/s00784-018-2763-9.

[59] L.Y. Shi, A. Wang, F.Z. Zang, J.X. Wang, X.W. Pan, H.J. Chen, Tantalum-coated pedicle screws enhance implant integration. Colloids and Surfaces B: Biointerfaces. 160 (2017) 22–32. https://doi.org/10.1016/j.colsurfb.2017.08.059.

[60] A. Bandyopadhyay, I. Mitra, A. Shivaram, N. Dasgupta, S. Bose, Direct comparison of additively manufactured porous titanium and tantalum implants towards in vivo osseointegration. Additive Manufacturing. 28 (2019) 259–266. https://doi.org/10.1016/j.addma.2019.04.025.

CHAPTER THREE

pH dependent silver nanoparticles releasing titanium implant: A novel therapeutic approach to control peri-implant infection.

Yiwen Dong[1, 2, *], Hui Ye[3, *], Yi Liu[2, *], Lihua Xu[4], Zuosu Wu[1], Xiaohui Hu[1], Jianfeng Ma[1], Janak L. Pathak[5], Jinsong Liu[1], Gang Wu[2]

[1] School and Hospital of Stomatology, Wenzhou Medical University, Wenzhou, China

[2] Department of Oral Implantology and Prosthetic Dentistry, Academic Centre for Dentistry Amsterdam (ACTA), Research Institute MOVE, VU University and University of Amsterdam, Amsterdam, The Netherlands

[3] School of Basic Medical Science, Wenzhou Medical University, China

[4] General Medicine Department, First Affiliated Hospital, Wenzhou Medical University, Wenzhou, China

[5] School of Pharmaceutical Science and Technology, Health Sciences Platform, Tianjin University, Tianjin, China

[*] Shared first authorship

Colloids and Surfaces B: Biointerfaces. 158 (2017) 127–136.

Abstract

Peri-implant infection control is crucial for implant fixation and durability. Antimicrobial administration approaches to control peri-implant infection are far from satisfactory. During bacterial infection, the pH level around the peri-implant surface decreases as low as pH 5.5. This change of pH can be used as a switch to control antimicrobial drug release from the implant surface. Silver nanoparticles (AgNPs) have broad-spectrum antimicrobial properties. In this study, we aimed to design a pH-dependent AgNPs releasing titania nanotube arrays (TNT) implant for peri-implant infection control. The nanotube arrays were fabricated on the surface of titanium implant as containers; AgNPs were grafted on TNT implant surface via a low pH-sensitive acetal linker (TNT-AL-AgNPs). SEM, TEM, AFM, FTIR as well as XPS data showed that AgNPs have been successfully linked to TNT via acetal linker without affecting the physicochemical characteristics of TNT. The pH 5.5 enhanced AgNPs release from TNT-AL-AgNPs implant compared with pH 7.4. AgNPs released at pH 5.5 robustly increased antimicrobial activities against gram-positive and gram-negative bacteria compared with AgNPs released at pH 7.4. TNT-AL-AgNPs implant enhanced osteoblast proliferation, differentiation, and did not affect osteoblast morphology *in vitro*. In conclusion, the incorporation of AgNPs in TNT via acetal linker maintained the surface characteristics of TNT. TNT-AL-AgNPs implant was biocompatible to osteoblasts and showed pro-osteogenic properties. AgNPs were released from TNT-AL-AgNPs implant in high doses at pH 5.5, and this release showed strong antimicrobial properties *in vitro*. Therefore, this novel design of low pH-triggered AgNPs releasing TNT-AL-AgNPs could be an infection-triggered antimicrobial releasing implant model to control peri-implant infection.

Keywords: Peri-implant infection; pH-dependent drug release; Silver nanoparticles; Antibacterial properties; Titanium implant; Titania nanotube arrays

Graphical abstract

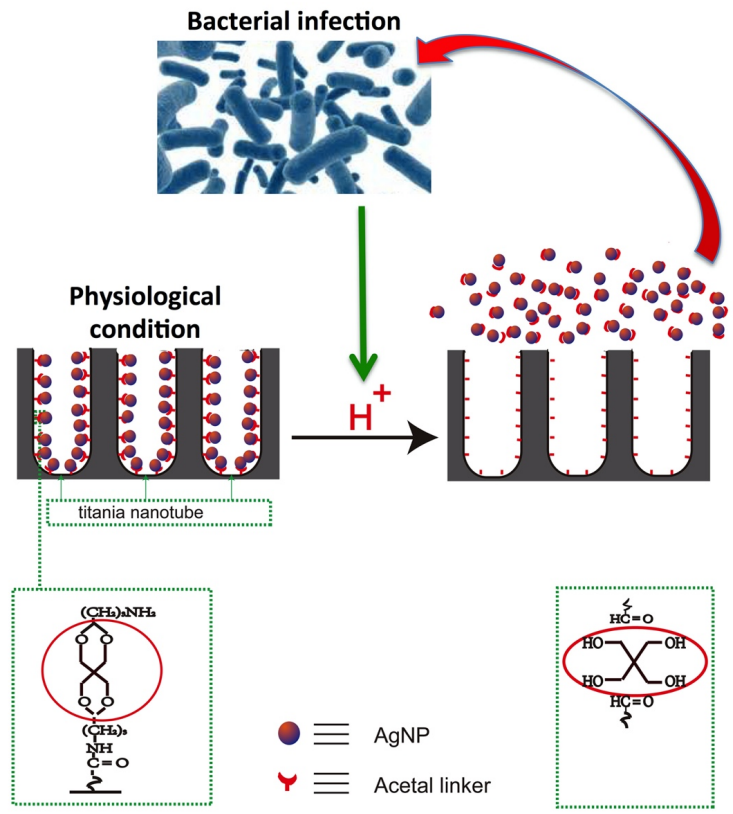

1. Introduction

Titanium (Ti) implants have been used in clinic for decades as dental and endo-osseous implants [1–5]. Peri-implant infection is still a major challenge for proper implant fixation and durability [6–9]. Dental or endo-osseous implants can be infected by local or systemic infection. Bacterial infection on implants extends rapidly into bone marrow, which accelerates bone loss, and causes implant failure [10–13]. Therapeutic approaches such as disinfection of implant and implantation site, stringent aseptic surgical protocols, antimicrobial agents coated on implant surface, and postoperative systemic antibiotic administration are frequently used to prevent postoperative peri-implant infection [14]. However, the effectiveness of such therapeutic approaches in the prevention of peri-implant infection is far from satisfactory. Conventional antibacterial treatment methods such as oral medication or systematic administration cannot control peri-implant infection since rapidly formed biofilm blocks drug penetration to the infection site [15,16]. Implants are at constant risk of infection by a variety of bacterial species from early days to years later of implantation [8,9,17]. Antimicrobials applied locally or adsorbed on implant surfaces cannot sustain for long periods due to burst release [15,18,19]. Therefore, antibacterial directly loaded on implants or biodegradable polymer can only treat peri-implant infection in the early days of implantation. Antimicrobial-loaded implants give uncontrolled drug release with inappropriate doses which increases the risk of antimicrobial resistance [20]. Therefore, novel approaches of loading broad-spectrum antimicrobial agents on implant surfaces that can store antimicrobial agents for long periods of time and release them only during the infection are desperately needed.

The special tunable pore structure and large surface area of the TNT not only enhance implant osteointegration but also provide a reservoir for a high amount of antimicrobial drugs [21,22]. Physicochemical properties of TNT affect osteogenic cell adhesion on implant, proliferation of those cells, and implant osteointegration [21,22]. Therefore, implant surface modification of nanotube arrays and/or antimicrobial incorporation should maintain the physicochemical properties of the implants. Drug-release duration of the super-hydrophilic TNT is still limited to a few weeks, which is still not sufficient to control peri-implant infection during the late stage of implantation [23]. Therefore, drug loading approaches, which can store the antimicrobial on TNT surface, and release only during infection could be an ideal approach to control infections in long term.

Under physiological conditions, the pH level around the implant surface is 7.4. During bacterial infection, the pH level around the implant surface goes as low as 5.5 [24]. This effect of bacterial infection on pH level can be used as a switch to trigger antimicrobial release from the implant surface [25,26]. For this purpose, a low pH-liable acetal linker (AL) has been previously used to incorporate drugs in biomaterials [25]. Silver has a broad-spectrum antimicrobial property at low concentrations [27–29]. AgNPs loading on biomaterial surfaces shows sustained silver-releasing ability, broad-spectrum antimicrobial properties, and biocompatibility with mammalian cells [30–32]. Therefore, AgNPs loading on TNT via pH-sensitive AL can be a novel implant design that triggers silver release in high doses during bacterial infection to control peri-implant infection.

In this study, we aimed to design a low pH-triggered silver-releasing TNT-AL-AgNPs implant to control peri-implant infection. We developed TNT with novel surface modification and anchored AgNPs into the inner wall of TNT via low pH-sensitive AL. We characterized the physicochemical properties of TNT-AL-AgNPs, analyzed a pH-dependent release of AgNPs from TNT-AL-AgNPs, and tested the antibacterial efficiency of the released AgNPs. Furthermore, we evaluated the biocompatibility of TNT-AL-AgNPs, as well as its effect on osteoblast morphology and differentiation *in vitro*.

2. Materials and methods

2.1. TNT preparation

Pure Ti foils (PT, Advent research materials, England, 20 × 20 × 0.25 mm^3) were polished by silicate-carbon sandpapers, ultrasonically cleaned with acetone (AR, Aladdin, Shanghai, China) and deionized water sequentially. Electrochemical anodization of Ti was carried out in a conventional two-electrode cell with Ti foil as the anode and Pt foil as the cathode. The distance between the two electrodes was 1 cm. Glycerin with 0.5% (w/v) ammonium fluoride (NH_4F, AR, Aladdin, Shanghai, China) in 10% (v/v) distilled water was used as an electrolyte [33]. TNT was prepared on Ti foil by anodization at 20 V for 12 h. TNT samples were cleaned with distilled water and dried by nitrogen flow.

2.2. Synthesis of carboxylic acid-functionalized TNT (TNT-COOH)

TNT samples were immersed in the 25 g/l toluene solution of 3-aminopropyltriethoxysilane (AR, Aladdin, Shanghai, China) under stirring at ambient temperature for 15 min. Toluene was evaporated by a rotary evaporator at 80°C for 2 h to obtain amine-functionalized TNT. The samples were immersed in 15 ml DMSO solution that contained succinic anhydride (120 mg) and triethylamine (120 mg). The solution was stirred at 40°C for 48 h [25]. Afterwards, the specimens were washed with ethanol.

2.3. Synthesis of TNT incorporated with AL (TNT-AL)

TNT-COOH was immersed in 15 ml H_2O with 250 mg 1-ethyl-3-(3-dimethylaminopropyl) carbodiimide-HCl (AR, Aladdin, Shanghai, China) and 100 mg N-hydroxysuccinimide (AR, Aladdin, Shanghai, China). Then 650 mg of 3,9-Bis(3-aminopropyl)-2,4,8,10-tetraoxaspiro[5.5]undecane (AR, Aladdin, Shanghai, China) was added and agitated at 35°C for 8 h. The obtained TNT-AL was refluxed in hot acetone for 48 h for cleaning.

2.4. AgNPs preparation

AgNPs were prepared following J. Justin Gooding's method with minor modification [34]. $AgNO_3$ (AR, Aladdin, Shanghai, China) aqueous solution (3 ml, 1 g/l) and trisodium citrate dehydrate (AR, Aladdin, Shanghai, China) aqueous solution (3 ml, 1 g/l) were added to ultrapure water (17 ml). Sodium borohydride (AR, Aladdin, Shanghai, China) aqueous solution (9 ml, 1 g/l) was then added dropwise into the solution, under vigorous stirring. The solution was stirred for 2 h until the color turned yellow. The synthesis of AgNPs was confirmed by Transmission electron microscopy (TEM, CM20, Philips, The Netherlands).

2.5. The AgNPs loaded TNT (TNT-AL-AgNPs) preparation

TNT-AL was immersed in 4 ml AgNPs solution for 2 h at ambient temperature, which facilitates AgNPs binding with AL [35]. After immersing, the sample was immediately soaked in the ultrapure water for 4 h and then ultrasonically cleaned to remove the remaining AgNPs and undesired remaining organic compounds. Hereafter, the specimens were dried at ambient temperature.

The AgNPs solution after immersion and the solution after the sample's ultrasonically clean were sampled, mixed with aqua regia solution in a 1:1 vol ratio to dissolve the silver and tested by inductively coupled plasma-atomic emission spectroscopy (ICP-AES, OPTIMA8000, PerkinElmer, USA) to calculate the amount of loaded AgNPs. The formula to calculate the amount of loaded AgNPs is as below. $M\ (mg) = m_o - a_1 \times v_1 - a_2 \times v_2$. M denotes the mass of loaded AgNPs, a_1, a_2 denote the concentration of the AgNPs solution after immersion and the solution after ultrasonic cleaning, respectively. v_1 and v_2 denote the volume of the AgNPs solution after immersion and the solution after ultrasonic cleaning, respectively.

2.6. Sample characterization

The surface morphology was evaluated by scanning electron microscopy (SEM, Nova NanoSEM200, FEI Co., USA) and atomic force microscopy (AFM, VeecoMultiMode, NanoscopeIIIa controller, Veeco Co., USA). X-ray photoelectron spectroscopy (XPS, K-Alpha, Thermo) using monochromatic Al Kαradiation (6 mA, 12 kV, and 1486.68 eV) as excitation source was employed to determine the surface elemental composition and chemical states of elements. The Fourier transform infrared spectroscopy (FTIR, Equinox 55, Bruker Co., Germany) was used to analyze the chemical group of the samples.

The static contact angles were tested by the static sessile drop method using the easy drop standard instrument (KRUSS) at ambient temperature and humidity. The microstructure of AgNPs anchored to the wall of the TNT was examined by TEM.

2.7. Assessment of AgNPs release kinetics

AgNPs' release profile in different pH was evaluated. The cleaned TNT-AL-AgNPs specimens were divided into three groups. Group one was immersed in 5 ml pH buffer solution (pH 5.5) while the second group was immersed in the same volume of neutral buffer solution (pH 7.4) and agitated at 100 rpm at 37°C. At 2, 4, 6, 8, 10, 12, 24 h, 2, 4, 6, 8, 10, 12, 14, 16, 18, 20, 22, 24, 26, 28, and 30 days samples were taken out from the solution, washed with PBS solution for three times, and immersed into fresh buffer solution. On day 28, in the pH 7.4 group, we suddenly changed the pH to 5.5 to analyze the effect of infection after a month of implantation. In the third group, the samples were immersed in the neutral buffer solution (pH 7.4), then agitated at 100 rpm at 37°C. TNT-AL-AgNPs were taken out from the solution, washed and immersed in fresh buffer solution at 2, 4, and 6 h. After 6 h immersion, TNT-AL-AgNPs were taken out, washed and immersed in an acidic buffer solution (pH 3). At 8, 12, 24, and 36 h the samples were taken out, washed and immersed in fresh buffer. Buffer solutions were mixed with aqua regia solution in a 1:1 vol ratio to dissolve the silver. The concentration of dissolved silver ions in the buffer solutions was analyzed by inductively coupled plasma-atomic emission spectroscopy (ICP-AES, OPTIMA8000, PerkinElmer, USA). Accumulated silver ion concentration directly correlates with the AgNPs release from TNT-AL-AgNPs implants.

2.8. Antibacterial activity of AgNPs released at pH 5.5 and 7.4

The antibacterial efficiency of AgNPs released from TNT-AL-AgNPs at different pH was tested against *S. aureus* (gram-positive bacteria) and *E. coli* (gram-negative bacteria). TNT-AL-AgNPs were immersed into buffer solutions with pH 7.4 and pH 5.5 separately and agitated at 100 rpm at 37°C. Buffer solution containing released AgNPs (0.5 ml) was collected at 2, 8, and 24 h, and 0.5 ml fresh buffer solution was added. AgNPs released solutions were neutralized by

traces of 1 M NaOH and 1 M HNO_3 [36,37]. Then, 1000 µl of *S. aureus* (ATCC25923) or *E. coli* (ATCC25922) (10^6 CFU/ml) were added to 1000 µl of neutralized AgNPs containing buffer solutions into centrifuge tubes. Specimens were incubated for 24 h at 37°C under aerobic conditions. In the control group, 1000 µl PBS was used instead of AgNPs containing solution.

3-(4, 5-dimethylthiazol-2-yl)-2, 5-diphenyltetra-zolium bromide (MTT assay, 0.5 mg/ml, Aladdin, Shanghai, China) was applied to detect the bacterial viability. A 200 µl volume of each bacterial culture solution was transferred into 1.5 ml centrifuge tube. Afterwards, 20 µl MTT stock solution was added to the centrifuge tube to initiate the reaction, mixed manually for 10 s and incubated at 37°C for 20 min. The mixture was centrifuged and the supernatant was removed by pipette. Then, 150 µl DMSO (AR, Aladdin, Shanghai, China) was added to the pellets of the cell-formazan crystal complexes and mixed with a pipette. The mixture was transferred to 96-well plates and absorbance was measured at 540 nm in a microplate reader (Bio-Rad Model 680, US) [38]. DMSO was used as the reference.

2.9. Effect of TNT-AL-AgNPs on osteoblast proliferation, cell morphology, and differentiation

Osteoblasts attach on the implant surface and deposit calcium phosphate matrix during implant osteointegration. MC3T3-E1 murine osteoblasts (ATCC; Chinese Academy of science, Shanghai, China) were cultured in α-Minimum essential medium (α-MEM) with 10% fetal bovine serum (FBS) (Gibco, Invitrogen, Grand Island, NY, USA), 10 µg/ml penicillin, 10 µg/ml streptomycin, and 50 µg/ml fungizone (complete medium). Medium was changed every 3 days. Osteoblasts were harvested using 0.25% trypsin and 0.1% EDTA, seeded onto Ti disc, TNT, and TNT-AL-AgNPs (φ = 1.77 cm) at 1×10^4 cells/cm^2, and cultured in a Petri dish with complete medium.

AlamarBlue cell viability assay (Invitrogen Corporation, Carlsbad, CA, USA) was carried out to determine osteoblast proliferation and viability on day 1 and 3. A fluorescence spectrometer (SpectraMax M5 Molecular Devices, Sunnyvale, CA, USA) at 540 nm/excitation 590 nm emission was used to measure the fluorescence intensity [39]. The alkaline phosphatase activity and total protein content were measured on day 3 of culture. A LabAssay™ ALP

colorimetric assay kit (Wako Pure Chemicals, Osaka, Japan) was used to determine the ALP activity in the cell lysate (Sigma-Aldrich, St. Louis, MO, USA). The total protein content was measured at 570 nm with a commercial BCA Protein Assay kit (Beyotime, Beijing, China). ALP activity was expressed in nanomole per microgram protein. To analyze the cell morphology on the implant surface, osteoblasts cultured on Ti disc, TNT, and TNT-AL-AgNPs for 1 and 3 days were rinsed with sterile PBS for three times, fixed with paraformaldehyde for 10 min and permeabilized with Triton X-100 (AR, Aladdin, Shanghai, China) at 4°C for 5 min. Cells were stained with phalloidin-FITC (Aladdin) overnight at 4°C and counterstained with DAPI (AR Aladdin, Shanghai, China). Cells were observed under a fluorescence microscope (FM, OLYMPUS IX71, Japan).

2.10. Statistical analysis

The results are reported as the mean ± standard deviation (SD). Statistical analysis was performed by one-way analysis of variance (ANOVA) with Bonferroni's post hoc test to test differences between groups. Data were analyzed using Graphpad Prism® 6.0 (GraphPad Software Inc., La Jolla, CA, USA). For the data in Figure 6C and D, we used two independent-sample t-test. Difference at $p < 0.05$ was considered to be significant.

3. Results and discussion

3.1. Physicochemical characterization

3.1.1. SEM, TEM, AFM observation

Optimal nanotube diameter and homogeneous distribution of nanotubes on implant surface are crucial for implant osteointegration [21]. SEM is a useful tool for surface morphology analysis of biomaterials. The surface morphology of the TNTs clearly exhibited that a well-aligned structure of circular opening with homogeneous and uniform nanotubes with an average diameter of approximately 70 nm can be fabricated on Ti foil (Fig. 1). After treatment with AL-AgNPs, the surface of TNT was slightly changed. Consistent with the SEM images, TEM images showed the diameter of TNT was about 70 nm (Fig. 2A) and the TNT wall was intact after TNT-AL-AgNPs preparation (Fig. 2B). Wang and colleagues have reported that the 70 nm diameter of titanium nanotubes is optimum for implant osteointegration [21]. The AgNPs ranging from 5 to 20 nm in diameter were anchored onto the inner wall of the TNT (Fig. 2B). The AgNPs distributed along the wall of the TNT without significant aggregation. This confirms that adding AL and AL-AgNPs did not affect the nanotube diameter. After the introduction of the AL and AgNPs, the nanotube morphology was maintained with sporadically occurring debris. The cross-sectional views showed that the TNT layer was about 2.5 μm and the surface modification didn't significantly change the length of TNT (Fig. 1). Nanotubes with 70 nm diameter and 2.5 μm length provide enough space to incorporate AgNPs that could give sustained silver release.

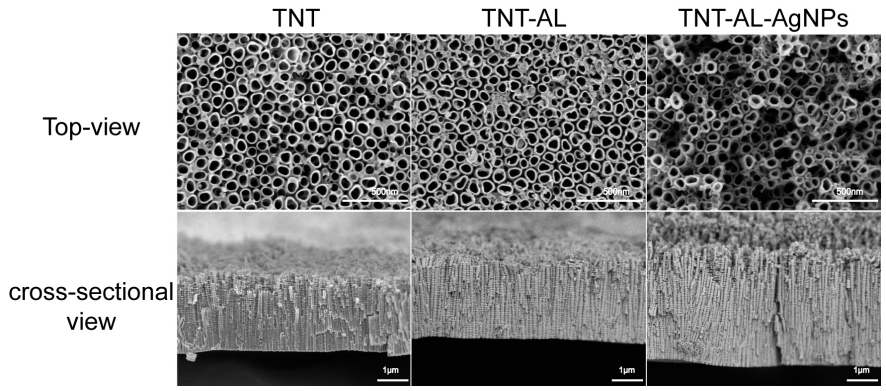

Figure. 1 SEM top view images and cross-sectional images of nanotube layer on TNT, TNT-AL, and TNT-AL-AgNPs.

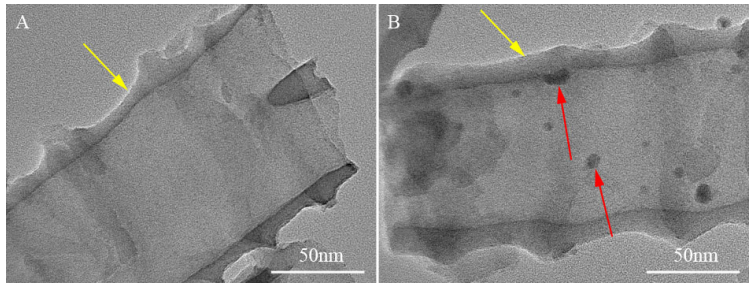

Figure 2: TEM image of TNT(A) and TNT-AL-AgNPs(B). The yellow arrow indicates the wall of the TNT. The red arrows denote AgNPs incorporated inside TNT.

Surface roughness measurements were calculated from the AFM images and it is demonstrated in Fig. 3A–C. We found that the surface roughness of the TNT increased with the incorporation of AL-AgNPs (Fig. 3C). It may be caused by the ultrasonically cleaned step after the introduction of AL-AgNPs. AFM analysis showed mean roughness of TNT and TNT-AL was 31.78 nm (Fig. 3A) and 24.45 nm (Fig. 3B) respectively. The mean roughness of TNT-AL-AgNPs was 75.73 nm (Fig. 3C). Higher surface micro-roughness of implants has been reported to accelerate bone tissue regeneration and increase

mechanical retention in the bone bed at short periods of implantation [40]. Therefore, increased surface roughness of TNT-AL-AgNPs could be beneficial for implant fixation and osteointegration.

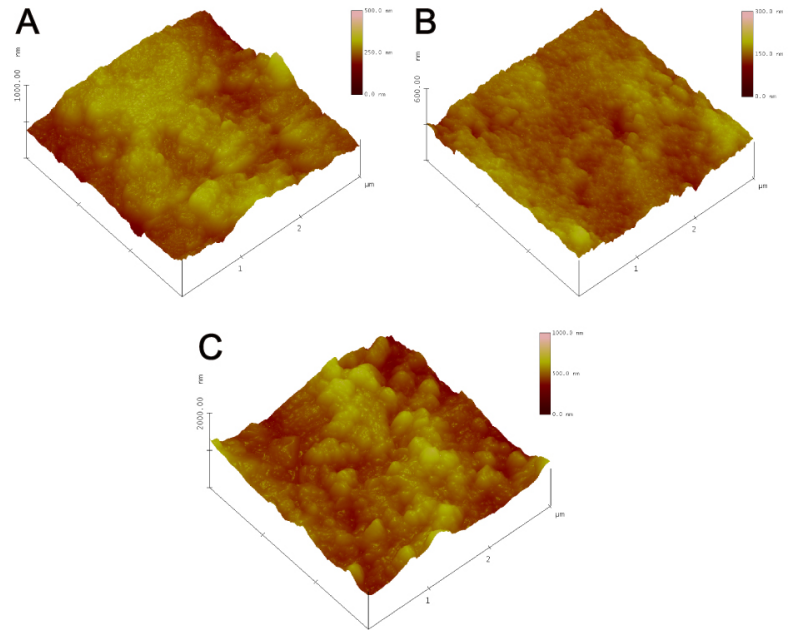

Figure. 3 Samples characteristics analyzed by AFM. (A) TNT, (B) TNT-AL, and (C) TNT-AL-AgNPs.

3.2. XPS analysis

The XPS survey spectra and high-resolution Ag3d are shown in Fig. 4. XPS analysis indicated the presence of Ti, O, C, F, N and Si elements on TNT-AL (Fig. 4A). The XPS spectra of TNT-AL revealed the presence of carbon (1s and 2p), nitrogen (1s), oxygen (1s), fluoride (1s), Ti (2p), Si (2p) on the surface (Fig. 4A). The Ti $2p_{3/2}$ maximum (458.9 eV) was used as binding energy reference. The same data were obtained when C 1s (adventitious carbon at 285.1 eV), or O 1s lattice oxygen (530.4 eV) was used as reference. Whereas for the TNT-AL-AgNPs corresponding spectrum exhibited the photoelectron peaks of

carbon (1s and 2p), nitrogen (1s), oxygen (1s), fluoride (1s), Ti (2p), Si (2p) from TNT-AL and Ag (3d) from the AgNPs. Fig. 4A and B show the O 1s peaks of the nanoparticles and nanotubes with the peak amplitude at 530.54 and 530.20, respectively. The peaks at 530.54 and 530.20 can be attributed to the Ti-O in the titanium dioxide materials. The presence of C, N, F, and Si elements should be due to the surface contamination from the organic electrolyte and aminopropyltriethoxysilane. The peak for Ag element occurred only in TNT-AL-AgNPs (Fig. 4B). Consistent with the TEM result, the $Ag3d_{5/2}$ and $Ag3d_{3/2}$ (367.36 eV and 373.35 eV) (Fig. 4C) were close to the metallic Ag^0 spectra absorption. This finding indicated that AgNPs were successfully immobilized onto the wall of TNT. Surface chemical properties, surface roughness, wettability, and surface energy are important parameters that can influence cell–materials interactions, cell adhesion, and proliferation [41,42]. Our results confirmed that the incorporation of AgNPs on TNT via AL did not affect the physicochemical properties of the TNT.

3.3 FTIR analysis

Fourier transform infrared (FTIR) spectra are used to analyze the surface functional groups of the TNT-AL and TNT-AL-AgNPs and results are shown in Fig. 4D. The FTIR spectra of TNT-AL showed a broad and strong bond at 3418 cm^{-1} corresponded to the stretching vibrations of hydroxyl (-OH) or amine (-NH) groups, which suggested a significant interaction between AgNPs and parts of the amino-groups. The characteristic adsorption at 3418 $cm^{-1}$was corresponding to N-H stretch vibrations from AL [34]. The peaks at 2920 and 2850 cm^{-1} were attributed to the stretching vibration of $-CH_2$ groups (Fig. 4D). The pH sensitive AL has been successfully linked with mesoporous silica, hydrogel, and microgel as a drug carrier [25,26]. Physicochemical characterization of TNT-AL-AgNPs by SEM, AFM, TEM, FTIR, and XPS showed that AgNPs were properly linked in TNT via AL. This is the first study reporting the successful incorporation of AgNPs homogeneously in TNT via AL without affecting the physicochemical characteristics of TNT and the diameter of nanotubes.

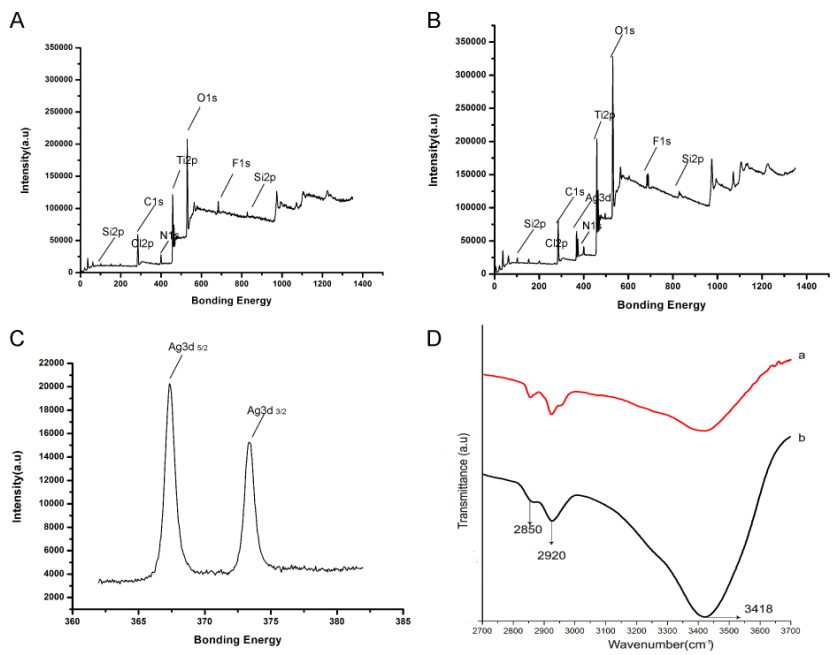

Figure. 4 XPS spectra of TNT-AL and TNT-AL-AgNPs. (A) XPS survey spectra of TNT-AL, (B) XPS survey spectra of TNT-AL-AgNPs, and (C) high-resolution XPS spectra of Ag3d of TNT-AL-AgNPs. (D) FTIR absorption spectroscopy of TNT-AL-AgNPs (a) and TNT-AL (b).

3.4 Contact angles measurement

The wetting ability of nonporous materials plays a crucial role in biomedical applications by promoting the adhesion and spreading of host cells to the implant surface as well as adsorption processes [23]. More hydrophilic material has higher wettability, and lower contact angle. The contact angle is the resultant between adhesive (droplet-surface) and cohesive (droplet-droplet) forces. In other words, the tendency of a drop to spread out over a flat, solid surface (wettability) increases as the contact angle decreases. The contact angle magnitude of TNT displays a decreasing trend with a loading nanotube array, indicating that the nanotubes layer exhibits a hydrophilic character. It is

generally recognized that TNT displays a hydrophilic behavior due to the presence of surface hydroxyl (-OH) groups [23]. As shown in Fig. 5, the Ti foil had the highest contact angle, corresponding to the lowest hydrophilicity. In the case of TNT, a lower contact angle was observed in comparison with Ti foil (Fig. 5B and C). TNT and TNT-AL-AgNPs had almost similar values in contact angles (Fig. 5D). This result indicated that the surface hydrophilicity of TNT and TNT-AL-AgNPs was significantly higher than Ti foil, and incorporation of AL-AgNPs didn't reduce the hydrophilicity of TNT (Fig. 5D). Our findings indicate that TNT and TNT-AL-AgNPs designed in this study have a hydrophilic surface, which is suitable for cell adhesion and spreading.

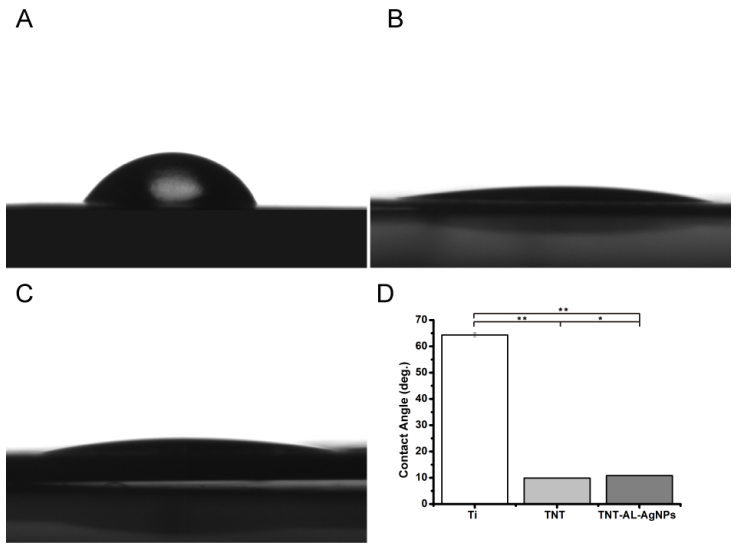

Figure. 5 Water contact angles measured on (A) Ti foil, (B) TNT, (C) TNT-AL-AgNPs, and (D) Quantification of to water contact angle in Ti foil, TNT, and TNT-AL-AgNPs. Values are mean ± SD from 6 different experiments. Significant effect, *$p < 0.05$, **$p < 0.01$.

3.5. Antimicrobial effect of AgNPs release from TNT-AL-AgNPs at pH 5.5 and 7.4

Implants, coated with antimicrobial agents directly or via biodegradable polymers, are frequently used to control peri-implant infection [16,18,19]. Although TNT provides a larger space for loading antimicrobial agents than Ti, antimicrobials loaded in TNT exhaust in 30 days [23]. Therefore, drugs directly loaded in TNT cannot control one-month post-implantation infection. Moreover, the antimicrobial agents directly loaded in TNT fail to respond to the subtle variations of the peri-implant microenvironment, such as an infection-mediated change in pH level or degree of inflammation. Therefore, in this study, we loaded AgNPs in TNT via pH-sensitive AL, which allowed drug release based on peri-implant pH level. In this study, the total amount of loaded AgNPs was 0.017 mg/implant, which is shown in Table 1. The amount of loaded AgNPs is lower than the minimal toxic dose of silver, which indicated the admirable biosafety of this new biomaterial [43]. AgNPs showed a burst release from TNT-AL-AgNPs at a rate of 0.392 ppm/h at pH 5.5 in the initial 2 h (Fig. 6A). The pH 5.5 corresponds to the pH in the peri-implant surface during bacterial infection. The pH 5.5 increased AgNPs release from TNT by 3.77, 3.26, 2.44, 2.22, 2.09, 2.24, and 2.36- fold in comparison to pH 7.4 at 2, 4, 6, 8, 10, 12, and 24 h, respectively (Fig. 6A). From 2–12 h, the release rates of AgNPs at pH 5.5 decreased, but still sustained ~ 2.5- fold higher release rate up to 30 days in comparison to release at pH 7.4 (Fig. 6A). When the pH was changed from 7.4 to 5.5 on 28th day, there was a sharp increase in AgNPs release (Fig. 6A). This result indicates that AgNPs can be stored at physiological state for a long time (>30 days) at pH7.4 and infection (pH 5.5) can quickly trigger the release of AgNPs.

	Samples				Mean
	1	2	3	4	
m_0 (mg)	0.448	0.448	0.448	0.448	0.448
a_1 (ppm)	55	52	52	53	53
v_1 (ml)	7	7	7	7	7
a_2 (ppm)	7	11	11	9	10
v_2 (ml)	6	6	6	6	6
M (mg)	0.018	0.017	0.015	0.017	0.017

Table 1: Amount of AgNPs loaded per TNT-AL-AgNPs implant. m_o, the mass of AgNPs dissolved in solution; M, the mass of AgNPs loaded; a_1, the concentration of the AgNPs solution after immersion; a_2, the concentration of AgNPs solution after ultrasonic cleaning; v_1, the volume of the AgNPs solution after immersion; v_2, the volume of the AgNPs solution after ultrasonic cleaning.

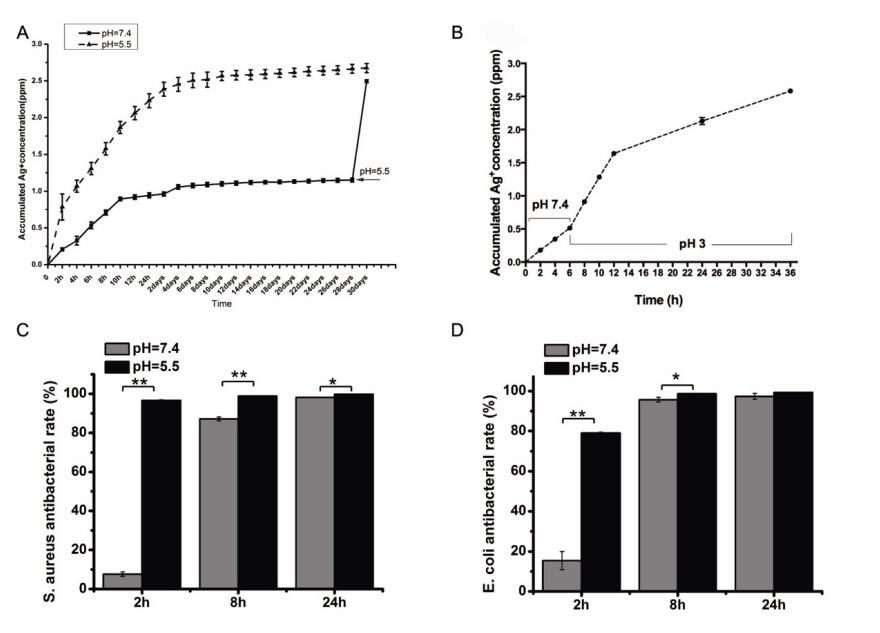

Figure. 6 The release profiles of AgNPs. (A) at pH 7.4 and pH 5.5 at different time points. (B) at pH 7.4 from 0 to 6 h and at pH 3.0 from 6 to 36 h. Antibacterial effect of AgNPs release from TNT-AL-AgNPs at pH 5.5 and 7.4 against *S. aureus* (C), and *E. coli* (D). Values are mean ± SD from 3 independent experiments.

Furthermore, the release rate of AgNPs was enhanced from 0.084 to 0.198 ppm/h when the microenvironment was changed from pH 7.4 to pH 3 (Fig. 6B). This finding supports the pH-sensitivity of AL, which is the middle part of the TNT-AL-AgNPs sandwich. The AL was able to hold AgNPs for long period at pH 7.4 and gave quick burst release followed by sustained high dose release at pH 5.5, which is in accordance with the previous findings [25,44]. Our result suggests that the infection-dependent decrease in pH around the TNT-AL-AgNPs can be used as a switch to release the AgNPs.

The selection of appropriate antibiotics to control implant-related infection is too difficult since such infections can be caused by different bacterial species [45]. Silver has broad-spectrum antibacterial ability in low concentration with no adverse effect on mammalian cells [27–29]. Moreover, silver reduces the possibility of developing drug-resistant bacterial strains [14,29,46–49]. AgNPs released in 2 h at pH 5.5, increased antimicrobial efficiency on *S. aureus* by 12.7- fold, and on *E. coli* by 5.1- fold in comparison to AgNPs released at pH 7.4 (Fig. 6C, D). The antibacterial activity of AgNPs released at pH 5.5 from TNT-AL-AgNPs was significantly higher than at pH 7.4 (Fig. 6C, D). Moreover, the antibacterial ability of AgNPs released solution showed a positive correlation to AgNPs' concentration. Wang and colleagues reported that AgNPs functionalized titanium surface inhibits bacterial adhesion and biofilm formation [30]. Results in Fig. 6A indicate that at physiological pH 7.4, TNT-AL-AgNPs allowed AgNPs to attach more firmly on the TNT surface for > 30 days compared to at pH 5.5. Due to limitations related to AgNPs directly loaded TNT, we propose that TNT-AL-AgNPs implant can be a potent therapeutic approach to inhibit bacterial adhesion and biofilm formation, which reduces the risk of peri-implant infection. However, further *in vitro* and *in vivo* studies are needed to evaluate this hypothesis. Our findings indicate that the efficient pH-

responsive release and antibacterial activity of AgNPs from TNT-AL-AgNPs pave the way towards better satisfying the clinical needs.

3.6. Cell proliferation and differentiation assay

The effect of the implant on cell viability and proliferation indicates the biocompatibility of the implants. For implant fixation and durability, implant biomaterial should be biocompatible, allow cell adhesion and cell growth [45–48]. We found that TNT increased osteoblast proliferation by 1.7- fold and 1.5-fold compared with Ti disc on day 1 and 3 respectively (Fig. 7A). TNT-AL-AgNPs increased osteoblast proliferation by 1.4- fold and 1.5- fold compared with Ti disc on day 1 and 3 respectively (Fig. 7A). TNT-AL-AgNPs reduced osteoblast proliferation on day 1 by 15% compared with TNT (Fig. 7A). Interestingly, TNT-AL-AgNPs did not inhibit osteoblast proliferation on day 3 compared with TNT (Fig. 7A). It indicated that the special nanotubular structure and homogeneously distributed AgNPs of TNT-AL-AgNPs promotes the cell proliferation effectively. This result was consistent with the findings from previous studies [21,40]. Our results showed the biocompatibility of TNT-AL-AgNPs with osteoblasts, which are major cells present around the implants and play important role in implant osteointegration.

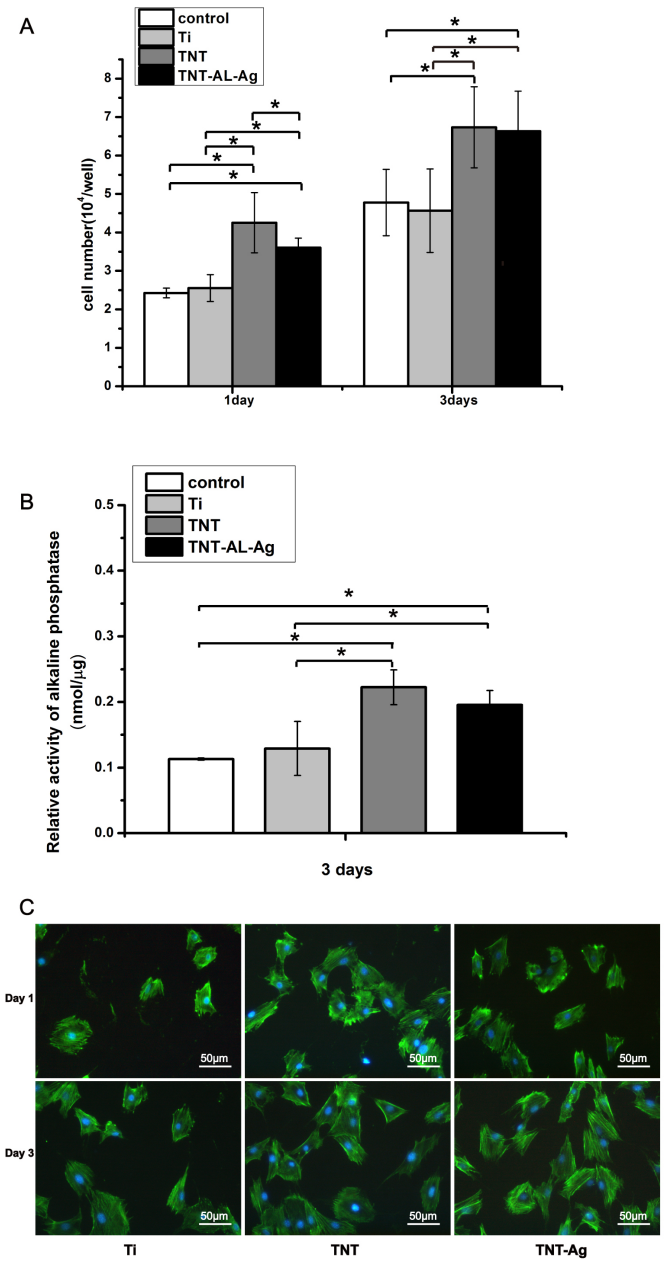

Figure. 7 Effect of Ti disc, TNT, and TNT-AL-AgNPs on (A) MC3T3-E1 osteoblast proliferation on day 1 and 3, (B) ALP activities of MC3T3-E1 osteoblasts on day 3, and (C) MC3T3-E1 osteoblast morphology on day 1 and

3 (phalloidin-FITC in green and DAPI in blue color). All data are presented as the mean values together with the standard deviation (SD). Values are mean ± SD from 6 independent experiments. Significant effect: *$p < 0.05$.

Differentiated osteoblasts deposit calcium phosphate in the gap between implant and bone, thereby facilitating implant osteointegration, and reducing the risk of infection [50]. ALP activity is an osteoblast differentiation marker. Fig. 7B showed the relative ALP activity of MC3T3-E1 cells seeded on Ti disc, TNT, and TNT-AL-AgNPs on day 3. TNT increased the ALP activity of osteoblasts by 1.7- fold compared with Ti disc (Fig. 7B). TNT-AL-AgNPs increased osteoblast ALP activity by 1.5- fold compared with Ti disc (Fig. 7B). TNT-AL-AgNPs did not inhibit the ALP activity compared with TNT (Fig. 7B). Our findings are strongly supported by data reported by De Giglio and colleagues showing that silver ion release from TNT-AgNPs has been properly tuned in order to assure antibacterial activity while preserving osteoblasts' response at the implant interface [51]. Delayed osteointegration in metabolic bone diseases increases the risk of frequent peri-implant infections [52]. TNT-AL-AgNPs along with osteoinductive agents such as bone morphogenetic protein 2 (BMP-2) may be a promising strategy to accelerate osteointegration and control infection, in patients with metabolic bone diseases [53,54]. Our results showed that loading AgNPs on the TNT surface via AL maintained the pro-osteogenic properties of TNT.

Both TNT and TNT-AL-AgNPs did not affect the osteoblast attachment and morphology compared with Ti disc on day 1 and 3 (Fig. 7C). There was a notable difference in the values of cell number between TNT and TNT-AL-AgNPs on the first day, while the values turned out to be similar on the third day, which may be due to the residual AgNPs absorbed on the surface of TNT. The cells showed elongated and spread out on TNT and TNT-AL-AgNPs, in addition, the F-actin filaments extended in numerous directions (Fig. 7C), which revealed good cytocompatibility of TNT-AL-AgNPs. Our findings showed that this novel design of pH dependent antimicrobial releasing TNT-AL-AgNPs implant is biocompatible, pro-osteogenic, and capable to control peri-implant bacterial infection.

4. Conclusion

In this study, we developed a novel design of a pH dependent silver nanoparticle releasing titanium implant to control peri-implant infection. Broad-spectrum antimicrobial (AgNPs) was successfully loaded in TNT via pH sensitive AL, without affecting the physicochemical characteristics of TNT. The pH 5.5, mimicking the pH level in peri-implant surface during bacterial infection, was able to trigger AgNPs release from TNT, and released AgNPs efficiently controlled bacterial growth *in vitro*. This novel design of the implant was biocompatible and pro-osteogenic. Our findings suggest that low pH-triggered AgNPs releasing TNT-AL-AgNPs implant could be a potent therapeutic approach to control peri-implant infection.

Conflicts of interest

The authors declare no conflict of interest.

Acknowledgments

The authors would like to thank Miss Youyun Zeng for technical support and data collection. Authors acknowledge financial support provided by the Nature Science Foundation of Zhejiang Province (No. LY13H140005 and No.LY17H140007), the National Natural Science Foundation of China (No. 81371182 and No.81271186), Zhejiang Provincial Foundation for Health Department (No. 2015KYA150 and No. 2013KYA124), Zhejiang Provincial Science and Technology Project for Public Welfare (No. 2015C33139), Technology Innovation Plan for Students in Zhejiang Province (Xinmiao Talents Program) (No.2016R413065) and Wenzhou Municipal Science and Technology Project for Public Welfare (No.Y20140662 and No.Y20150074).

References

[1] M. Geetha, A.K. Singh, R. Asokamani, A.K. Gogia, Ti based biomaterials, the ultimate choice for orthopaedic implants–a review. Progress in Materials Science. 54 (2009) 397–425. https://doi.org/10.1016/J.PMATSCI.2008.06.004.

[2] D.A. Puleo, R.A. Kissling, M.S. Sheu, A technique to immobilize bioactive proteins, including bone morphogenetic protein-4 (BMP-4), on titanium alloy. Biomaterials. 23 (2002) 2079–2087. https://doi.org/10.1016/S0142-9612(01)00339-8.

[3] M. Cioffi, D. Gilliland, G. Ceccone, R. Chiesa, A. Cigada, Electrochemical release testing of nickel-titanium orthodontic wires in artificial saliva using thin layer activation. Acta Biomaterialia. 1 (2005) 717–724. https://doi.org/10.1016/j.actbio.2005.07.008.

[4] M. Long, H.J. Rack, Titanium alloys in total joint replacement–a materials science perspective. Biomaterials. 19 (1998) 1621–1639. https://doi.org/10.1016/S0142-9612(97)00146-4.

[5] H.-J. Han, S. Kim, D.-H. Han, Multifactorial evaluation of implant failure: A 19-year retrospective study. The International Journal of Oral & Maxillofacial Implants. 29 (2014) 303–310. https://doi.org/10.11607/JOMI.2869.

[6] D. Campoccia, L. Montanaro, C.R. Arciola, The significance of infection related to orthopedic devices and issues of antibiotic resistance. Biomaterials. 27 (2006) 2331–2339. https://doi.org/10.1016/J.BIOMATERIALS.2005.11.044.

[7] Y.H. An, R.J. Friedman, Concise review of mechanisms of bacterial adhesion to biomaterial surfaces. Journal of Biomedical Materials Research. 43 (1998) 338–348. https://doi.org/10.1002/(SICI)1097-4636(199823)43:3<338::AID-JBM16>3.0.CO;2-B.

[8] J.M. Schierholz, J. Beuth, Implant infections: A haven for opportunistic bacteria. Journal of Hospital Infection. 49 (2001) 87–93. https://doi.org/10.1053/jhin.2001.1052.

[9] A. Mombelli, N.P. Lang, The diagnosis and treatment of peri-implantitis. Periodontology 2000. 17 (1998) 63–76. https://doi.org/10.1111/J.1600-0757.1998.TB00124.X.

[10] T. Bechert, P. Steinrücke, J.P. Guggenbichler, A new method for screening anti-infective biomaterials. Nature Medicine. 6 (2000) 1053–1056. https://doi.org/10.1038/79568.

[11] J. Hardes, C. Gebert, A. Schwappach, H. Ahrens, A. Streitburger, W. Winkelmann, G. Gosheger, Characteristics and outcome of infections associated with tumor endoprostheses. Archives of Orthopaedic and Trauma Surgery. 126 (2006) 289–296. https://doi.org/10.1007/S00402-005-0009-1.

[12] A. Abudu, R.J. Grimer, R.M. Tillman, S.R. Carter, Endoprosthetic replacement of the distal tibia and ankle joint for aggressive bone tumours. International Orthopaedics. 23 (1999) 291–294. https://doi.org/10.1007/s002640050374.

[13] R.J. Grimer, M. Belthur, C. Chandrasekar, S.R. Carter, R.M. Tillman, Two-stage revision for infected endoprostheses used in tumor surgery. Clinical Orthopaedics and Related Research. 395 (2002) 193–203. https://doi.org/10.1097/00003086-200202000-00022.

[14] J. Hardes, H. Ahrens, C. Gebert, A. Streitbuerger, H. Buerger, M. Erren, A. Gunsel, C. Wedemeyer, G. Saxler, W. Winkelmann, G. Gosheger, Lack of toxicological side-effects in silver-coated megaprostheses in humans. Biomaterials. 28 (2007) 2869–2875. https://doi.org/10.1016/j.biomaterials.2007.02.033.

[15] D. Neut, O.S. Kluin, B.J. Crielaard, H.C. van der Mei, H.J. Busscher, D.W. Grijpma, A biodegradable antibiotic delivery system based on poly-(trimethylene carbonate) for the treatment of osteomyelitis. Acta Orthopaedica. 80 (2009) 514–519. https://doi.org/10.3109/17453670903350040.

[16] A.G. Gristina, M. Oga, L.X. Webb, C.D. Hobgood, Adherent bacterial colonization in the pathogenesis of osteomyelitis. Science. 228 (1985) 990–993. https://doi.org/10.1126/SCIENCE.4001933.

[17] T.P. Schmalzried, H.C. Amstutz, M.K. Au, F.J. Dorey, Etiology of deep sepsis in total hip arthroplasty: The significance of hematogenous and recurrent infections. Clinical Orthopaedics and Related Research. 280 (1992) 200–207. https://doi.org/10.1097/00003086-199207000-00026.

[18] W.J.E.M. Habraken, J.G.C. Wolke, J.A. Jansen, Ceramic composites as matrices and scaffolds for drug delivery in tissue engineering. Advanced Drug Delivery Reviews. 59 (2007) 234–248. https://doi.org/10.1016/j.addr.2007.03.011.

[19] H.I. Chang, Y. Perrie, A.G.A. Coombes, Delivery of the antibiotic gentamicin sulphate from precipitation cast matrices of polycaprolactone. Journal of Controlled Release. 110 (2006) 414–421. https://doi.org/10.1016/j.jconrel.2005.10.028.

[20] D. Campoccia, L. Montanaro, P. Speziale, C.R. Arciola, Antibiotic-loaded biomaterials and the risks for the spread of antibiotic resistance following their prophylactic and therapeutic clinical use. Biomaterials. 31 (2010) 6363–6377. https://doi.org/10.1016/J.BIOMATERIALS.2010.05.005.

[21] N. Wang, H. Li, W. Lü, J. Li, J. Wang, Z. Zhang, Y. Liu, Effects of TiO2 nanotubes with different diameters on gene expression and osseointegration of implants in minipigs. Biomaterials. 32 (2011) 6900–6911. https://doi.org/10.1016/j.biomaterials.2011.06.023.

[22] L. Zhao, H. Wang, K. Huo, L. Cui, W. Zhang, H. Ni, Y. Zhang, Z. Wu, P.K. Chu, Antibacterial nano-structured titania coating incorporated with silver nanoparticles. Biomaterials. 32 (2011) 5706–5716. https://doi.org/10.1016/j.biomaterials.2011.04.040.

[23] A. Gao, R. Hang, X. Huang, L. Zhao, X. Zhang, L. Wang, B. Tang, S. Ma, P.K. Chu, The effects of titania nanotubes with embedded silver oxide nanoparticles on bacteria and osteoblasts. Biomaterials. 35 (2014) 4223–4235. https://doi.org/10.1016/j.biomaterials.2014.01.058.

[24] L. Ma, M. Liu, H. Liu, J. Chen, D. Cui, In vitro cytotoxicity and drug release properties of pH- and temperature-sensitive core-shell hydrogel microspheres. International Journal of Pharmaceutics. 385 (2010) 86–91. https://doi.org/10.1016/j.ijpharm.2009.10.037.

[25] R. Liu, Y. Zhang, X. Zhao, A. Agarwal, L.J. Mueller, P. Feng, pH-responsive nanogated ensemble based on gold-capped mesoporous silica through an acid-labile acetal linker. Journal of the American Chemical Society. 132 (2010) 1500–1501. https://doi.org/10.1021/ja907838s.

[26] N. Murthy, Y.X. Thng, S. Schuck, M.C. Xu, J.M.J. Fréchet, A novel strategy for encapsulation and release of proteins: Hydrogels and microgels with acid-labile acetal cross-linkers. Journal of the American Chemical Society. 124 (2002) 12398–12399. https://doi.org/10.1021/ja026925r.

[27] J.B. Wright, K. Lam, D. Hansen, R.E. Burrell, Efficacy of topical silver against fungal burn wound pathogens. American Journal of Infection Control. 27 (1999) 344–350. https://doi.org/10.1016/S0196-6553(99)70055-6.

[28] J.B. Wright, K. Lam, R.E. Burrell, Wound management in an era of increasing bacterial antibiotic resistance: A role for topical silver treatment. American Journal of Infection Control. 26 (1998) 572–577. https://doi.org/10.1053/ic.1998.v26.a93527.

[29] N.H. Ahmad Barudin, S. Sreekantan, M.T. Ong, C.W. Lai, Synthesis, characterization and comparative study of nano-Ag-TiO2 against Gram-positive and Gram-negative bacteria under fluorescent light. Food Control. 46 (2014) 480–487. https://doi.org/10.1016/J.FOODCONT.2014.05.046.

[30] J. Wang, J. Li, G. Guo, Q. Wang, J. Tang, Y. Zhao, H. Qin, T. Wahafu, H. Shen, X. Liu, X. Zhang, Silver-nanoparticles-modified biomaterial surface resistant to staphylococcus: New insight into the antimicrobial action of silver. Scientific Reports. 6 (2016) 1–16. https://doi.org/10.1038/srep32699.

[31] M. Bosetti, A. Massè, E. Tobin, M. Cannas, Silver coated materials for external fixation devices: In vitro biocompatibility and genotoxicity. Biomaterials. 23 (2002) 887–892. https://doi.org/10.1016/S0142-9612(01)00198-3.

[32] B. Tian, W. Chen, D. Yu, Y. Lei, Q. Ke, Y. Guo, Z. Zhu, Fabrication of silver nanoparticle-doped hydroxyapatite coatings with oriented block arrays for enhancing bactericidal effect and osteoinductivity. Journal of the Mechanical Behavior of Biomedical Materials. 61 (2016) 345–359. https://doi.org/10.1016/j.jmbbm.2016.04.002.

[33] J. Yu, X.F. Xiao, J.H. Liang, R.F. Liu, C.Y. Wang, D. Mao, Filling TiO2 nanotubes with biological apatite by alternative loop immersion method. Wuji Cailiao Xuebao/Journal of Inorganic Materials. 26 (2011) 78–84. https://doi.org/10.3724/SP.J.1077.2011.00078.

[34] X. Chen, X. Cheng, J.J. Gooding, Multifunctional modified silver nanoparticles as ion and pH sensors in aqueous solution. Analyst. 137 (2012) 2338–2343. https://doi.org/10.1039/C2AN35147A.

[35] A. Kumar, S. Mandal, P.R. Selvakannan, R. Pasricha, A.B. Mandale, M. Sastry, Investigation into the interaction between surface-bound alkylamines and gold nanoparticles. Langmuir. 19 (2003) 6277–6282. https://doi.org/10.1021/la034209c.

[36] L. Pichavant, G. Amador, C. Jacqueline, B. Brouillaud, V. Héroguez, M.C. Durrieu, pH-controlled delivery of gentamicin sulfate from orthopedic

devices preventing nosocomial infections. Journal of Controlled Release. 162 (2012) 373–381. https://doi.org/10.1016/j.jconrel.2012.06.033.

[37] A. Gaudin, G. Amador Del Valle, A. Hamel, V. le Mabecque, A.F. Miegeville, G. Potel, J. Caillon, C. Jacqueline, A new experimental model of acute osteomyelitis due to methicillin-resistant Staphylococcus aureus in rabbit. Letters in Applied Microbiology. 52 (2011) 253–257. https://doi.org/10.1111/j.1472-765X.2010.02992.x.

[38] Y. Wen, W. Zhou, X. Zhu, S. Cheng, G. Xiao, Y. Li, Y. Zhu, Z. Wang, C. Wan, An investigation of circadian rhythm in Escherichia coli. Biological Rhythm Research. 46 (2015) 753–762. https://doi.org/10.1080/09291016.2015.1052650.

[39] W. Bi, Z. Gu, Y. Zheng, X. Zhang, J. Guo, Heterodimeric BMP-2/7 antagonizes the inhibition of all-trans retinoic acid and promotes the osteoblastogenesis. PLoS ONE. 8 (2013) e78198. https://doi.org/10.1371/journal.pone.0078198.

[40] E. Velasco, L. Monsalve-Guil, A. Jimenez, I. Ortiz, J. Moreno-Muñoz, E. Nuñez-Marquez, M. Pegueroles, R.A. Pérez, F.J. Gil, Importance of the roughness and residual stresses of dental implants on fatigue and osseointegration behavior. In vivo study in rabbits. Journal of Oral Implantology. 42 (2016) 469–476. https://doi.org/10.1563/aaid-joi-D-16-00088.

[41] K.S. Brammer, S. Oh, C.J. Cobb, L.M. Bjursten, H. van der Heyde, S. Jin, Improved bone-forming functionality on diameter-controlled TiO2 nanotube surface. Acta Biomaterialia. 5 (2009) 3215–3223. https://doi.org/10.1016/j.actbio.2009.05.008.

[42] K. Das, S. Bose, A. Bandyopadhyay, TiO2 nanotubes on Ti: Influence of nanoscale morphology on bone cell-materials interaction. Journal of Biomedical Materials Research-Part A. 90 (2009) 225–237. https://doi.org/10.1002/JBM.A.32088.

[43] F. Sambale, S. Wagner, F. Stahl, R.R. Khaydarov, T. Scheper, D. Bahnemann, Investigations of the toxic effect of silver nanoparticles on mammalian cell lines. Journal of Nanomaterials. 2015 (2015) 1–13. https://doi.org/10.1155/2015/136765.

[44] L. Zhang, J. Bernard, T.P. Davis, C. Barner-Kowollik, M.H. Stenzel, Acid-degradable core-crosslinked micelles prepared from thermosensitive glycopolymers synthesized via RAFT polymerization. Macromolecular Rapid Communications. 29 (2008) 123–129. https://doi.org/10.1002/MARC.200700663.

[45] K. D. Kuhn, Release of active ingredients. Bone Cements, Springer, Berlin. (2000) 253--258.

[46] V. Alt, T. Bechert, P. Steinrücke, M. Wagener, P. Seidel, E. Dingeldein, E. Domann, R. Schnettler, An in vitro assessment of the antibacterial properties and cytotoxicity of nanoparticulate silver bone cement. Biomaterials. 25 (2004) 4383–4391. https://doi.org/10.1016/j.biomaterials.2003.10.078.

[47] W. Chen, Y. Liu, H.S. Courtney, M. Bettenga, C.M. Agrawal, J.D. Bumgardner, J.L. Ong, In vitro anti-bacterial and biological properties of magnetron co-sputtered silver-containing hydroxyapatite coating. Biomaterials. 27 (2006) 5512–5517. https://doi.org/10.1016/j.biomaterials.2006.07.003.

[48] M. Ramstedt, B. Ekstrand-Hammarström, A. v. Shchukarev, A. Bucht, L. Österlund, M. Welch, W.T.S. Huck, Bacterial and mammalian cell response to poly(3-sulfopropyl methacrylate) brushes loaded with silver halide salts. Biomaterials. 30 (2009) 1524–1531. https://doi.org/10.1016/j.biomaterials.2008.12.008.

[49] L. Zhao, P.K. Chu, Y. Zhang, Z. Wu, Antibacterial coatings on titanium implants. Journal of Biomedical Materials Research - Part B Applied Biomaterials. 91 (2009) 470–480. https://doi.org/10.1002/JBM.B.31463.

[50] P.-I. Bra-nemark, G.A. Zarb, T. Albrektsson, H.M. Rosen, Tissue-integrated prostheses: Osseointegration in clinical dentistry. Plastic and Reconstructive Surgery. 77 (1986) 496–497. https://doi.org/10.1097/00006534-198603000-00037.

[51] E. de Giglio, D. Cafagna, S. Cometa, A. Allegretta, A. Pedico, L.C. Giannossa, L. Sabbatini, M. Mattioli-Belmonte, R. Iatta, An innovative, easily fabricated, silver nanoparticle-based titanium implant coating: Development and analytical characterization. Analytical and Bioanalytical Chemistry. 405 (2013) 805–816. https://doi.org/10.1007/S00216-012-6293-Z.

[52] T. Beikler, T.F. Flemmig, Implants in the medically compromised patient. Critical Reviews in Oral Biology and Medicine. 14 (2003) 305–316. https://doi.org/10.1177/154411130301400407.

[53] R.M. Díaz-Sánchez, R.M. Yáñez-Vico, A. Fernández-Olavarría, R. Mosquera-Pérez, A. Iglesias-Linares, D. Torres-Lagares, Current approaches of bone morphogenetic proteins in dentistry. Journal of Oral Implantology. 41 (2015) 337–342. https://doi.org/10.1563/AAID-JOI-D-13-00012.

[54] T. Liu, Y. Zheng, G. Wu, D. Wismeijer, J.L. Pathak, Y. Liu, BMP2-coprecipitated calcium phosphate granules enhance osteoinductivity of deproteinized bovine bone, and bone formation during critical-sized bone defect healing. Scientific Reports. 7 (2017) 41800. https://doi.org/10.1038/srep41800.

CHAPTER FOUR

Antimicrobial and pro-osteogenic coaxially-electrospun magnesium oxide nanoparticles-polycaprolactone /parathyroid hormone-polycaprolactone composite barrier membrane for guided bone regeneration

Yiwen Dong[1-3], Litao Yao[2-4], Lei Cai[1], Mi Jin[1], Tymour Forouzanfar[2, 3], Lianjun Wu[1], Jinsong Liu[1], Gang Wu[2, 3]

[1]School and Hospital of Stomatology, Wenzhou Medical University, Wenzhou, China

[2] Department of Oral and Maxillofacial Surgery/Pathology, Amsterdam UMC and Academic Center for Dentistry Amsterdam (ACTA), Vrije Universiteit Amsterdam, Amsterdam Movement Science, Amsterdam, Amsterdam, The Netherlands

[3] Department of Oral Cell Biology, Academic Centre for Dentistry Amsterdam (ACTA), University of Amsterdam (UvA) and Vrije Universiteit Amsterdam (VU), Amsterdam, The Netherlands

[4] Department of Dentistry, Sir Run Run Shaw Hospital, School of Medicine, Zhejiang University, Hangzhou, Zhejiang, China

International Journal of Nanomedicine. 18 (2023) 369—383.

Abstract

Introduction: An antibacterial and pro-osteogenic coaxially-electrospun nanofiber guided bone regeneration (GBR) membrane was fabricated to satisfy the complicated and phased requirements of the GBR process.

Methods: In this study, we synthesize dual-functional coaxially-electrospun nanofiber GBR membranes by encapsulating parathyroid hormone (PTH) in the core layer and magnesium oxide nanoparticles (MgONPs) in the shell layer (MgONPs-PCL/PTH-PCL). Herein, the physicochemical characterization of MgONPs-PCL/PTH-PCL, the release rates of MgONPs and PTH, and the antibacterial efficiency of the new membrane were evaluated. Furthermore, the pro-osteogenicity of the membranes was assessed both *in-vitro* and *in-vivo.*

Results: We successfully fabricated a coaxially-electrospun nanofiber MgONPs-PCL/PTH-PCL membrane with the majority of nanofibers (> 65%) ranging from 0.40 ~ 0.60 μm in diameter. MgONPs-PCL/PTH-PCL showed outstanding antibacterial potential against *Escherichia coli* (*E. coli*) and *Staphylococcus aureus* (*S. aureus*) through the release of MgONPs. We also discovered that the incorporation of MgONPs significantly prolonged the release of PTH. Furthermore, both the *in-vivo* and *in-vitro* studies demonstrated that high dosages of PTH promoted pro-osteogenicity of the membrane to improve bone regeneration efficacy with the presence of MgONPs.

Conclusion: The new composite membrane is a promising approach to enhance bone regeneration in periodontitis or peri-implantitis patients with large-volume bone defects.

Keywords: antibacterial property; pro-osteogenicity; coaxially-electrospun; barrier membrane; guided bone regeneration

1. Introduction

The guided bone regeneration (GBR) technique is the most widely used surgical procedure that adopts barrier membranes and particulate bone-defect-filling materials to restore bone volume and dimensions surrounding natural teeth or artificial implants [1]. In the classic GBR concept, barrier membranes mainly function to prevent the invasion of surrounding connective tissues to provide a favorable microenvironment to facilitate osteoblast proliferation, migration, differentiation, and finally bone tissue regeneration [1]. However, the efficacy of GBR may be greatly challenged by many adverse conditions, such as inflammation and large-volume bone defects that are resulted from severe periodontitis or peri-implantitis [2,3]. On one hand, large-volume bone defects may largely surpass the spontaneous healing ability of bone tissue and will be healed only by connective tissues. One approach to this problem is the adoption of autologous bone chips, whose use is, whereas, associated with limited availability, donor site pain, and morbidity [4]. Furthermore, periodontitis or peri-implantitis-derived inflammation may further compromise the healing capacity of bone tissue [5,6]. On the other hand, residual bacteria that escape from the chemical and mechanical elimination procedures may rapidly proliferate and form biofilms, resulting in a series of complications, such as post-operative infection, bone graft exposure, and impeded bone regeneration [7]. In clinic, systemic administration of antibiotics is conventionally applied to combat these complications. However, its application is also associated with certain concerns, such as dysbacteriosis, poor biodistribution, toxicity, and bacterial resistance [8,9]. In recent years, multi-functionalized biomaterials used for GBR membranes with antibacterial and pro-osteogenic properties have shown promising application potential to cope with these complicated adverse conditions.

One of the commonly used approaches to synthesize a multi-functionalized membrane is coaxial electrospinning which involves the arrangement of multiple solution feed systems to simultaneously electrospun two or more polymer solutions to form core-shell structured nanofibers. This technique allows for the encapsulation of two different bioactive agents respectively into core and shell layers, enabling their sustained releases [10].

Due to the complexity of the oral flora, broad-spectrum antibiotics are frequently applied in the membrane in previous studies [11]. However, compared with clinically available antibiotics, antibacterial metallic nanoparticles are a promising alternative due to their significantly broader antimicrobial spectrum while lowering the risk of bacterial resistance [10,12]. Silver-based nanoparticles, a frequently used antibacterial metallic nanoparticle, are associated with several concerns, such as local accumulation of heavy metal elements causing cytotoxicity [13]. In contrast, magnesium oxide nanoparticles (MgONPs) possess biodegradability and lower toxicity [14]. Furthermore, the benefits of MgONPs, which include pro-osteogenic property [15] and significant inhibition of biofilm formation and maturation, have attracted increasing interest in membrane applications [14]. As for the pro-osteogenic drug applied in GBR membrane, PTH is a suitable candidate. As a commonly used drug for bone regeneration, PTH promotes osteogenesis by activating osteoblast cells and the secretion of SOST through the receptor PTHr1 [16,17]. Additionally, the cost of PTH is much lower than that of bone morphogenetic proteins, making it more readily available for clinical applications. At the same time, previous studies have proven that locally delivered PTH significantly promotes bone regeneration [16,18]. Moreover, Vetter *et al*. also demonstrated the synergistic effects of Mg and PTH in promoting bone regeneration [18]. Polycaprolactone (PCL) has been widely used as the scaffold in bone regeneration engineering [19,20], therefore, we applied PCL in the nanofiber as the main scaffold.

In this study, we aimed to synthesize dual-functional coaxially-electrospun nanofiber GBR membranes to achieve a sustained release by encapsulating PTH in the core layer and MgONPs in the shell layer (MgONPs-PCL/PTH-PCL). Herein, the physicochemical characterization of MgONPs-PCL/PTH-PCL, the release rates of MgONPs and PTH, and the antibacterial efficiency of the new membrane were evaluated. Furthermore, the pro-osteogenicity of the membranes was assessed both *in-vitro* and *in-vivo.* The scheme of preparation and functional assessments of MgONPs-PCL/PTHn-PCL coaxially-electrospun barrier membrane is listed in Fig. 1.

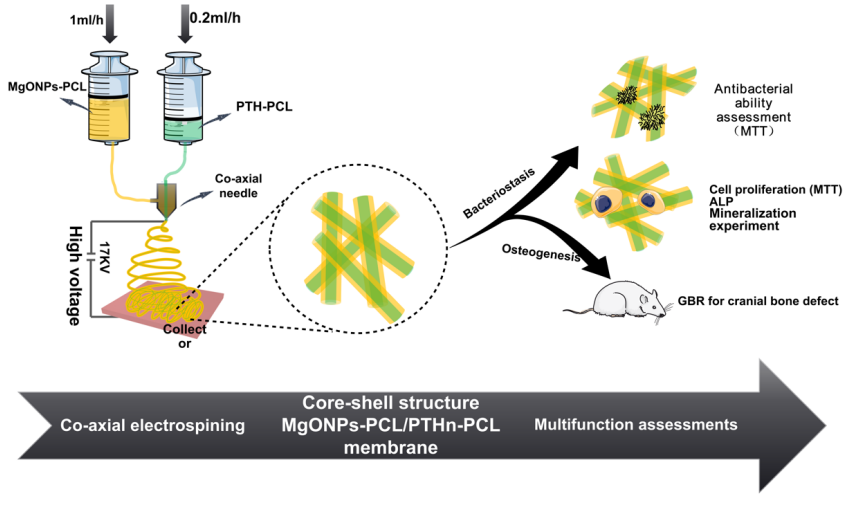

Figure. 1 Scheme of preparation and functional assessments of MgONPs-PCL/PTHn-PCL coaxially-electrospun barrier membrane.

2. Materials and methods

2.1 PCL and MgONPs-PCL/PTHn-PCL coaxial electrospinning barrier membrane preparation

In the coaxial electrospinning process, two needles of different gauge diameters were used. The diameter of the needle for the core layer was 0.33 mm and for the shell layer was 1.10 mm. The two needles were arranged concentrically to dispense two separate solutions at the same time. The base solution was made up of polycaprolactone (PCL, Mn 70,000–90,000) and 2,2,2-Trifluoroethanol (TFE, purity > 99.0) with a concentration of PCL at 150 mg/ml. The core solution was made by combining the base solution with different concentrations of PTH; the shell solution was made by mixing the base solution with or without MgONPs (nano-powder, diameter < 50 nm, PCL: MgONPs = 1:0.3). The concentration of MgONPs was altered by the pre-experiment results of SEM (supplementary data Fig. S1) and antibacterial assay (supplementary data Fig. S2). All the drugs were purchased from Sigma Aldrich. The voltage was 17 kV and the distance between the top of the needles and the receptor was 10 cm.

The feed rate for the core was 0.2 ml/h and for the shell it was 1 ml/h. The procedure was kept at room temperature for 7 h. The results of a scanning electron microscope (SEM) (Nova NanoSEM200, FEI Co., USA) and an antibacterial test were used to determine the optimum concentrations for the base solution and MgONPs. The PCL membrane was fabricated with only the base solution in the same electrospinning parameter of MgONPs-PCL/PTHn-PCL (n represented the different concentrations of PTH). The MgONPs-PCL/PTHn-PCL membrane was labeled as group B and the PCL membrane was labeled as group A.

2.2 Sample characterization

The surface morphology and surface elemental composition of PCL and MgONPs-PCL/PTHn-PCL membrane were assessed by Field-emission scanning electron microscopy (Nova NanoSEM200, FEI Co., Houston, TX, USA) coupled with Energy dispersive X-ray (EDX) spectroscopy. The pore size and nanofiber diameter distribution of each membrane were estimated by the software ImageJ (National Institutes of Health, Bethesda, MD, USA) from the representative SEM images. For calculating the pore size, the threshold function was applied to separate the pore area from the whole image. Subsequently, the analyze particles function was used to calculate individual pores. The quantitative analysis of EDX was selected randomly from the SEM results and repeated three times. The chemical groups of the materials were evaluated by FTIR (Equinox 55, Bruker Co., Germany). The XRD (D8 Focus, Bruker Co.) with operating settings of 35 kV and 30 mA was used to assess the crystalline phase in PCL and MgONPs-PCL/PTHn-PCL membranes. The data was collected at a scanning rate of 0.06°/s in the 2θ range of 10°~80°.

2.3 In-vitro evaluation of MgONP and PTH release kinetics

To test the release profiles of MgONPs *in-vitro*, group A and B (0.5 × 1.5 × 1.5 cm) were immersed individually in 10 ml of phosphate buffered solution (PBS) at 37°C and agitated at 100 rpm. At 1, 3, 5, 7, 9, 11, 13, 15, 17, 19, 21, 23, 25, 27, and 29 days, samples were removed from the solution and rinsed three times with fresh PBS before soaking in fresh buffer solutions of the same volume. Afterwards, the solutions were mixed with aqua regia solution in a 1:1

vol ratio to dissolve the MgONPs. The inductively coupled plasma-atomic emission spectroscopy (ICP-AES, OPTIMA8000, PerkinElmer, USA) was used to examine the magnesium ion concentration of solutions. The accumulative magnesium ion concentration was calculated using the formula: $c=(c_1-c_0)+(c_2-c_0)+(c_3-c_0)+\ldots(c_n-c_0)$. c refers to the accumulative magnesium ion concentration; c_1 refers to the magnesium ion concentration of the solution on day 1; c_2 refers to the magnesium ion concentration of the solution on day 3 and so on; c_0 refers to the magnesium ion concentration of the fresh PBS solution.

The MgONPs released from the MgONPs-PCL/PTHn-PCL coaxial electrospinning barrier membrane were exactly proportional to the accumulative magnesium ion concentration. PTH was substituted by the model protein bovine serum albumin, which had been conjugated with fluorescein isothiocyanate (FITC-BSA, sigma), marked as group C (PCL/ FITC-BSA-PCL) and group D (MgONPs-PCL/ FITC-BSA-PCL). To evaluate the release kinetics of PTH from the membrane, 6 μg of FITC-BSA was added to the core of the nanofibers of the membrane. The samples of group C and group D were immersed in 10 ml PBS solution, respectively. Subsequently, the process of group A and group B samples was repeated for Group C and D. According to the methodology reported previously, the spectrophotometer was used to examine the sampled solutions of groups C and D [21]. In each group, three replicates were set.

2.4 Antibacterial efficacy of PCL and MgONPs-PCL/PTH-PCL Coaxial electrospinning Barrier

All the samples used in antibacterial ability tests, cell experiments, and animal experiments were sterilized by submerging them in a 75% ethyl alcohol solution for 1 h and then drying them before use. The entire procedure was carried out on a clean bench with laminar flow.

S. aureus (gram-positive bacteria) and *E. coli* (gram-negative bacteria) were used to test the antibacterial efficacy of PCL and MgONPs-PCL/PTH-PCL. The method was used in our earlier study with modification [22]. Briefly, samples (φ= 14 mm) were separated into groups, co-cultured with 500 μl *S. aureus* (ATCC 25923) or *E. coli* (ATCC 25922) (1×10^6 CFU/ml) buffer solution and

500 μl Luria-Bertani culture and agitated at 100 rpm at 37°C for 24 h. After that, the samples were removed and rinsed three times with fresh PBS.

The bacterial viability was detected by 3-(4, 5-dimethylthiazol-2-yl)-2, 5-diphenyltetra-zolium bromide (MTT assay, Aladdin, Shanghai, China). 200 μl of each co-culture solution was put into a 1.5 ml centrifuge tube, along with 20 μl of MTT (0.5 mg/ml) stock solution, manually mixed for 10 s, and incubated for 20 min at 37°C. The mixture was centrifuged, and the supernatant was removed. Using a pipette, added 150 μl DMSO (AR, Aladdin, Shanghai, China) into the pellets of the cell-formazan crystal complex. Afterwards, we transferred the mixtures to 96-well plates and used a microplate reader (Bio-Rad Model 680, US) to detect absorbance at 540 nm [23]. DMSO was applied as a control. In each group, three replicates were set.

2.5. Effect of PCL and MgONPs-PCL/PTH-PCL coaxial electrospinning barrier membrane on osteoblast proliferation, differentiation, and Mineralization

The pure PCL membrane and MgONPs-PCL/PTH-PCL membranes (φ=14 mm) with varied concentrations of PTH were separated into distinct groups and indicated in cell tests. According to the results of the pre-experiment, we screened out two concentrations (20 μg/ml and 40 μg/ml) of PTH with significant differences in cell experiments (supplementary data Fig. S3); labeled them as MgONPs-PCL/PTH20-PCL and MgONPs-PCL/PTH40-PCL, respectively. It was divided into four groups: A (MgONPs-PCL/PTH20-PCL), B (MgONPs-PCL/PTH40-PCL), C (MgONPs-PCL/PCL), and D (PCL). The mouse embryonic precursor osteoblast cells (MC3T3-E1 cells, ATCC, Chinese Academy of science, Shanghai, China) were cultured in alpha-minimum essential medium (α-MEM) with 10% fetal bovine serum (FBS) (Gibco, Invitrogen, Grand Island, NY, USA), 10 μg/ml penicillin, 10 μg/ml streptomycin, and 50 μg/ml fungizone (complete medium) under the condition of 5% CO_2, at 37°C. The medium was changed every 3 days. When the cell confluence reached about 80% - 90%, cell passage was carried out. 0.25% trypsin and 0.1% EDTA were used for harvesting osteoblasts. Cells were then seeded onto 4 groups of membranes at 2 × 10^4 cells/well, respectively, and cultured in a Petri dish with complete medium.

2.5.1 Cell proliferation assay

The proliferation of MC3T3-E1 seeded on the different membranes was detected using Cell Counting Kit-8 reagent (CCK-8, Beyotime Biotechnology, Shanghai, China) by measuring absorbance after incubation for 4 and 7d. MC3T3-E1 cells were seeded on different membranes at a density of 2 × 10^4 cells/well in the 24-well culture plates. After culturing for 4 and 7 days, the medium was removed, cells were rinsed with PBS and incubated with 10% CCK-8 for 2 h at 37°C in the dark. Afterwards, 100 μl solution of each well was taken out and added to the 96-well culture plates. The absorbance value was determined at an optical density of 490 nm using a Bio Rad microplate reader (Bio-Rad 680, USA). Four replicates were set in each group.

2.5.2 Alkaline phosphatase (ALP) activity characterization

MC3T3-E1 cells were seeded on different groups in α-MEM at a concentration of 2 × 10^4 cells/well. After incubation for 24 h in the 24-well culture plates, the α-MEM was replaced by a mineralized induction medium (supplemented with 10 mmol/l β-glycerophosphate, 0.05 mmol/l acetic acid, and 100 mmol/l dexamethasone) and it was changed every 3 days in the following process. The membranes and cells were cultured in the mineralized induction medium for 7 d. MC3T3-E1 cells on different membranes were lysed by 1% Triton X-100 at 0°C for 30 min. Then, the lysates were measured via LabAssayTM ALP colorimetric assay kit (Wako Pure Chemicals, Japan), and the total intracellular protein content was tested by BCA Protein Assay Kit (Beyotime, China). In each group, four replicates were set.

2.5.3 Mineralization measurement

For the measurement of calcium deposits, MC3T3-E1 cells were cultured on different membranes in mineralized induction medium (quadruplicates per group) for 14 days. The medium culture was freshly changed every 3 days. After 14 days of culture on four groups of membranes, MC3T3-E1 cells were rinsed with fresh cold PBS and fixed using 4% paraformaldehyde solution for 30 min. Subsequently, extracellular matrix mineralization was evaluated by alizarin red staining (ARS, Solarbio, China). The dyed calcium nodules were

finally dissolved in 10 wt% cetylpyridinium chloride solution and measured by a Bio Rad microplate reader at OD540 nm.

2.6 The assessment of bone reconstruction promoting effect of PCL, MgONPs-PCL/PCL, and MgONPs-PCL/PTH-PCL coaxial electrospinning membrane in-vivo

2.6.1 Animals

In a pathogen-free environment, sixteen male Sprague-Dawley rats (Animal Centre, Wenzhou Medical University, 200 - 300g) were housed in pairs. The rats were acclimated to a regular rat chow diet, tap water, and a controlled temperature (25°C, relative humidity of 45–62%, and a 12 h light-dark cycle). Animals were cared in accordance with the ethical guidelines of the Wenzhou Medical University Animal Care and Use Committee. The Animal Experimental Ethical Panel, Wenzhou Medical University, accepted the study protocol (Approval number: wydw2019-0658).

2.6.2 Implantation procedure

After a week of acclimation, 16 rats were placed into four groups randomly. Briefly, the rats were anesthetized by intraperitoneal injections of 10% chloral hydrate (3.3 ml/kg). All the defects were 8 mm in diameter and were smooth punched with burs. As previously described [24], critical size defects were created in calvaria, membranes were cut to the same size (φ = 10 mm), and S. aureus (1×10^6 CFU/ml, 10 μl) was mixed with deproteinized bovine bone mineral (DBBM, Geistlich Trading (Beijing) Co. Ltd, China, 0.2 g) and divided into four groups: A.PCL + DBBM + S. aureus, B.MgONPs-PCL/PCL + DBBM + S. aureus, C.MgONPs-PCL/PTH20-PCL + DBBM + S. aureus and D.MgONPs-PCL/PTH40-PCL+DBBM+S. aureus. We implanted the four different groups of grafts into the defects separately and closed the wound with tight suture. A month after implantation, the rats were sacrificed and the calvaria bone was harvested. The calvarial specimens were fixed in 4% paraformaldehyde (Yili FineChemical Co., Ltd, China) for 48 h. Micro-CT and histological analysis were used to assess the samples.

2.6.3 Micro-CT Analysis

A micro-CT scanner (μCT100, SCANCO Medical AG, Switzerland) was used to monitor the samples for new bone regeneration in the defect areas. For qualitative and quantitative evaluation, about 300 binary images were rebuilt into three-dimensional images. The bone volume/total bone ratio (BV/TV), trabecular thickness (Tb.Th), trabecular number (Tb.N), and trabecular separation (Tb.Sp) were calculated to detect the quality and quantity of new bone in different groups.

2.6.4 Histology sample preparation

After micro-CT scanning, 10% EDTA solution was applied for the demineralization of calvarial specimens, and the solution was replaced every day for 3 months. The samples were grade dehydration using an ethanol series, which further replaced by a xylene, and routinely embedded in paraffin. A sliding microtome (EXAKT300CP, Germany) was used to cut the specimens. The thickness of paraffin sections was set to 5 μm. Hematoxylin and Eosin (H&E) staining was used on the central sections of each defect. The Leica DMI4000B microscope was used to examine them in sagittal perspectives. Quantity analysis of the samples (new bone surface/ graft materials surface) were analyzed by Image J.

2.7. Statistical analysis

Data are presented as the mean ± standard deviation (SD). Statistical analysis was performed by one-way analysis of variance (ANOVA). Data normality was tested with a Shapiro-Wilk test ($p < 0.05$). Homogeneity of variance was tested with a Levene's test ($p < 0.01$). Post hoc Bonferroni was performed. If normality was violated a Kruskall Wallis test was performed. Data were analyzed using Graphpad Prism® 7.5 (GraphPad Software Inc., La Jolla, CA, USA). Difference at $p < 0.05$ was considered to be significant.

3. Results and Discussion

3.1. Physicochemical characterization

3.1.1. SEM and EDX observation

The representative SEM morphology of pure PCL and MgONPs-PCL/PTH-PCL composite membranes were depicted in Fig. 2A1 and A2, respectively. The surface morphology of both membranes was composed of randomly oriented fibers without bead-like structure, indicating the successful fabrication of the electrospun nanofibers. The fibers in pure PCL (Fig. 2A1) were smooth, while those in the composite membrane (Fig. 2A2) exhibited some lumps, which may be due to the occasional aggregation of MgONPs [25,26]. The diameter size distribution of nanofibers in each membrane was measured from the micrographs and listed in Fig. 2B1 and B2, respectively. The fiber diameter of pure PCL was at a range of 0.22 ~ 2.06 μm and that of MgONPs-incorporated membrane was 0.33 ~ 1.51 μm. The majority of nanofibers (> 65%) that ranged from 0.40 ~ 0.60 μm in diameter, has been proved by Chen *et al.* to be more optimal in promoting cell adhesion and proliferation [27]. The pore sizes of pure PCL and the composite membrane were 0.99 ± 0.12 μm and 1.30 ± 0.18 μm, respectively, which could provide a sufficient barrier function since the pore sizes < 10 μm had been shown to efficiently prevent the invasion of surrounding connective tissue-derived fibroblasts and bacteria through the membrane [25,28]. Simultaneously, this also allowed the passage of essential chemicals and nutrients for bone regeneration [29]. The representative EDX spectra of the membranes were listed in Fig. 2C1 and C2. Compared with pure PCL membrane, the composite membrane exhibited the presence of peak corresponded to Mg element and increased intensity of peak corresponded to O element (Fig. 2C1), which indicated the incorporation of MgONPs in PCL (Fig. 2C2). In addition, the quantitative EDX analysis of three randomly selected areas from the composite membranes was listed in Table 1. The data showed that the weight percentages of Mg in three different areas were 14.92%, 15.27%, and 15.35%, respectively. In the meantime, the atomic percentages were 8.50%, 8.72%, and 8.78%, respectively. The similar intensities of Mg peaks in the composite membrane revealed the homogeneous distribution of MgONPs.

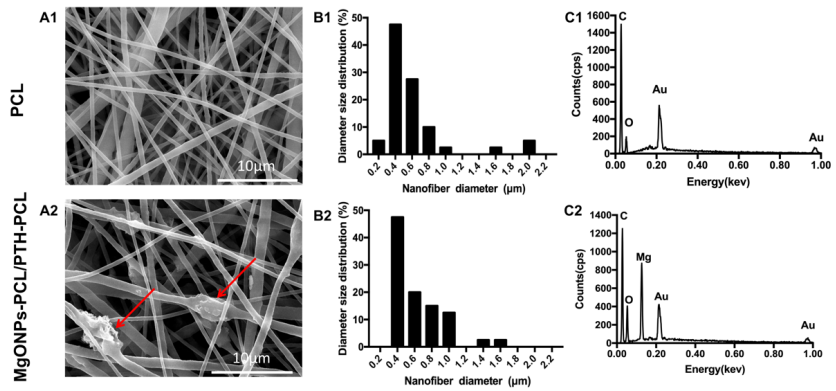

Figure. 2 SEM image, fiber diameter distribution and EDX spectra of PCL and MgONPs-PCL/PTH-PCL membranes.

Element	Area 1		Area 2		Area 3	
	Wt%	At%	Wt%	At%	Wt%	At%
C	62.11	71.62	61.56	71.17	61.02	70.67
O	22.97	19.88	23.17	20.11	23.63	20.55
Mg	14.92	8.50	15.27	8.72	15.35	8.78

Table 1. Quantitative EDX analysis of different areas in MgONPs-PCL/PTH-PCL composite membrane (wt%: weight percent, At%: atom percent).

3.1.2 XRD and FTIR test

The FTIR spectra of the membranes were exhibited in Fig. 3A. The FTIR spectrum of pure PCL fiber (black curve) exhibited the stretching vibration at 2949, 2864, 1727, 1297, and 1241 cm^{-1}, which corresponded to asymmetric CH_2 stretching, symmetric CH_2 stretching, carbonyl stretching, C-O and C-C stretching in the crystalline phase, and asymmetric COC stretching, respectively [29,30]. These characteristic bands of PCL accordingly occurred

at 2941, 2873, 1724, 1299, and 1243 cm^{-1} in the composite membrane. The spectrum of MgONPs exhibited the stretching vibration at 870 cm^{-1}, which corresponded to Mg-O bands [31]. The characteristic bands of PTH exhibited the stretching vibration at 1548 and 1646 cm^{-1}, which corresponded to amide bands [32]. The absorption peak of MgONPs (red curve) was not very prominent due to its much lower intensity than those of PCL. The XRD patterns of the pure PCL and MgONPs-PCL/PTH-PCL composite membranes were shown in Fig. 3B. The pure PCL displayed two intense and sharp diffraction peaks at 21.6° and 23.9° 2θ, which were attributed to the orthorhombic crystal structure of semi-crystalline PCL [33]. In addition of the characteristic peaks of PCL, the presence of MgONPs in the composite membrane resulted in the occurrence of two sharp diffraction peaks at 43.0° and 62.1°, which corresponded to its crystallographic planes [33]. The intensity of both the PCL peaks at 21.6° and 23.9° in the composite membrane decreased, which may be due to the incorporation of hydrophilic MgONPs and PTH leading to a decrease in the degree of crystallinity of PCL [34,35]. All these results indicated that MgONPs and PTH were successfully incorporated into PCL fibers.

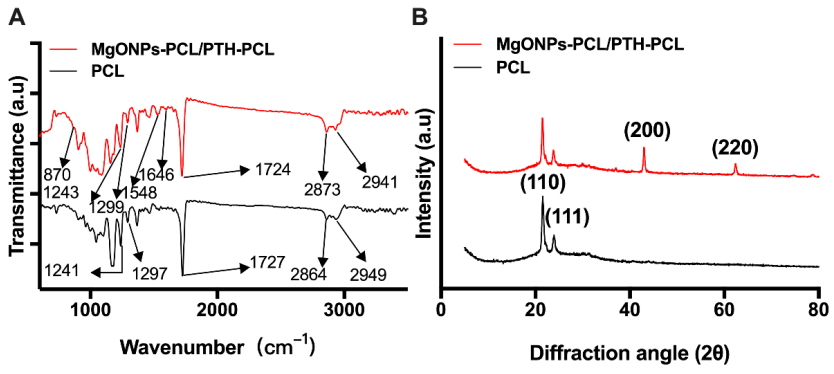

Figure. 3 (A) FTIR absorption spectroscopy and (B) XRD spectroscopy of PCL and MgONPs-PCL/PTH-PCL.

3.2 Biological evaluation

3.2.1 PTH and MgONPs release profiles in-vitro

Fig. 4A depicted the 29 days accumulative release profiles of MgONPs from different membranes. The observed release profile of MgONPs from the MgONPs-PCL/PTH-PCL membrane comprised of two distinct phases: the initial burst release on the first day (stage I) and a sustained release (stage II). At the initial stage, a concentration of approximately 29.57 ± 1.53 µg/ml (14%) of MgONPs was released. This phenomenon may be attributed to the quick detachment of superficially distributed MgONPs on the nanofiber, resulting in a burst release [34]. Joyshree *et al.* claim that MgONPs at a concentration of 7.50 µg/ml is sufficient to eliminate both gram-negative and gram-positive bacteria [36]. Furthermore, a previous study has also proposed that MgONPs at a concentration lower than 500 µg/ml are not cytotoxic [37]. This indicated that the abrupt release of MgONPs at stage 1 (within 24 h) would contribute to eliminate the residual bacteria in periodontal tissues, thus preventing post-operative infections. Conversely, it was apparent that there was a sustained release of MgONPs for the remaining period at stage II with an average rate of 2.35% per day. This would aid in the inhibition of new bacterial invasion. According to the consensuses of the 15th European Workshop on Periodontology on Bone Regeneration, exposure tolerance of GBR membrane is one of the basic requirements [38]. The early exposure of GBR membrane significantly compromises the regenerative outcomes of GBR [38]. Exposure tolerance is defined as “In case of exposure, the exposed membrane should be kept in situ and continue to function during the regenerative process, although in case of overt infections.”[38] In contrast to the limited exposure tolerance of commercially available GBR membranes [39], the slow and sustained release of MgONPs and the low degradation rate of PCL (at pH= 7, the PCL membrane just lose 11% of the initial weight after 50 days degradation in PBS)[40] made MgONPs-PCL/PTH-PCL membrane possible to achieve exposure tolerance in the first month after implantation. Systemic administration of antibiotics and antiseptic mouthwash applied for a month post-operation were commonly used to prevent subsequent bacterial contamination for bone grafts through exposed wounds [41]. The exposure tolerance of the membranes exhibited the potential

to replace conventional methods, thereby avoiding the side effects such as drug resistance or disorders of normal oral flora.

To analyze the release profile of PTH, we utilized the FITC-BSA conjugate as a model protein [42]. The accumulative release profiles of FITC-BSA from different membranes *in-vitro* for 29 days were listed in Fig. 4B. FITC-BSA released from the membranes within 24 h at rates of 8.58 ± 1.40% (MgONPs-PCL/FITC-BSA-PCL) and 21.95 ± 5.02% (PCL/FITC-BSA-PCL) per day of the total amount of encapsulated FITC-BSA, respectively. The FITC-BSA in the core layer can easily diffuse through the shells of nanofibers, resulting in the initial burst release [43]. Interestingly, the release profiles of FITC-BSA in different membranes showed a significant difference. The cumulative release percentage of FITC-BSA from the PCL/FITC-BSA-PCL membrane on day 29 was 70.83 ± 2.26%, whereas only 27.16 ± 4.38% of FITC-BSA was released from the MgONPs-PCL/FITC-BSA-PCL membrane. Ajay *et al.* indicate that the degradation of the PCL membrane will slowly release chain oligomers with acidic carboxyl groups, causing slight acidification [40] in the surrounding milieu, which may reversely accelerate PCL degradation. It has been shown that the release and degradation of MgONPs will first cause a steep rise of pH to 8.1 and subsequent decrease at a slow rate, finally settling near 7.6 [44]. Therefore, MgONPs-incorporation may regulate the release of PCL and thus FITC-BSA through neutralizing the pH of the surrounding milieu [40]. Thereby regenerated slow release of incorporated PTH was good to prevent bone resorption [45]. Additionally, the neutralized pH of the surrounding milieu prevented the negative effect on bone formation resulting from the acid environment [46]. The release periods of PTH applied in the local delivery system in previous studies were limited in 2 weeks [32,47], which was unable to cover the whole osteogenesis process (4 weeks) [48], thereby may compromise the efficacy of GBR. Conversely, according to the result of FITC-BSA release profile of MgONPs-PCL/FITC-BSA-PCL membrane, there was approximately 70% FITC-BSA in storage at the end of the release study (29 days), which satisfied the long-term osteogenesis process.

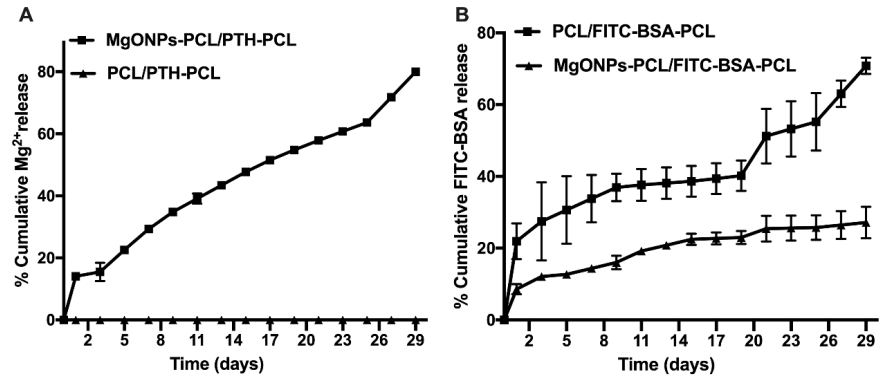

Figure. 4 The release profiles of (A) Mg^{2+} and (B) FITC-BSA from different membranes for 29 days.

3.2.2 In-vitro antibacterial efficacy

G. Rutger *et al.* demonstrate that T. forsythia and S. aureus are associated with peri-implantitis [49]. Ter Boo *et al.* declaim that gram-positive (such as *S. aureus* and S. epidermidis) and gram-negative (such as Pseudomonas aeruginosa and *E. coli*) bacteria are present in infected bone defects [50]. Hence, the antibacterial agent applied in the membrane should have a broad spectrum. For this purpose, we adopted two most widely used bacteria — *S. aureus* and *E. coli* to evaluate the antibacterial effect on gram-positive and gram-negative bacteria, respectively. Additionally, Gabrijela *et al.* indicate that the bacteria adhesion on the membrane, which is considered a crucial initial stage for the formation of a biofilm, occurs in 4 h [51]. Therefore, the elimination of residual bacteria in the initial 24 h was crucial for high efficacy of GBR. Based on this, we further evaluated the antibacterial efficacy of the membranes with or without MgONPs, which were co-cultured with bacteria for 24 h using an MTT assay and listed it in Fig. 5. Our data showed that MgONPs-PCL/PTH-PCL killed 95.04% *S. aureus* and 88.76% *E. coli* after incubation for one day. In contrast, the non-MgONPs-containing membrane exhibited no significant antibacterial effect, instead, both types of bacteria proliferated in the presence of PCL/PTH-PCL membranes and culture medium. The dramatic reversal of antibacterial efficacy between the two membranes may attribute to the reactive

oxygen species (ROS) of MgONPs. The free Mg^{2+} ions produced from the nanoparticle induced the uncontrolled ROS generation in bacteria, resulted in excessive oxidative stress, distorted cellular membrane, leakage of proteins, carbohydrates, and lipids, and eventually bacteria damage [52]. Hence, MgONPs-PCL/PTH-PCL was suggested as a promising candidate for preventing post-operative infection.

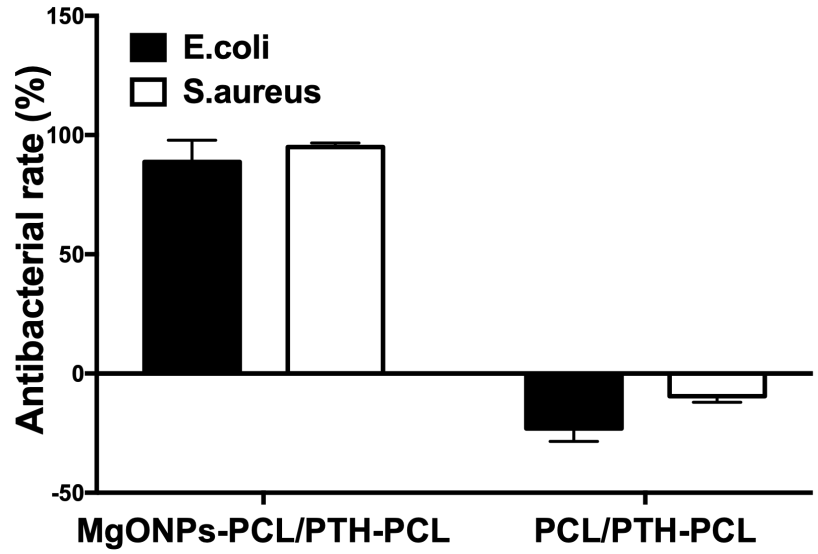

Figure. 5 Antibacterial effects of MgONPs-PCl/PTH-PCL and PCL/PTH-PCL against *S. aureus* and *E. coli.* Values are mean ± SD from 3 independent experiments.

3.2.3 The effect of MgONPs-PCL/PTH-PCL membrane on in-vitro osteoblastic activity

One desired property of the MgONPs-PCL/PTH-PCL membrane for GBR technique is to promote the proliferation and osteogenic differentiation of osteogenic cells. One potential contributor to this property may be the

MgONPs-derived Mg, that has been shown to stimulate the proliferation of osteoblasts [53]. On the other hand, overdosed MgONPs may be detrimental to cell viability by blocking DNA synthesis and cell cycle processes [54]. Therefore, a proper incorporation amount of MgONPs is highly important. In fact, the amount of incorporated MgONPs is mainly determined by the fabrication process and the antibacterial efficacy of MgONPs-PCL/PTH-PCL membrane. A relatively higher amount will result in high inhomogeneity with extensive bead-like structure on the nanofibers (supplementary data Fig. S1), while a relatively lower amount may not be sufficient to yield adequate antibacterial efficacy (supplementary data Fig. S2). In our preliminary study, we screened the optimal dosage of MgONPs by assessing the morphology and antibacterial property, from which we determined the ratio of PCL: MgONPs at 1:0.3. With this dosage, the OD value of MC3T3-E1 pre-osteoblasts seeded on MgONPs-PCL/PCL was slightly higher than that seeded on pure PCL membrane (Fig. 6A), which suggested no significant cytotoxicity of MgONPs at the current dosage. Albeit so, we did find that the presence of MgONPs was associated with significantly enhanced ALP activity — the early osteogenic differentiation markers (Fig. 6B). One potential mechanism accounting for this promoting effect may be due to the MgONPs-derived Mg^{2+} triggered upregulation of Akt phosphorylation and enhanced expression of osteogenic related genes [55]. Additionally, MgONPs-derived OH^- stimulated the release of bone morphogenetic protein 2 and alkaline phosphatase [56]. However, MgONPs at the current dosage failed to significantly enhance extracellular matrix mineralization — the early osteogenic differentiation markers. To approach this problem, we adopted PTH to further enhance the pro-osteogenic property of the membrane. We showed that MgONPs-PCL/PTH20-PCL did significantly enhance cell proliferation (Fig. 6A), ALP activity (Fig. 6B), and extracellular matrix mineralization (Fig. 6C) in comparison with both the pure PCL membrane and the MgONPs-PCL/PCL membrane. The potential mechanism accounting for this enhancing effect may be attribute to PTH can stimulate the expression of osteoblast-specific transcription factors, thus promoting the proliferation and differentiation of osteoblasts [57,58]. Mediated by PTH1R in early differentiated osteoblasts, PTH inactivates the proapoptotic factor Bad and the apoptosis-inducing factor CARP-1, while increasing the

expression of Bcl-2 and enhancing DNA repair, thus reducing osteoblast apoptosis [59].

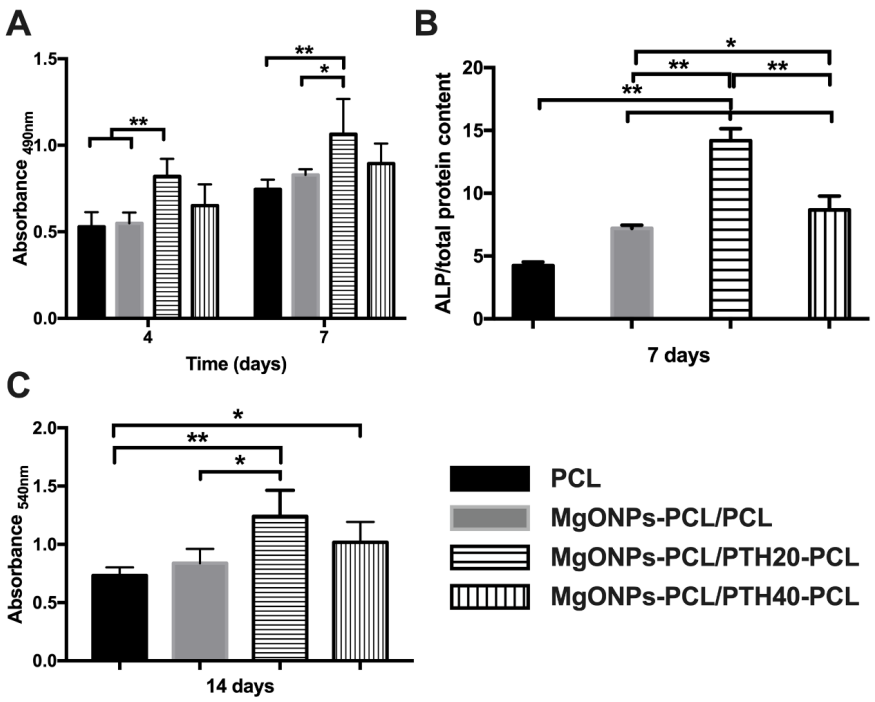

Figure. 6 The effects of PCL and MgONPs-PCL/PTHn-PCL membranes on (A) Proliferation of MC3T3-E1 cells, (B) Relative ALP activities of MC3T3-E1 cells and (C) Quantitatively detect of mineralization of MC3T3-E1 cells. Significant effect of treatment, $^{**}p < 0.01$, $^{*}p < 0.05$.

3.2.4 Micro-CT observation

Calvarial bone defect in SD rats is one of the most widely used models to assess the osteogenic efficacy of biomaterials [60]. In previous literature, 8-mm-in-diameter calvarial bone defects are regarded as critical-size bone defects with a maximum 10% healing within 13 months [24,61]. In this study, we adopted the 8-mm-in-diameter calvarial bone defects to assess the osteogenic potential of MgONPs-PCL/PTH-PCL membranes in bacteria-contaminated defects.

4 weeks post implantation, the implanted materials and surrounding tissues were retrieved, fixed, and subjected to micro-CT analysis. In comparison with histological evaluation, Micro-CT is superior in both qualitatively and quantitatively evaluating the microstructure and mineral density of mineralized tissues [62,63]. As shown in the representative 3D reconstructed Micro-CT images of the pure PCL group, the defects remained partially unfilled and largely unhealed with part of transplanted DBBM particles dislocated out of defects (Figure 7). In comparison, the addition of MgONPs resulted in significantly increased BV/TV and BV, as well as significantly decreased Tb.Sp and DBBM dislocation, which might be due to the inhibition of bacterial activities of MgONPs. Interestingly, further significant improvement in BV/TV, Tb.N, and Tb.Sp. was detected not in the group of MgONPs-PCL/PTH20-PCL but in the group of MgONPs-PCL/PTH40-PCL. This was inconsistent with our *in-vitro* cell result where MgONPs-PCL/PTH20-PCL but not MgONPs-PCL/PTH40-PCL resulted in significantly enhanced osteogenic differentiation of MC3T3-E1 cells. This was not unreasonable since the optimal dosage of bioactive agents in the in-vivo model is often higher than that in the *in-vitro* model [58,64]. Furthermore, the presence of bacteria in this *in-vivo* model might also partially deactivate PTH, which necessitates a higher concentration to exhibit significant efficacy.

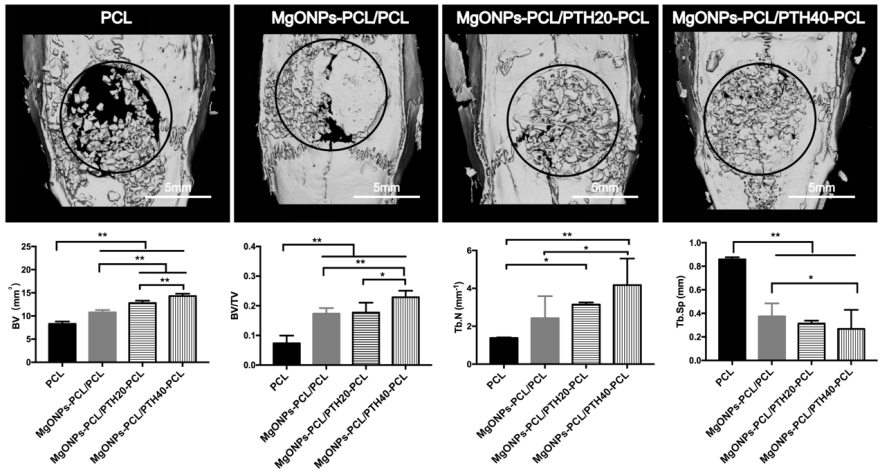

Figure. 7 Representative 3D micro-CT images of infective cranial bone defect rats with GBR process covering with different membranes from overall at week 4 post-operatively (The surgical regions are marked by black circle). Datas of the selected regions are evaluated by micro-CT. Quantity analysis: Bone volume/Total volume (BV/TV), Bone volume (BV), Trabecular number (Tb. N) and Trabecular separation (Tb. Sp). Significant effect of treatment, $*p < 0.05$, $**p < 0.01$.

3.2.5. Histological assessment

We further adopted histological observations and histomorphometric analysis to assess the newly formed bone tissue [65]. DBBM are deproteinized, decellularized, and sintered bovine cancellous bone chips and its major component is hydroxyapatite [66]. Due to its excellent biocompatibility and osteoconductivity, DBBM is one of the most frequently used materials in GBR technique [67]. After demineralization in the histological process, most of DBBM was dissolved, showing a morphology of vacuole. In some of the vacuoles, the undissolved DBBM formed an isolated island. In the group of PCL membrane, most of the vacuoles were surrounded by dense fibrous connective tissues. In the group of MgONPs-PCL/PCL, the fibrous newly formed tissue surrounding

the vacuoles appeared to be less dense and there were some islands of new bone distributed within the connective tissues. There seemed no direct contact between new bone and vacuoles. In the two PTH-containing groups, more new bone tissues were detected and formed direct contact with vacuoles. It seemed to be that the PTH-containing groups achieved a better bone-formation activity, thereby the presence of the osseous tissue suppressed the fibrous encapsulation of the DBBM. The quantity analysis of the new bone as a ratio of the graft material (new bone surface/entire graft materials surface; NB/GM) was calculated by ImageJ (National Institutes of Health, Bethesda, MD) software according to Young's study [68], which was used to assess the osteogenesis efficacy. Consistent with the micro-CT finding, the histomorphometric analysis showed a slight promotion of NB/GM in MgONPs-PCL/ PCL while significant promotion of that in the two PTH-containing groups compared with PCL. Furthermore, although there was no significant difference between the two PTH-containing groups, the MgONPs-PCL/PTH40-PCL group showed a significant promotion compared with MgONPs-PCL/ PCL group. It suggested that the osteogenesity of the MgONPs-PCL/PTH40-PCL membrane was mainly attributed to the incorporation of PTH. The existence of MgONPs mainly acted as an antibacterial agent thus assisting osteogenesity. Similar osteogenesis effects have also been observed by incorporating PTH in local drug delivery systems, for instance, PTH-bound PEG hydrogel, PTH-fibrin matrix, and PTH-incorporated CaP coating [32,47,69], which indicated the local delivery system with an appropriate PTH dosage was a promising strategy for achieving osteogenesis.

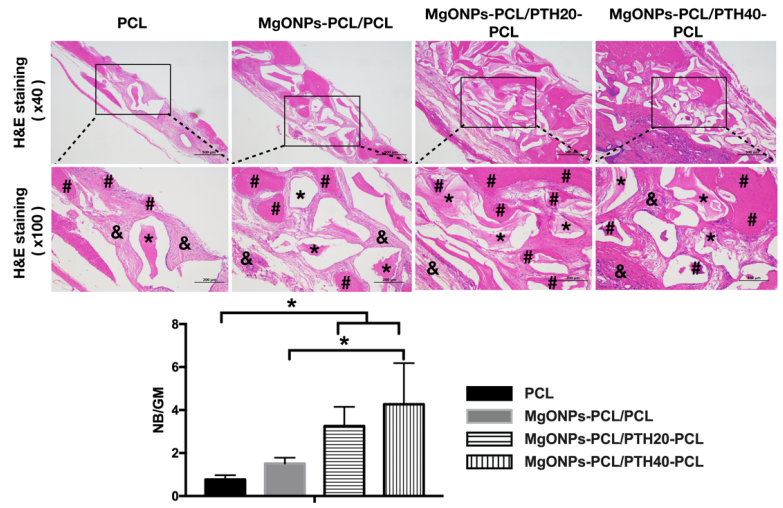

Figure. 8 H&E staining of infective cranial bone defect rats with GBR process covering with different membranes at week 4 post-operatively. DBBM granules (*), new bone (#) and loose connective tissue (&) were marked in different groups H&E staining images. Quantity analysis of new bone as a percentage of graft material (new bone surface /entire graft materials surface; NB/GM). Significant effect of treatment, *$p < 0.05$.

4. Conclusion

In this study, we have successfully synthesized a dual-functional nanofiber GBR membrane with antimicrobial and pro-osteogenic properties. The coaxial electrospinning procedure was used and successfully encapsulate a broad-spectrum antibacterial (MgONPs) agent in the shell layer and a pro-osteogenic drug (PTH) in the core layer of the nanofibers. The sustained release of MgONPs and PTH significantly promoted antibacterial properties, which were shown *in-vitro.* This indicated that the membrane could effectively eliminate the residual bacteria in periodontal tissues. Furthermore, the results of release profiles and antibacterial assessments of the GBR membrane indicated its exposure tolerance for the first month after implantation. This would contribute to prevent GBR failure caused by early exposure. The significant improvement of osteogenesis in bacterial-contaminated models *in-vivo,* especially with the presence of high dosage PTH, proved to be a promising approach to satisfy the complicated and phased requirements of the GBR process in periodontitis or peri-implantitis patients with large-volume bone defects. In-depth mechanism research for the MgONPs and PTH interaction in micro-environment for the infection-defect bone area still needs further work.

Acknowledgments

Authors acknowledge financial support provided by Wenzhou Municipal Science and Technology Project for Public Welfare (No. Y20190107 and No.2019Y0597).

Disclosure

The author reports no conflicts of interest in this work.

References

[1] M.C. Bottino, V. Thomas, G. Schmidt, Y.K. Vohra, T.M.G. Chu, M.J. Kowolik, G.M. Janowski, Recent advances in the development of GTR/GBR membranes for periodontal regeneration-a materials perspective. Dental Materials. 28 (2012) 703–721. https://doi.org/10.1016/j.dental.2012.04.022.

[2] J.M. Latimer, S. Maekawa, Y. Yao, D.T. Wu, M. Chen, W. v. Giannobile, Regenerative medicine technologies to treat dental, oral, and craniofacial defects. Frontiers in Bioengineering and Biotechnology. 9 (2021) 637. https://doi.org/10.3389/fbioe.2021.704048.

[3] Z. Sheikh, N. Hamdan, Y. Ikeda, M. Grynpas, B. Ganss, M. Glogauer, Natural graft tissues and synthetic biomaterials for periodontal and alveolar bone reconstructive applications: A review. Biomaterials Research. 21 (2017) 1–20. https://doi.org/10.1186/s40824-017-0095-5.

[4] A. Stahl, Y.P. Yang, Regenerative approaches for the treatment of large bone defects. Tissue Engineering-Part B: Reviews. 27 (2021) 539–547. https://doi.org/10.1089/ten.teb.2020.0281.

[5] E. Shoba, R. Lakra, M.S. Kiran, P.S. Korrapati, 3D nano bilayered spatially and functionally graded scaffold impregnated bromelain conjugated magnesium doped hydroxyapatite nanoparticle for periodontal regeneration. Journal of the Mechanical Behavior of Biomedical Materials. 109 (2020) 103822. https://doi.org/10.1016/j.jmbbm.2020.103822.

[6] R. Zhang, J. Yang, J. Wu, L. Xiao, L. Miao, X. Qi, Y. Li, W. Sun, Berberine promotes osteogenic differentiation of mesenchymal stem cells with therapeutic potential in periodontal regeneration. European Journal of Pharmacology. 851 (2019) 144–150. https://doi.org/10.1016/j.ejphar.2019.02.026.

[7] S. Calamak, R. Shahbazi, I. Eroglu, M. Gultekinoglu, K. Ulubayram, An overview of nanofiber-based antibacterial drug design. Expert Opinion on Drug Discovery. 12 (2017) 391-406. https://doi.org/10.1080/17460441.2017.1290603.

[8] G. Isola, A. Polizzi, S. Santonocito, D. Dalessandri, M. Migliorati, F. Indelicato, New frontiers on adjuvants drug strategies and treatments in periodontitis. Scientia Pharmaceutica. 89 (2021) 46. https://doi.org/10.3390/scipharm89040046.

[9] P. Makvandi, U. Josic, M. Delfi, F. Pinelli, V. Jahed, E. Kaya, M. Ashrafizadeh, A. Zarepour, F. Rossi, A. Zarrabi, T. Agarwal, E.N. Zare, M. Ghomi, T. Kumar Maiti, L. Breschi, F.R. Tay, Drug delivery (nano)platforms for oral and dental applications: Tissue regeneration, infection control, and cancer management. Advanced Science. 8 (2021) 2004014. https://doi.org/10.1002/advs.202004014.

[10] K. Blecher, A. Nasir, A. Friedman, The growing role of nanotechnology in combating infectious disease. Virulence. 2 (2011) 395–401. https://doi.org/10.4161/viru.2.5.17035.

[11] C.C. Sanders, W.E. Sanders, D.J. Harrowe, Bacterial interference: Effects of oral antibiotics on the normal throat flora and its ability to interfere with group A streptococci. Infection and Immunity. 13 (1976) 808–812. https://doi.org/10.1128/iai.13.3.808-812.1976.

[12] J. Hornak, Synthesis, properties and selected technical applications of magnesium oxide nanoparticles: A review. International Journal of Molecular Sciences. 22 (2021) 12752. https://doi.org/10.3390/ijms222312752.

[13] R. Eivazzadeh-Keihan, E. Bahojb Noruzi, K. Khanmohammadi Chenab, A. Jafari, F. Radinekiyan, S.M. Hashemi, F. Ahmadpour, A. Behboudi, J. Mosafer, A. Mokhtarzadeh, A. Maleki, M.R. Hamblin, Metal-based nanoparticles for bone tissue engineering. Journal of Tissue Engineering and Regenerative Medicine. 14 (2020) 1687–1714. https://doi.org/10.1002/term.3131.

[14] S. Hayat, S. Muzammil, M.H. Rasool, Z. Nisar, S.Z. Hussain, A.N. Sabri, S. Jamil, In vitro antibiofilm and anti-adhesion effects of magnesium oxide nanoparticles against antibiotic resistant bacteria. Microbiology and Immunology. 62 (2018) 211–220. https://doi.org/10.1111/1348-0421.12580.

[15] G.K. Meenashisundaram, N. Wang, S. Maskomani, S. Lu, S.K. Anantharajan, S.T. Dheen, S.M.L. Nai, J.Y.H. Fuh, J. Wei, Fabrication of Ti + Mg composites by three-dimensional printing of porous Ti and subsequent pressureless infiltration of biodegradable Mg. Materials Science and Engineering C. 108 (2020) 110478. https://doi.org/10.1016/j.msec.2019.110478.

[16] B. Safari, S. Davaran, A. Aghanejad, Osteogenic potential of the growth factors and bioactive molecules in bone regeneration. International Journal of Biological Macromolecules. 175 (2021) 544–557. https://doi.org/10.1016/j.ijbiomac.2021.02.052.

[17] J.B. Cannata-andía, N. Carrillo-lópez, O.D. Messina, N.A.T. Hamdy, S. Panizo, S.L. Ferrari, Pathophysiology of vascular calcification and bone loss: Linked disorders of ageing? Nutrients. 13 (2021) 3835. https://doi.org/10.3390/nu13113835.

[18] T. Vetter, M.J. Lohse, Magnesium and the parathyroid. Current Opinion in Nephrology and Hypertension. 11 (2002) 403–410. https://doi.org/10.1097/00041552-200207000-00006.

[19] P. Feng, R. Zhao, L. Yang, S. Chen, D. Wang, H. Pan, C. Shuai, Hydrothermal synthesis of hydroxyapatite nanorods and their use in PCL bone scaffold. Ceramics International. 48 (2022) 33682–33692. https://doi.org/10.1016/J.CERAMINT.2022.07.314.

[20] P. Feng, K. Wang, Y. Shuai, S. Peng, Y. Hu, C. Shuai, Hydroxyapatite nanoparticles in situ grown on carbon nanotube as a reinforcement for

poly (ε-caprolactone) bone scaffold. Materials Today Advances. 15 (2022) 100272. https://doi.org/10.1016/j.mtadv.2022.100272.

[21] G. Wu, E.B. Hunziker, Y. Zheng, D. Wismeijer, Y. Liu, Functionalization of deproteinized bovine bone with a coating-incorporated depot of BMP-2 renders the material efficiently osteoinductive and suppresses foreign-body reactivity. Bone. 49 (2011) 1323–1330. https://doi.org/10.1016/j.bone.2011.09.046.

[22] Y. Dong, H. Ye, Y. Liu, L. Xu, Z. Wu, X. Hu, J. Ma, J.L. Pathak, J. Liu, G. Wu, pH dependent silver nanoparticles releasing titanium implant: A novel therapeutic approach to control peri-implant infection. Colloids and Surfaces B: Biointerfaces. 158 (2017) 127–136. https://doi.org/10.1016/j.colsurfb.2017.06.034.

[23] Y. Wen, W. Zhou, X. Zhu, S. Cheng, G. Xiao, Y. Li, Y. Zhu, Z. Wang, C. Wan, An investigation of circadian rhythm in Escherichia coli. Biological Rhythm Research. 46 (2015) 753–762. https://doi.org/10.1080/09291016.2015.1052650.

[24] J.P. Schmitz, J.O. Hollinger, The critical size defect as an experimental model for craniomandibulofacial nonunions. Clinical Orthopaedics and Related Research. 205 (1986) 299–308. https://doi.org/10.1097/00003086-198604000-00036.

[25] X. Liu, X. He, D. Jin, S. Wu, H. Wang, M. Yin, A. Aldalbahi, M. El-Newehy, X. Mo, J. Wu, A biodegradable multifunctional nanofibrous membrane for periodontal tissue regeneration. Acta Biomaterialia. 108 (2020) 207–222. https://doi.org/10.1016/j.actbio.2020.03.044.

[26] F. Yang, S.K. Both, X. Yang, X.F. Walboomers, J.A. Jansen, Development of an electrospun nano-apatite/PCL composite membrane for GTR/GBR application. Acta Biomaterialia. 5 (2009) 3295–3304. https://doi.org/10.1016/j.actbio.2009.05.023.

[27] M. Chen, P.K. Patra, S.B. Warner, S. Bhowmick, Role of fiber diameter in adhesion and proliferation of NIH3T3 fibroblast on electrospun polycaprolactone scaffolds. Tissue Engineering. 13 (2007) 579–587. https://doi.org/10.1089/ten.2006.0205.

[28] S.B. Qasim, R.M. Delaine-Smith, T. Fey, A. Rawlinson, I.U. Rehman, Freeze gelated porous membranes for periodontal tissue regeneration. Acta Biomaterialia. 23 (2015) 317–328. https://doi.org/10.1016/j.actbio.2015.05.001.

[29] S. Mallakpour, N. Nouruzi, Effect of modified ZnO nanoparticles with biosafe molecule on the morphology and physiochemical properties of novel polycaprolactone nanocomposites. Polymer. 89 (2016) 94–101. https://doi.org/10.1016/j.polymer.2016.02.038.

[30] A. Polini, D. Pisignano, M. Parodi, R. Quarto, S. Scaglione, Osteoinduction of human mesenchymal stem cells by bioactive composite scaffolds without supplemental osteogenic growth factors. PLoS ONE. 6 (2011) e26211. https://doi.org/10.1371/journal.pone.0026211.

[31] L.Z. Peia, L.Z. Yinb, J.F. Wanga, J. Chena, C.G. Fana, Q.F. Zhanga, Low temperature synthesis of magnesium oxide and spinel powders by a sol-gel process. Materials Research. 13 (2010) 339–343. https://doi.org/10.1590/s1516-14392010000300010.

[32] X. Yu, M. Wei, Preparation and evaluation of parathyroid hormone incorporated CaP coating via a biomimetic method. Journal of Biomedical Materials Research-Part B Applied Biomaterials. 97 B (2011) 345–354. https://doi.org/10.1002/jbm.b.31820.

[33] K.H. Lee, H.Y. Kim, M.S. Khil, Y.M. Ra, D.R. Lee, Characterization of nano-structured poly(ε-caprolactone) nonwoven mats via electrospinning. Polymer. 44 (2003) 1287–1294. https://doi.org/10.1016/S0032-3861(02)00820-0.

[34] U. Adhikari, X. An, N. Rijal, T. Hopkins, S. Khanal, T. Chavez, R. Tatu, J. Sankar, K.J. Little, D.B. Hom, N. Bhattarai, S.K. Pixley, Embedding magnesium metallic particles in polycaprolactone nanofiber mesh

improves applicability for biomedical applications. Acta Biomaterialia. 98 (2019) 215–234. https://doi.org/10.1016/j.actbio.2019.04.061.

[35] C.C. Coelho, R. Araújo, P.A. Quadros, S.R. Sousa, F.J. Monteiro, Antibacterial bone substitute of hydroxyapatite and magnesium oxide to prevent dental and orthopaedic infections. Materials Science and Engineering C. 97 (2019) 529–538. https://doi.org/10.1016/j.msec.2018.12.059.

[36] J. Maji, S. Pandey, S. Basu, Synthesis and evaluation of antibacterial properties of magnesium oxide nanoparticles. Bulletin of Materials Science. 43 (2020) 1–10. https://doi.org/10.1007/s12034-019-1963-5.

[37] C.L. Wetteland, N.Y.T. Nguyen, H. Liu, Concentration-dependent behaviors of bone marrow derived mesenchymal stem cells and infectious bacteria toward magnesium oxide nanoparticle. Acta Biomaterialia. 35 (2016) 341–356. https://doi.org/10.1016/j.actbio.2016.02.032.

[38] M. Sanz, C. Dahlin, D. Apatzidou, Z. Artzi, D. Bozic, E. Calciolari, H. de Bruyn, H. Dommisch, N. Donos, P. Eickholz, J.E. Ellingsen, H.J. Haugen, D. Herrera, F. Lambert, P. Layrolle, E. Montero, K. Mustafa, O. Omar, H. Schliephake, Biomaterials and regenerative technologies used in bone regeneration in the craniomaxillofacial region: Consensus report of group 2 of the 15th European Workshop on Periodontology on Bone Regeneration. Journal of Clinical Periodontology. 46 (2019) 82–91. https://doi.org/10.1111/jcpe.13123.

[39] K. Chen, G. Zhou, Q. Li, H. Tang, S. Wang, P. Li, X. Gu, Y. Fan, In vitro degradation, biocompatibility and antibacterial properties of pure zinc: assessing the potential of Zn as a guided bone regeneration membrane. Journal of Materials Chemistry. B. 9 (2021) 5114–5127. https://doi.org/10.1039/d1tb00596k.

[40] R. Scaffaro, F. Lopresti, L. Botta, Preparation, characterization and hydrolytic degradation of PLA/PCL co-mingled nanofibrous mats

prepared via dual-jet electrospinning. European Polymer Journal. 96 (2017) 266–277. https://doi.org/10.1016/j.eurpolymj.2017.09.016.

[41] R.P. Ocaña, G.D. Rabelo, L.M. Sassi, V.P. Rodrigues, F.A. Alves, Implant osseointegration in irradiated bone: An experimental study. Journal of Periodontal Research. 52 (2017) 505–511. https://doi.org/10.1111/jre.12416.

[42] N. Coq, T. van Bommel, R.A. Hikmet, H.R. Stapert, W.U. Dittmer, Self-supporting hydrogel stamps for the microcontact printing of proteins. Langmuir. 23 (2007) 5154–5160. https://doi.org/10.1021/la0700321.

[43] J.S. Choi, H.S. Yoo, Nano-inspired fibrous matrix with bi-phasic release of proteins. Journal of Nanoscience and Nanotechnology. 10 (2010) 3038–3045. https://doi.org/10.1166/jnn.2010.2164.

[44] A. Suryavanshi, K. Khanna, K.R. Sindhu, J. Bellare, R. Srivastava, Magnesium oxide nanoparticle-loaded polycaprolactone composite electrospun fiber scaffolds for bone-soft tissue engineering applications: In-vitro and in-vivo evaluation. Biomedical Materials (Bristol). 12 (2017) 055011. https://doi.org/10.1088/1748-605X/aa792b.

[45] R.L. Jilka, C.A. O'Brien, S.M. Bartell, R.S. Weinstein, S.C. Manolagas, Continuous elevation of PTH increases the number of osteoblasts via both osteoclast-dependent and -independent mechanisms. Journal of Bone and Mineral Research. 25 (2010) 2427–2437. https://doi.org/10.1002/jbmr.145.

[46] J. Liu, D.G. Kerns, Mechanisms of Guided Bone Regeneration: A Review. The Open Dentistry Journal. 8 (2014) 56. https://doi.org/10.2174/1874210601408010056.

[47] R.E. Jung, D.L. Cochran, O. Domken, R. Seibl, A.A. Jones, D. Buser, C.H.F. Hammerle, The effect of matrix bound parathyroid hormone on bone regeneration. Clinical Oral Implants Research. 18 (2007) 319–325. https://doi.org/10.1111/j.1600-0501.2007.01342.x.

[48] P.S. Gomes, M.H. Fernandes, Rodent models in bone-related research: The relevance of calvarial defects in the assessment of bone regeneration strategies. Laboratory Animals. 45 (2011) 14–24. https://doi.org/10.1258/la.2010.010085.

[49] G.R. Persson, S. Renvert, Cluster of bacteria associated with peri-implantitis. Clinical Implant Dentistry and Related Research. (2014) 783–793. https://doi.org/10.1111/cid.12052.

[50] G.J.A. ter Boo, D.W. Grijpma, T.F. Moriarty, R.G. Richards, D. Eglin, Antimicrobial delivery systems for local infection prophylaxis in orthopedic- and trauma surgery. Biomaterials. 52 (2015) 113–125. https://doi.org/10.1016/j.biomaterials.2015.02.020.

[51] G. Begić, M. Petković Didović, S. Lučić Blagojević, I. Jelovica Badovinac, J. Žigon, M. Perčić, O. Cvijanović Peloza, I. Gobin, Adhesion of oral bacteria to commercial d-PTFE membranes: Polymer microstructure makes a difference. International Journal of Molecular Sciences. 23 (2022) 2983. https://doi.org/10.3390/ijms23062983.

[52] P. Bhattacharya, A. Dey, S. Neogi, An insight into the mechanism of antibacterial activity by magnesium oxide nanoparticles. Journal of Materials Chemistry B. 9 (2021) 5329–5339. https://doi.org/10.1039/d1tb00875g.

[53] K.M. Pang, J.W. Lee, J.Y. Lee, J.B. Lee, S.M. Kim, M.J. Kim, J.H. Lee, Clinical outcomes of magnesium-incorporated oxidised implants: A randomised double-blind clinical trial. Clinical Oral Implants Research. 25 (2014) 616–621. https://doi.org/10.1111/clr.12091.

[54] A. Mahmoud, Ö. Ezgi, A. Merve, G. Özhan, In vitro toxicological assessment of magnesium oxide nanoparticle exposure in several mammalian cell types. International Journal of Toxicology. 35 (2016) 429–437. https://doi.org/10.1177/1091581816648624.

[55] J. Wang, X.Y. Ma, Y.F. Feng, Z.S. Ma, T.C. Ma, Y. Zhang, X. Li, L. Wang, W. Lei, Magnesium ions promote the biological behaviour of rat calvarial

osteoblasts by activating the PI3K/Akt signalling pathway. Biological Trace Element Research. 179 (2017) 284–293. https://doi.org/10.1007/s12011-017-0948-8.

[56] R. Radha, D. Sreekanth, Insight of magnesium alloys and composites for orthopedic implant applications–a review. Journal of Magnesium and Alloys. 5 (2017) 286–312. https://doi.org/10.1016/j.jma.2017.08.003.

[57] D.H. Balani, N. Ono, H.M. Kronenberg, Parathyroid hormone regulates fates of murine osteoblast precursors in vivo. Journal of Clinical Investigation. 127 (2017) 3327–3338. https://doi.org/10.1172/JCI91699.

[58] M.G. Jang, J.Y. Lee, J.Y. Yang, H. Park, J.H. Kim, J.E. Kim, C.S. Shin, S.Y. Kim, S.W. Kim, Intermittent PTH treatment can delay the transformation of mature osteoblasts into lining cells on the periosteal surfaces. Journal of Bone and Mineral Metabolism. 34 (2016) 532–539. https://doi.org/10.1007/s00774-015-0707-x.

[59] B.C. Silva, J.P. Bilezikian, Parathyroid hormone: Anabolic and catabolic actions on the skeleton. Current Opinion in Pharmacology. 22 (2015) 41–50. https://doi.org/10.1016/j.coph.2015.03.005.

[60] Y.H. An, R.J. Friedman, Animal models of bone defect repair. in: Animal models in orthopaedic research. CRC Press. (2020) pp. 241–260. https://doi.org/10.1201/9780429173479-16.

[61] K. Takagi, M.R. Urist, The reaction of the dura to bone morphogenetic protein (BMP) in repair of skull defects. Annals of Surgery. 196 (1982) 100. https://doi.org/10.1097/00000658-198207000-00020.

[62] Y. Jiang, J. Zhao, E.Y. Liao, R.C. Dai, X.P. Wu, H.K. Genant, Application of micro-CT assessment of 3-D bone microstructure in preclinical and clinical studies. Journal of Bone and Mineral Metabolism. 23 (2005) 122–131. https://doi.org/10.1007/BF03026336.

[63] J.S. Thomsen, A. Laib, B. Koller, S. Prohaska, L. Mosekilde, W. Gowin, Stereological measures of trabecular bone structure: Comparison of 3D micro computed tomography with 2D histological sections in human

proximal tibial bone biopsies. Journal of Microscopy. 218 (2005) 171–179. https://doi.org/10.1111/j.1365-2818.2005.01469.x.

[64] J. Wang, J. Li, L. Yang, Y. Zhou, Y. Wang, Dose-dependence of PTH-related peptide-1 on the osteogenic induction of MC3T3-E1 cells in vitro. Medicine (United States). 96 (2017) e6637. https://doi.org/10.1097/MD.0000000000006637.

[65] J.P. D'Lima, J. Paul, P. Palathingal, B.R.R. Varma, M. Bhat, M. Mohanty, Histological and histometrical evaluation of two synthetic hydroxyapatite based biomaterials in the experimental periodontal defects in dogs. Journal of Clinical and Diagnostic Research. 8 (2014) ZC52. https://doi.org/10.7860/JCDR/2014/9892.4860.

[66] M. Retzepi, N. Donos, Guided Bone Regeneration: Biological principle and therapeutic applications. Clinical Oral Implants Research. 21 (2010) 567–576. https://doi.org/10.1111/j.1600-0501.2010.01922.x.

[67] A. Verket, S.P. Lyngstadaas, H. Tiainen, H.J. Rønold, J.C. Wohlfahrt, Impact of particulate deproteinized bovine bone mineral and porous titanium granules on early stability and osseointegration of dental implants in narrow marginal circumferential bone defects. International Journal of Oral and Maxillofacial Surgery. 47 (2018) 1086–1094. https://doi.org/10.1016/j.ijom.2018.02.007.

[68] Y.K. Kim, S.G. Kim, S.C. Lim, H.J. Lee, P.Y. Yun, A clinical study on bone formation using a demineralized bone matrix and resorbable membrane. Oral Surgery, Oral Medicine, Oral Pathology, Oral Radiology and Endodontology. 109 (2010) e6–e11. https://doi.org/10.1016/j.tripleo.2010.01.012.

[69] I. Arrighi, S. Mark, M. Alvisi, B. von Rechenberg, J.A. Hubbell, J.C. Schense, Bone healing induced by local delivery of an engineered parathyroid hormone prodrug. Biomaterials. 30 (2009) 1763–1771. https://doi.org/10.1016/j.biomaterials.2008.12.023.

Supplementary data:

Antimicrobial and pro-osteogenic coaxially-electrospun magnesium oxide nanoparticles-polycaprolactone /parathyroid hormone-polycaprolactone composite barrier membrane for guided bone regeneration

Yiwen Dong[1-3], Litao Yao[2-4], Lei Cai[1], Mi Jin[1], Tymour Forouzanfar[2, 3], Lianjun Wu[1], Jinsong Liu[1], Gang Wu[2, 3]

[1]School and Hospital of Stomatology, Wenzhou Medical University, Wenzhou, China

[2] Department of Oral and Maxillofacial Surgery/Pathology, Amsterdam UMC and Academic Center for Dentistry Amsterdam (ACTA), Vrije Universiteit Amsterdam, Amsterdam Movement Science, Amsterdam, Amsterdam, The Netherlands

[3] Department of Oral Cell Biology, Academic Centre for Dentistry Amsterdam (ACTA), University of Amsterdam (UvA) and Vrije Universiteit Amsterdam (VU), Amsterdam, The Netherlands

[4] Department of Dentistry, Sir Run Run Shaw Hospital, School of Medicine, Zhejiang University, Hangzhou, Zhejiang, China

International Journal of Nanomedicine. 18 (2023) 369—383.

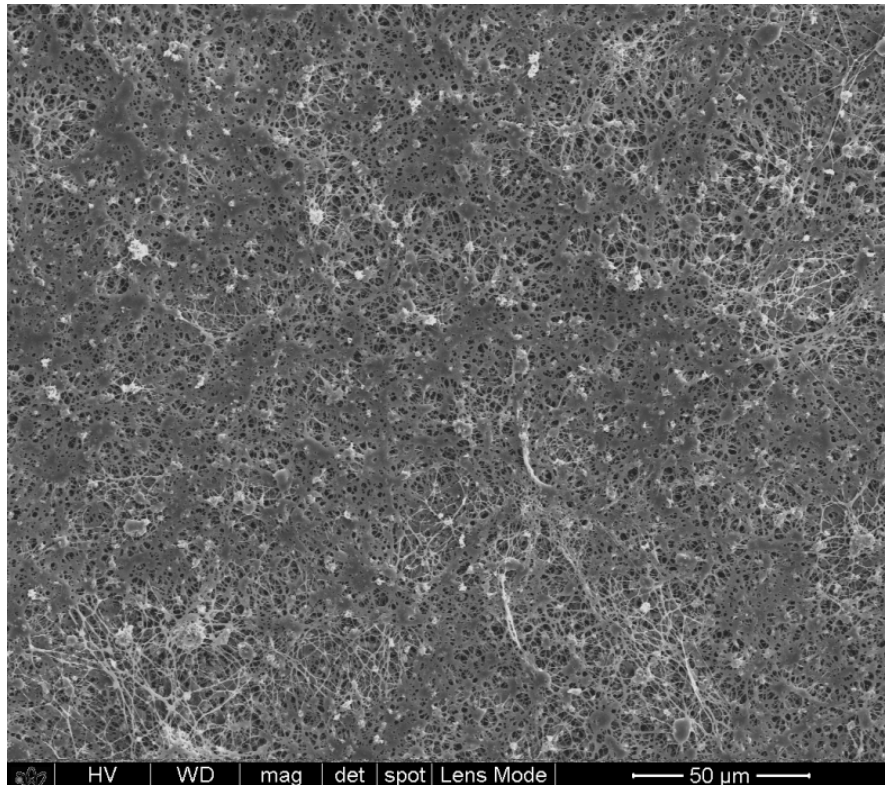

Fig. S1: SEM image of MgONPs-PCL/PTH-PCL nanofibers (MgONPs=0.5)

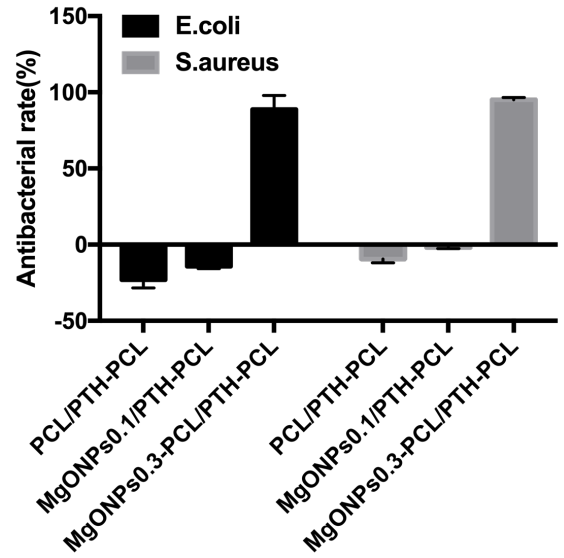

Fig. S2: Antibacterial effects of MgONPs-PCl/PTH-PCL (MgONPs=0.1 and 0.3) and PCL/PTH-PCL against *S. aureus* and *E. coli.* Values are mean ± SD from 3 independent experiments.

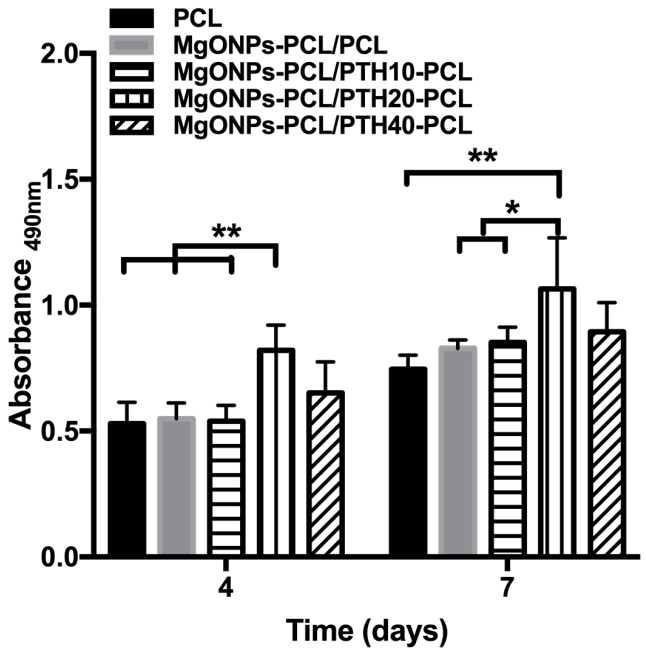

Fig. S3: The effects of PCL and MgONPs-PCL/PTHn-PCL membranes on proliferation of MC3T3-E1 cells. Values are mean ± SD from 4 independent experiments. Significant effect of treatment, **p < 0.01, *p < 0.05.*

CHAPTER FIVE

Antibacterial and pro-osteogenic functionalized gallium-coated magnesium alloy membrane for guided bone regeneration.

Yiwen Dong[1-3], Litao Yao[2-4], Lei Cai[1], Mi Jin[1], Tymour Forouzanfar[2, 3], Lianjun Wu[1], Jinsong Liu[1], Gang Wu[2, 3]

[1]School and Hospital of Stomatology, Wenzhou Medical University, Wenzhou, China

[2] Department of Oral and Maxillofacial Surgery/Pathology, Amsterdam UMC and Academic Center for Dentistry Amsterdam (ACTA), Vrije Universiteit Amsterdam, Amsterdam Movement Science, Amsterdam, Amsterdam, The Netherlands

[3] Department of Oral Cell Biology, Academic Centre for Dentistry Amsterdam (ACTA), University of Amsterdam (UvA) and Vrije Universiteit Amsterdam (VU), Amsterdam, The Netherlands

[4] Department of Dentistry, Sir Run Run Shaw Hospital, School of Medicine, Zhejiang University, Hangzhou, Zhejiang, China

Submitted.

magnesium-supported GBR/GTR barrier membrane. International Journal of Molecular Sciences. 21 (2020) 3098. https://doi.org/10.3390/ijms21093098.

[35] Q. Wei, Y. Xu, Y. Wang, Textile surface functionalization by physical vapor deposition (PVD). Surface Modification of Textiles. (2009) 58–90. https://doi.org/10.1533/9781845696689.58.

[36] G.R. Persson, S. Renvert, Cluster of bacteria associated with peri-implantitis. Clinical Implant Dentistry and Related Research. (2014) 783–793. https://doi.org/10.1111/cid.12052.

[37] G.J.A. ter Boo, D.W. Grijpma, T.F. Moriarty, R.G. Richards, D. Eglin, Antimicrobial delivery systems for local infection prophylaxis in orthopedic- and trauma surgery. Biomaterials. 52 (2015) 113–125. https://doi.org/10.1016/j.biomaterials.2015.02.020.

[38] N. Gómez-Cerezo, E. Verron, V. Montouillout, F. Fayon, P. Lagadec, J.M. Bouler, B. Bujoli, D. Arcos, M. Vallet-Regí, The response of pre-osteoblasts and osteoclasts to gallium containing mesoporous bioactive glasses. Acta Biomaterialia. 76 (2018) 333–343. https://doi.org/10.1016/J.ACTBIO.2018.06.036.

[39] L. Pompa, Z.U. Rahman, E. Munoz, W. Haider, Surface characterization and cytotoxicity response of biodegradable magnesium alloys. Materials Science and Engineering C. 49 (2015) 761–768. https://doi.org/10.1016/j.msec.2015.01.017.

[40] L. Pompa, Z.U. Rahman, E. Munoz, W. Haider, Surface characterization and cytotoxicity response of biodegradable magnesium alloys. Materials Science and Engineering C. 49 (2015) 761–768. https://doi.org/10.1016/j.msec.2015.01.017.

CHAPTER SIX

GENERAL DISCUSSION

Since the emergence of titanium (Ti) implants in 1965 [1], continuous efforts have been made on developing surface modification technologies with an aim to improve the interaction between dental implants and peri-implant supporting tissues [2]. The original dental implants introduced by Brånemark bear a smooth machined surface [3]. Smooth-surface implants have been shown a 15-year survival rate of 84% in the mandible and 78% in the maxilla [4]. A large variety of surface modification technologies have been developed to improve cell adhesion, migration, differentiation, and eventually implant osteointegration by modifying the surface topography, energy, and chemical composition of implants [5]. Sandblasting acid etching (SLA) is the most representative and widely used surface modification method in current implants. A well-established SLA treatment significantly improves the roughness, hydrophilicity, surface energy, cell adhesion of the implants and finally enhances the implant osteointegration [6]. The 15-year survival rate of SLA Ti implant is more than 90% in healthy bone conditions [7]. In recent years, SLActive surface implants are carried out to further enhance implant osteointegration. The surface of the SLActive implant is produced with the same sandblasting and acid-etching technique but rinsed under nitrogen protection and stored in sealed glass tubes containing isotonic NaCl solution to prevent exposure to oxygen [8]. These implants with higher surface energy and hydrophilicity easily achieve more osteointegration. However, none of these current surface modifications are adequate to cope with various adverse bone abnormalities in peri-implant supporting tissues, such as low bone density, periimplantitis, and large-volume bone defects [9,10]. A new generation of surface modification technology is highly needed to specifically functionalize dental implants with pro-osteogenic and antibacterial functions. The aims of the studies presented in this thesis were:

1) To fabricate a diameter-controllable tantalum nanoporous arrays (TaNS) on Zr implant surface and examined whether the TaNS improved the osteointegration of zirconia implants (**Chapter 2**).
2) To load antimicrobial agents in the nanotube arrays with a pH-sensitive acid cleavable acetal linker (AL), which can store antimicrobial agents for long periods in normal conditions (pH=7.4) and release only during the infection (pH=5.5) (**Chapter 3**).

3) To encapsulate two different bioactive agents into the nanofibers membrane for realizing the sustained release and achieving antibacterial and pro-osteogenic functions with lower toxicity (**Chapter 4**).
4) To fabricate a coating on Mg alloys' surface so that reducing the degradation rate. To test the coated Mg alloys' effects on bacteria viability and osteogenesis (**Chapter 5**).

Bioactive coatings to improve implant osteointegration in adverse conditions

Nanoporous tantalum coating

The "tooth-like" color of zirconia (Zr) implants are suitable for patients with high smile line, thin gingival biotype, and/or gingival recession in the anterior aesthetic zone [11,12]. However, the oxide film on the Zr surface compromises the formation of hydroxyapatite compounds, which is unfavorable for bone formation [13]. Histological results show that fibrous cells will easily invade the implant-bone interface at the early stage of osteointegration, which results in loosening, micro-motion, and eventually the failure of osteointegration [13]. The osteointegration of Zr implant may be further impeded in adverse bone abnormalities [14]. Therefore, continuous efforts should be done to enhance the osteointegration of Zr. Zr is a brittle material with a thermal insulator, which is more susceptible to thermal shocks caused by high temperature gradients and finally deteriorates the mechanical properties [15]. Furthermore, sharp particle abrasion can cause deep micro-cracks and compromise the fatigue resistance of Zr [15]. Therefore, the modification methods of Zr implants with relatively milder conditions are preferred. The metallic coating — tantalum (Ta) and its oxides have emerged as promising candidates fabricated on Zr implant surface to improve osteointegration due to their excellent fragile resistance, anticorrosion, biocompatibility, and osteogenesis [16,17]. Ta coating significantly promotes osteogenic cell adhesion, aggregation, and proliferation both *in-vitro* and *vivo* compared with Ta-uncoated groups [18]. Magnetron sputtering is a high-rate vacuum coating technique to deposit alloys, compounds, and metals onto a wide range of materials without temperature gradients and sharp particle abrasion [19]. The high purity, excellent uniformity and high bond strength of the thereby generated coatings make it promising in

coating Ta on the surface of Zr implants [19].Whereas the high elastic modulus of Ta (186GPa) [20], which results in the mismatch between Ta-based biomaterials and bone tissue (human trabecular bone：0.1~30 GPa) [21], will induce the “stress shielding”, in which the Ta coating overtakes a considerable part of the occlusal load, and shield peri-implant bone tissue from the necessary stressing for maintaining the strength, density and healthy structure of bone. Stress shielding may cause bone loss, implant loosening, and finally implant failure [22]. The nanoporous structure is introduced to Ta coatings with the aim to decrease the modulus of elasticity (2.5~3.9 GPa) [20,23–25]. Previous studies have demonstrated that nanoporous Ta coating presents enhanced osteointegration in artificial joints and implants [26,27], which may be due to the increased surface roughness of the nanoporous structure. Heiden *et al*. indicate that nanoporous Ta coating with a diameter of 30 nm can significantly enhance surface roughness, improve cell adhesion, proliferation, and eventually enhance osteointegration by providing a framework for synthesizing new bone tissue [28,29]. The commonly applied methods to fabricate Ta nanoporous structure on the Zr surface include solid-state laser etching [30], selective infiltration etching [31] and electrochemical anodization [32]. However, solid-state laser etching is reported to damage the structure of Zr and reduces its mechanical strength [30]. Selective infiltration etching fails to fabricate ordered and controllable nanostructure arrays easily [31]. Therefore, electrochemical anodization has become the favorable method to fabricate nanopores with uniform, ordered, and controllable nanoporous structures. Another invaluable property of the nanoporous array of Ta coatings is its transparency that enables retaining the “tooth-like” color of Zr for aesthetic needs. Hitherto, few studies are performed to prepare and analyze the pro-osteogenic properties of homogeneous Ta coatings with nanoporous structure (TaNS) on the Zr substrates. In **Chapter 2**, the surface morphology of ZrO_2/TaNS showed homogeneous nanoporous arrays with a diameter of nanopores was about 30 nm, which was claimed to be beneficial for cellular proliferation, osteogenic differentiation, and mineralization [28,29]. The surface roughness of ZrO_2/TaNS significantly was increased when compared with ZrO_2 and ZrO_2/Ta, which resulted in enlarged surface area, enhancements of protein adsorption, and

subsequent cell osteogenic functions, thereby improving the percentage of bone-implant contact (BIC%) and eventually its osteointegration. Furthermore, our study showed that the TaNS coating could modulate MC3T3-E1 cells attachment, proliferation, osteogenic differentiation, and mineralization by up-regulating osteogenic-related gene expressions. In our study, Runx2 expressed in ZrO_2/TaNS was 3.6-, and 1.7-fold higher than ZrO_2 and ZrO_2/Ta on day 14, respectively. The expression of ALP in ZrO_2/TaNS was 3.14- and 1.4-fold higher compared to ZrO_2 and ZrO_2/Ta, respectively. Likewise, COL-1 showed 70% increased expression in ZrO_2/TaNS compared to ZrO_2, and a similar increase was observed in ZrO_2/Ta, with 1.9-fold higher than ZrO_2. Moreover, the animal experiment also showed that the TaNS coating significantly enhanced the new bone tissue formation around Zr implants. *In vitro* and *vivo* findings in our study indicated the nanoporous Ta-coated Zr implants could improve osteointegration of the Zr implant and will be a promising biomaterial for clinical application in anterior aesthetic zone.

pH-sensitive antibacterial coatings for periimplantitis prevention

One of the adverse conditions that challenges implant fixation and durability is periimplantitis [33,34]. It is a destructive inflammatory process, that finally leads to bone loss [33,34]. Almost 14.5% of the implants will suffer moderate to severe periimplantitis after 10-year function [35]. The risk factors of periimplantitis include diabetes mellitus, smoking, poor plaque control, and a history of periodontitis [36]. Among them, poor plaque control and a history of periodontitis are factors with strong supporting evidence [36]. The history of periodontitis is associated with early implant failure [37]. When implants are placed in extraction sockets with periodontitis, the residual bacteria in the peri-implant tissues may rapidly adhere to the surface of implants, form a biofilm, and cause periimplantitis, leading to even early implant failure (within 12 months) [38]. Poor plaque control is a high-risk factor associated with late implant failure [37]. Bacteria first adhere to peri-implant mucosa and lead to peri-implant mucositis with the characteristics of redness, swelling, and inflammation [39]. Afterwards, bacteria extend rapidly into bone marrow through the micro gap at the implant abutment connection and finally progress to significant bone loss [40–43]. Literature review shows that systemic

prophylactic antibiotics are useful in preventing postoperative infections post implant [44]. However, such an administration may raise a series of adverse events, such as diarrhea and life-threatening allergic reactions [45]. Local administration of antibiotics is less recommended in clinic due to the potential risk of the development of antibiotic-resistant bacteria [46]. To approach this issue, researchers have attempted slow-release systems of antibacterial metallic nanoparticles such as silver, copper, zinc, and so on [47,48]. In previous studies, metallic nanoparticles are loaded in the HA coatings or titanium nanotubes to realize the locally long-term drug release. The release duration could be prolonged to months [49]. Whereas the passive long-term release often results in lower drug concentrations than the minimum inhibitory concentration, which will compromise the antibacterial efficacy [50,51]. Therefore, approaches of loading antimicrobial agents on implant surfaces that can not only store antimicrobial agents for long periods but also release them adequately and timely only during infection are desperately needed. An ideal release system should be able to respond to microbial activity. The pH level around the implant surface during infection can decrease to as low as 5.5, while that under the physiological condition is 7.4 [52]. The difference of pH in different conditions can be used as a switch to trigger antimicrobial agents released from the implant surface [53,54]. In **Chapter 3,** the pH-sensitive acid cleavable acetal linker (AL) degraded accompanied with the release of silver nanoparticles when pH is 5.5. At pH 7.4, there was a burst release with an average release rate of 0.085 ppm/h within 10 h, which effectively prevented primary bacteria adhesion. Afterwards, the average release rate was almost zero for 28 days. Then, we changed the pH to 5.5, a sharp increase of drug release rate occurred (Fig. 6A). These *in-vitro* release test results indicated that the new biomaterial was able to store AgNPs for a long period at pH 7.4 while releasing sufficient doses timely at pH 5.5. Our findings suggested that low pH-triggered AgNPs releasing TNT-AL-AgNPs implant could be a potent therapeutic approach to prevent periimplantitis.

Antibacterial and pro-osteogenic functionalized guided bone regeneration membranes

Biodegradable synthetic polymers

Multi-functionalized GBR membranes with antibacterial and pro-osteogenic properties have shown promising application potential to enhance the osteogenesis efficacy in large-volume bone defects [46,55,56]. In this study, we applied coaxial electrospinning to encapsulate the antibacterial agent and pro-osteogenic agent respectively into core and shell layers and enabled their sustained releases [57]. In clinic, broad-spectrum antibiotics are frequently used to prevent post-surgy infection [58]. However, their application is associated with certain concerns, such as dysbacteriosis, poor biodistribution, toxicity, and bacterial resistance [59,60]. Compared with clinically available antibiotics, antibacterial metallic nanoparticles are a promising alternative due to their significantly broader antimicrobial spectrum and lower the risk of bacterial resistance [57,61]. In previous studies, silver nanoparticles are the most frequently used to endow the biomaterials with antibacterial properties. Whereas silver nanoparticles are associated with several concerns, such as local accumulation of heavy metal elements causing cytotoxicity [62]. In contrast, magnesium oxide nanoparticles (MgONPs) possess biodegradability and lower toxicity [63]. The benefits of MgONPs, which includes pro-osteogenic property [64] and significant inhibition of biofilm formation and maturation, have attracted increasing interest in membrane applications [63]. As for the pro-osteogenic drug applied in the GBR membrane, PTH is a suitable candidate. As a commonly used drug for bone regeneration, PTH promotes osteogenesis by activating osteoblast cells and the secretion of SOST through the receptor PTHr1 [65,66]. Additionally, the cost of PTH is much lower than that of bone morphogenetic proteins, making it more readily available for clinical applications. At the same time, previous studies have proven that locally delivered PTH significantly promotes bone regeneration [65,67]. Moreover, Dang *et al*. also demonstrated the synergistic effects of Mg and PTH in promoting bone regeneration [67]. The sustained release of the two drugs to satisfy the phased, long-term osteogenesis process was pursued in our study. In **Chapter 4**, the MgONPs release profiles *in-vitro* indicated a sustained release of MgONPs with an average rate of 2.35% per day after 24h, which would aid in the inhibition of new bacterial invasion. The cumulative release percentage of PTH from the PCL/PTH-PCL membrane at day 29 was 2.61-fold of PTH released from the MgONPs-PCL/PTH-PCL membrane, which may

attribute to the released MgONPs. Additionally, the MgONPs-PCL/PTH-PCL membrane killed 95.04% S. aureus and 88.76% E. coli after incubation for one day, which exhibited significant antibacterial effects. The new MgONPs-PCL/PTH-PCL membrane was suggested as a promising candidate for preventing postoperative infection. The assessments of MgONPs-PCL/PTH-PCL membrane on *in-vitro* osteoblastic activity showed that MgONPs-PCL/PTH20-PCL did significantly enhance cell proliferation, ALP activity and extracellular matrix mineralization in comparison with both the pure PCL membrane and the MgONPs-PCL/PCL membrane. The results of micro-CT and histomorphometric analysis showed that MgONPs-PCL/PTH40-PCL exhibited the best osteogenesis effects among all the groups, which was mainly attributed to the incorporation of PTH. The significant improvement of osteogenesis in bacterial-contaminated models *in-vivo*, especially with the presence of high dosage PTH, proved to be a promising approach to satisfy the complicated and phased requirements of the GBR process in periimplantitis patients with large-volume bone defects.

Biodegradable magnesium alloy

The resorbable membranes, that are mainly made of naturally-derived polymers, are usually associated with suboptimal mechanical stiffness, which cannot sufficiently shield exogenous forces, leading to membrane collapse and compromised osteogenesis [68,69]. Consequently, a resorbable membrane with sufficient stiffness, antibacterial property, and pro-osteogenic capacity will be more favorable to achieve desirable osteogenic efficacy in clinic. One promising material to fabricate such a membrane is magnesium (Mg) alloys because they are of sufficient mechanical strength, biodegradable, and biocompatible [70]. The fracture strength and compressive strength of Mg alloys are 3–16 times stronger than clinically available resorbable GBR membranes, which enables sufficient shielding to provide a mechanically stable microenvironment [71]. Additionally, the Mg alloys may also exhibit an antibacterial effect through releasing free Mg^{2+} ions so as to damage the cell membrane of bacteria [72]. Furthermore, the released Mg^{2+} ions are also shown to enhance osteogenesis via phosphatidyl-inositol 3-kinase/serine-threonine kinase (PI3K/Akt) signaling [73]. However, the naked Mg alloys degrade too fast *in vivo* [74]. Continuous efforts have been made to reduce its degradation rates so as to ensure an adequate functional duration [75]. One promising method is magnetron sputtering, a high-rate vacuum coating technique to deposit alloys, compounds, and metals onto a wide range of materials [19]. The high purity, excellent uniformity, and high bonding strength of the thereby generated coatings have been shown to significantly reduce the corrosion and degradation of Mg alloys [19]. In **Chapter 5**, to further improve the pro-osteogenic and antibacterial properties of Mg alloys, we adopted gallium (Ga) to coat Mg alloys. On one hand, the chemical properties of Ga are very similar to iron (Fe) so that it can replace Fe^{3+} in ribonucleotide reductase, thereby impairing bacterial DNA synthesis and causing their death [76,77]. On the other hand, Ga^{3+} ions are also shown to increase alkaline phosphatase (ALP) activity, accelerate calcium nodule formation, and upregulate expression levels of osteogenic proteins in osteoblasts through activating transient receptor potential melastatin 7/Akt signaling pathway [78]. The results of SEM and EDX of Ga/AZ31 membrane in our study indicated the successful deposition of Ga coating on the surface of Mg alloys with a homogeneous uniformed surface. The bacterial viability assessments suggested that the Ga-coated AZ31 membranes bore more potent antibacterial activity than the naked AZ31, which further helps to reduce the risk of post-operative infection. In addition, Ga100/AZ31 showed the highest ALP activity, which was about 2.85- fold that of AZ31. Our findings suggested that the antimicrobial and pro-osteogenic Ga/AZ31 was a promising material to enhance osteogenesis in periodontitis or peri-implantitis patients with large-volume bone defects.

Future perspective

Based on this thesis, different surface modifications have been applied to the implanted materials and endowed them antibacterial and/or pro-osteogenic functions. Several questions still need to be answered in future research:

1. Can pro-osteogenic TaNS coatings improve the osteointegration of zirconia implants in low-density bones? In this thesis, our findings revealed that TaNS coating effectively enhanced pre-osteoblast attachment, proliferation, and osteogenic differentiation. The results of *in-vivo* experiments demonstrated that

TaNS coatings significantly enhanced the osteointegration of zirconia implants in normal bone conditions. Low bone density is general caused by bad habits (smoking and alcoholism), poor diet (lacking vitamins and calcium), changes in hormones (from smoking or menopause), disuse, medical conditions (rheumatoid arthritis, chronic kidney disease, overactive parathyroid gland or celiac sprue). Low bone density is characterized by low bone mass due to an imbalance in bone remodeling where osteoclast-mediated bone resorption exceeds osteoblast-mediated bone formation. The activation of osteoclasts is a major issue of low bone density. The effect of TaNS coatings on osteoclasts should be investigated in the future to clarify its clinical application potential in low density bones.

2. Can TNT-AL-AgNPs release sufficient AgNPs timely to prevent periimplantitis years after implantation? The prevalence of periimplantitis after 9 years is 45%. According to the results of release profile listed in **Chapter 3**, the AgNPs were stored at physiological state for a long time (>30 days) at pH7.4 and infection (pH 5.5) quickly triggered the release of AgNPs. However, the whole time of release tests was just lasted for 30 days. It remains to be elucidated whether the pH-responsiveness of TNT-AL-AgNPs is still valid after a 5- to 10-year implantation.

3. What is the degradation rate of MgONPs-PCL/PTHn-PCL membrane *in-vivo*? In **Chapter 4**, we have adopted a coaxial electrospinning technique and successfully synthesized a dual-functional nanofiber GBR membrane (MgONPs-PCL/PTH-PCL) with antimicrobial and pro-osteogenic properties. On the other hand, the *in-vivo* degradation rate of the membrane remains unknown. Since the degradation rate of membrane also play an important role in facilitating GBR efficacy, the degradation rate of MgONPs-PCL/PTHn-PCL should be investigated in future study to further clarify its clinical application potential.

4. What are the degradation rates of the Ga/AZ31 membranes *in-vitro* and *in-vivo*? As abovementioned, the degradation rate of a GBR membrane is highly important for bone augmentation in alveolar bone. One desired function of Ga coating is to significantly reduce the degradation of Mg alloy membrane. However, the degradation rates of the Ga/AZ31 membranes *in-vitro* and *in-vivo* remain unknown. Consequently, the degradation rate of the Ga/AZ31 membranes *in-vivo* should also be performed in further work to further clarify its clinical application potential.

Conclusions

In this thesis, different surface modification technologies were introduced to functionalize biomaterials with pro-osteogenic and antibacterial functions with an aim to coping with various adverse bone abnormalities in peri-implant supporting tissues. Magnetron sputtering and electrochemical anodization were applied to fabricate diameter-controllable TaNS coatings on the surface of zirconia implants. TaNS coatings significantly enhanced the osteogenesis both *in-vitro* and *in-vivo*. To enhance the antibacterial property of titanium implants, we successfully synthesized TNTs via electrochemical anodization and loaded pH-sensitive AL linker and AgNPs in TNTs. TNT-AL-AgNPs could serve as a pH-responsive drug delivery system: AgNPs was stored in TNT in normal pH condition while could be released in sufficient doses when pH value of the surrounding milieu became to 5.5 due to bacterial activity. This TNT-AL-AgNPs might present an effective approach to prevent periimplantitis. To endow the GBR membranes with antibacterial and pro-osteogenic functions, MgONPs and PTH were encapsulated in nanofiber through coaxial electrospinning. MgONPs-PCL/PTH-PCL significantly enhanced cell proliferation, ALP activity and extracellular matrix mineralization. In animal experiments, MgONPs-PCL/PTH-PCL significantly improved osteogenesis in infected bone defects as well. Despite the nanofibers membranes, magnesium alloy (AZ31) is one of the promising membrane materials due to its sufficient mechanical strength, biodegradable, and biocompatible. The homogeneous uniformed Ga coatings were successfully deposited on the surface of AZ31 without obvious cracks through magnetron sputtering. Ga100/AZ31 significantly enhanced ALP activity and decreased the bacterial viability. In-depth mechanistic studies of how these new materials function under adverse conditions still need further work.

References

[1] S. Kligman, Z. Ren, C.-H. Chung, M.A. Perillo, Y.-C. Chang, H. Koo, Z. Zheng, C. Li, The impact of dental implant surface modifications on osseointegration and biofilm formation. Journal of Clinical Medicine. 10 (2021) 1641. https://doi.org/10.3390/jcm10081641.

[2] H. Dong, H. Liu, N. Zhou, Q. Li, G. Yang, L. Chen, Y. Mou, Surface modified techniques and emerging functional coating of dental implants. Coatings. 10 (2020) 1–25. https://doi.org/10.3390/coatings10111012.

[3] R. Adell, U. Lekholm, B. Rockler, P.I. Brånemark, A 15-year study of osseointegrated implants in the treatment of the edentulous jaw. International Journal of Oral Surgery. 10 (1981) 387–416. https://doi.org/10.1016/S0300-9785(81)80077-4.

[4] D.L. Cochran, A comparison of endosseous dental implant surfaces. Journal of Periodontology. 70 (1999) 1523. https://doi.org/10.1902/jop.1999.70.12.1523.

[5] H. Huang, Z. Xu, X. Shao, D. Wismeijer, P. Sun, J. Wang, G. Wu, J. Leicester Williams, Multivariate linear regression analysis to identify general factors for quantitative predictions of implant stability quotient values. PLoS ONE. 12 (2017) e0187010. https://doi.org/10.1371/journal.pone.0187010.

[6] R. Smeets, B. Stadlinger, F. Schwarz, B. Beck-Broichsitter, O. Jung, C. Precht, F. Kloss, A. Gröbe, M. Heiland, T. Ebker, Impact of dental implant surface modifications on osseointegration. BioMed Research International. (2016) 16. https://doi.org/10.1155/2016/6285620.

[7] C. Giannasi, S. Niada, G. Pagni, G. Rasperini, A.T. Brini, Monitoring oral and epithelial primary cells onto dental implants. in: GISM. (2016). https://hdl.handle.net/2434/470199.

[8] G.L. Stafford, L. Chambrone, J.A. Shibli, C.E. Mercúrio, B. Cardoso, P.M. Preshaw, Review found little difference between sandblasted and acid-

etched (SLA) dental implants and modified surface (SLActive) implants. Evidence-Based Dentistry. 15 (2014) 87–88. https://doi.org/10.1038/sj.ebd.6401047.

[9] S. Raikar, P. Talukdar, S. Kumari, S.K. Panda, V.M. Oommen, A. Prasad, Factors affecting the survival rate of dental implants: A retrospective study. Journal of International Society of Preventive and Community Dentistry. 7 (2017) 351. https://doi.org/10.4103/jispcd.JISPCD_380_17.

[10] P. Dhatrak, U. Shirsat, S. Sumanth, V. Deshmukh, Finite element analysis and experimental investigations on stress distribution of dental implants around implant-bone interface. Materials Today: Proceedings. 5 (2018) 5641–5648. https://doi.org/10.1016/j.matpr.2017.12.157.

[11] L. Wu, Y. Dong, L. Yao, C. Liu, A.M. Al-Bishari, K.H. Ru Yie, H. Zhang, J. Liu, G. Wu, Nanoporous tantalum coated zirconia implant improves osseointegration. Ceramics International. 46 (2020) 17437–17448. https://doi.org/10.1016/j.ceramint.2020.04.038.

[12] J. Han, J. Zhao, Z. Shen, Zirconia ceramics in metal-free implant dentistry. Advances in Applied Ceramics. 116 (2017) 138–150. https://doi.org/10.1080/17436753.2016.1264537.

[13] S. Roehling, K.A. Schlegel, H. Woelfler, M. Gahlert, Zirconia compared to titanium dental implants in preclinical studies—a systematic review and meta-analysis. Clinical Oral Implants Research. 30 (2019) 365–395. https://doi.org/10.1111/clr.13425.

[14] R. Depprich, C. Naujoks, M. Ommerborn, F. Schwarz, N.R. Kübler, J. Handschel, Current findings regarding zirconia implants. Clinical Implant Dentistry and Related Research. 16 (2014) 124–137. https://doi.org/10.1111/j.1708-8208.2012.00454.x.

[15] F.H. Schünemann, M.E. Galárraga-Vinueza, R. Magini, M. Fredel, F. Silva, J.C.M. Souza, Y. Zhang, B. Henriques, Zirconia surface modifications for implant dentistry. Materials Science and Engineering C. 98 (2019) 1294–1305. https://doi.org/10.1016/j.msec.2019.01.062.

[16] Y. Liu, C. Bao, D. Wismeijer, G. Wu, The physicochemical/biological properties of porous tantalum and the potential surface modification techniques to improve its clinical application in dental implantology. Materials Science and Engineering C. 49 (2015) 323–329. https://doi.org/10.1016/j.msec.2015.01.007.

[17] V.K. Balla, S. Bose, N.M. Davies, A. Bandyopadhyay, Tantalum—a bioactive metal for implants. The Journal of The Minerals, Metals & Materials Society. 62 (2010) 61–64. https://doi.org/10.1007/s11837-010-0110-y.

[18] I. Putrantyo, N. Anilbhai, R. Vanjani, B. de Vega, Tantalum as a novel biomaterial for bone implant: A literature review. Journal of Biomimetics, Biomaterials and Biomedical Engineering. 52 (2021) 55–65. https://doi.org/10.4028/www.scientific.net/JBBBE.52.55.

[19] I.V. Tudose, F. Comanescu, P. Pascariu, S. Bucur, L. Rusen, F. Iacomi, E. Koudoumas, M.P. Suchea, Chemical and physical methods for multifunctional nanostructured interface fabrication. Functional Nanostructured Interfaces for Environmental and Biomedical Applications. (2019) 15–26. https://doi.org/10.1016/B978-0-12-814401-5.00002-5.

[20] B.R. Levine, S. Sporer, R.A. Poggie, C.J. della Valle, J.J. Jacobs, Experimental and clinical performance of porous tantalum in orthopedic surgery. Biomaterials. 27 (2006) 4671–4681. https://doi.org/10.1016/j.biomaterials.2006.04.041.

[21] E.F. Morgan, G.U. Unnikrisnan, A.I. Hussein, Annual review of biomedical engineering bone mechanical properties in healthy and diseased states. Annual Review of Biomedical Engineering. 4 (2018) 119–143. https://doi.org/10.1146/annurev-bioeng-062117.

[22] Y. Song, D.S. Xu, R. Yang, D. Li, W.T. Wu, Z.X. Guo, Theoretical study of the effects of alloying elements on the strength and modulus of β-type

bio-titanium alloys. Materials Science and Engineering A. 260 (1999) 269–274. https://doi.org/10.1016/s0921-5093(98)00886-7.

[23] J.W. Lee, H.B. Wen, P. Gubbi, G.E. Romanos, New bone formation and trabecular bone microarchitecture of highly porous tantalum compared to titanium implant threads: A pilot canine study. Clinical Oral Implants Research. 29 (2018) 164–174. https://doi.org/10.1111/clr.13074.

[24] B.R. Levine, S. Sporer, R.A. Poggie, C.J. della Valle, J.J. Jacobs, Experimental and clinical performance of porous tantalum in orthopedic surgery. Biomaterials. 27 (2006) 4671–4681. https://doi.org/10.1016/j.biomaterials.2006.04.041.

[25] V.K. Balla, S. Bodhak, S. Bose, A. Bandyopadhyay, Porous tantalum structures for bone implants: Fabrication, mechanical and in vitro biological properties. Acta Biomaterialia. 6 (2010) 3349–3359. https://doi.org/10.1016/j.actbio.2010.01.046.

[26] Q. Wang, H. Zhang, H. Gan, H. Wang, Q. Li, Z. Wang, Application of combined porous tantalum scaffolds loaded with bone morphogenetic protein 7 to repair of osteochondral defect in rabbits. International Orthopaedics. 42 (2018) 1437–1448. https://doi.org/10.1007/s00264-018-3800-7.

[27] D. Fraser, G. Mendonca, E. Sartori, P. Funkenbusch, C. Ercoli, L. Meirelles, Bone response to porous tantalum implants in a gap-healing model. Clinical Oral Implants Research. 30 (2019) 156–168. https://doi.org/10.1111/clr.13402.

[28] M. Heiden, S. Huang, E. Nauman, D. Johnson, L. Stanciu, Nanoporous metals for biodegradable implants: Initial bone mesenchymal stem cell adhesion and degradation behavior. Journal of Biomedical Materials Research-Part A. 104 (2016) 1747–1758. https://doi.org/10.1002/jbm.a.35707.

[29] M.N. Aboushelib, E. Osman, I. Jansen, V. Everts, A.J. Feilzer, Influence of a nanoporous zirconia implant surface of on cell viability of human

osteoblasts. Journal of Prosthodontics. 22 (2013) 190–195. https://doi.org/10.1111/j.1532-849X.2012.00920.x.

[30] W. Nassif, M. Rifai, Surface characterization and cell adhesion of different zirconia treatments: An in vitro Study. Journal of Contemporary Dental Practice. 19 (2018) 181–188. https://doi.org/10.5005/JP-JOURNALS-10024-2234.

[31] M.N. Aboushelib, N.A. Salem, A.L.A. Taleb, N.M.A. el Moniem, Influence of surface nano-roughness on osseointegration of zirconia implants in rabbit femur heads using selective infiltration etching technique. Journal of Oral Implantology. 39 (2013) 583–590. https://doi.org/10.1563/AAID-JOI-D-11-00075.

[32] P. Roy, S. Berger, P. Schmuki, TiO2 nanotubes: Synthesis and applications. Angewandte Chemie International Edition. 50 (2011) 2904–2939. https://doi.org/10.1002/anie.201001374.

[33] S. Bauer, P. Schmuki, K. von der Mark, J. Park, Engineering biocompatible implant surfaces Part I: materials and surfaces Progress in Materials Science. 58 (2013) 261–326. https://doi.org/10.1016/j.pmatsci.2012.09.001.

[34] J. Lindhe, J. Meyle, Peri-implant diseases: Consensus Report of the Sixth European Workshop on Periodontology. Journal of Clinical Periodontology. 35 (2008) 282–285. https://doi.org/10.1111/j.1600-051X.2008.01283.x.

[35] C. Fransson, U. Lekholm, T. Jemt, T. Berglundh, Prevalence of subjects with progressive bone loss at implants. Clinical Oral Implants Research. 16 (2005) 440–446. https://doi.org/10.1111/j.1600-0501.2005.01137.x.

[36] H. Dreyer, J. Grischke, C. Tiede, J. Eberhard, A. Schweitzer, S.E. Toikkanen, S. Glöckner, G. Krause, M. Stiesch, Epidemiology and risk factors of peri-implantitis: A systematic review. Journal of Periodontal Research. 53 (2018) 657–681. https://doi.org/10.1111/jre.12562.

[37] S. Sakka, K. Baroudi, M.Z. Nassani, Factors associated with early and late failure of dental implants. Journal of Investigative and Clinical Dentistry. 3 (2012) 258–261. https://doi.org/10.1111/j.2041-1626.2012.00162.x.

[38] P.A. Norowski, J.D. Bumgardner, Biomaterial and antibiotic strategies for peri-implantitis. Journal of Biomedical Materials Research-Part B Applied Biomaterials. 88 (2009) 530–543. https://doi.org/10.1002/jbm.b.31152.

[39] L.J.A. Heitz-Mayfield, G.E. Salvi, Peri-implant mucositis. Journal of Clinical Periodontology. 45 (2018) S237–S245. https://doi.org/10.1111/jcpe.12953.

[40] S. Schou, P. Holmstrup, K. Stoltze, E. Hjørting-hansen, K.S. Kornman, Ligature-induced marginal inflammation around osseointegrated implants and ankylosed teeth. Clinical and radiographic observations in cynomolgus monkeys (Macaca fascicularis). Clinical Oral Implants Research. 4 (1993) 12–22. https://doi.org/10.1034/j.1600-0501.1993.040102.x.

[41] I. Ericsson, T. Berglundh, C. Marinello, B. Liljenberg, J. Lindhe, Long-standing plaque and gingivitis at implants and teeth in the dog. Clinical Oral Implants Research. 3 (1992) 99–103. https://doi.org/10.1034/j.1600-0501.1992.030301.x.

[42] P.E. Petersen, H. Ogawa, The global burden of periodontal disease: Towards integration with chronic disease prevention and control. Periodontology 2000. 60 (2012) 15–39. https://doi.org/10.1111/j.1600-0757.2011.00425.x.

[43] V. Candotto, F. Gabrione, L. Oberti, D. Lento, M. Severino, The role of implant-abutment connection in preventing bacterial leakage: A review. Journal of Biological Regulators and Homeostatic Agents. 33 (2019) 129–134.

[44] C.D. Dent, J.W. Olson, S.E. Farish, J. Bellome, A.J. Casino, H.F. Morris, S. Ochi, The influence of preoperative antibiotics on success of endosseous implants up to and including stage II surgery: A study of 2,641 implants. Journal of Oral and Maxillofacial Surgery. 55 (1997) 19–24. https://doi.org/10.1016/S0278-2391(16)31193-4.

[45] H. Surapaneni, P.S. Yalamanchili, M.H. Basha, S. Potluri, N. Elisetti, M.V.K. Kiran Kumar, Antibiotics in dental implants: A review of literature. Journal of Pharmacy and Bioallied Sciences. 8 (2016) S28–S31. https://doi.org/10.4103/0975-7406.191961.

[46] C. Ardila, J. Bedoya-García, D. Arrubla-Escobar, Antibiotic resistance in periodontitis patients: A systematic scoping review of randomized clinical trials. Oral Diseases. (2022) 1– 11. https://doi.org/10.1111/odi.14288.

[47] K.P. Nobles, A.V. Janorkar, R.S. Williamson, Surface modifications to enhance osseointegration–resulting material properties and biological responses. Journal of Biomedical Materials Research-Part B Applied Biomaterials. 109 (2021) 1909–1923. https://doi.org/10.1002/jbm.b.34835.

[48] W. Orapiriyakul, P.S. Young, L. Damiati, P.M. Tsimbouri, Antibacterial surface modification of titanium implants in orthopaedics. Journal of Tissue Engineering. 9 (2018) 1–16. https://doi.org/10.1177/2041731418789838.

[49] M.F. Kunrath, T.C. Muradás, N. Penha, M.M. Campos, Innovative surfaces and alloys for dental implants: What about biointerface-safety concerns? Dental Materials. 37 (2021) 1447–1462. https://doi.org/10.1016/j.dental.2021.08.008.

[50] T.P. Schmalzried, H.C. Amstutz, M.K. Au, F.J. Dorey, Etiology of deep sepsis in total hip arthroplasty: The significance of hematogenous and recurrent infections. Clinical Orthopaedics and Related Research. 280 (1992) 200–207. https://doi.org/10.1097/00003086-199207000-00026.

[51] W.J.E.M. Habraken, J.G.C. Wolke, J.A. Jansen, Ceramic composites as matrices and scaffolds for drug delivery in tissue engineering. Advanced

Drug Delivery Reviews. 59 (2007) 234–248. https://doi.org/10.1016/j.addr.2007.03.011.

[52] L. Ma, M. Liu, H. Liu, J. Chen, D. Cui, In vitro cytotoxicity and drug release properties of pH- and temperature-sensitive core-shell hydrogel microspheres. International Journal of Pharmaceutics. 385 (2010) 86–91. https://doi.org/10.1016/j.ijpharm.2009.10.037.

[53] R. Liu, Y. Zhang, X. Zhao, A. Agarwal, L.J. Mueller, P. Feng, pH-responsive nanogated ensemble based on gold-capped mesoporous silica through an acid-labile acetal linker. Journal of the American Chemical Society. 132 (2010) 1500–1501. https://doi.org/10.1021/ja907838s.

[54] N. Murthy, Y.X. Thng, S. Schuck, M.C. Xu, J.M.J. Fréchet, A novel strategy for encapsulation and release of proteins: Hydrogels and microgels with acid-labile acetal cross-linkers. Journal of the American Chemical Society. 124 (2002) 12398–12399. https://doi.org/10.1021/ja026925r.

[55] Y. Mu, S. Ma, P. Wei, Y. Wang, W. Jing, Y. Zhao, L. Zhang, J. Wu, B. Zhao, J. Deng, Z. Liu, Multifunctional modification of SIS membrane with chimeric peptides to promote its antibacterial, osteogenic, and healing-promoting abilities for applying to GBR. Advanced Functional Materials. 31 (2021) 2101452. https://doi.org/10.1002/adfm.202101452.

[56] Y. Yang, Y. Cheng, F. Deng, L. Shen, Z. Zhao, S. Peng, C. Shuai, A bifunctional bone scaffold combines osteogenesis and antibacterial activity via in situ grown hydroxyapatite and silver nanoparticles. Bio-Design and Manufacturing. 4 (2021) 452–468. https://doi.org/10.1007/s42242-021-00130-x.

[57] K. Blecher, A. Nasir, A. Friedman, The growing role of nanotechnology in combating infectious disease. Virulence. 2 (2011) 395–401. https://doi.org/10.4161/viru.2.5.17035.

[58] C.C. Sanders, W.E. Sanders, D.J. Harrowe, Bacterial interference: Effects of oral antibiotics on the normal throat flora and its ability to interfere with group A streptococci. Infection and Immunity. 13 (1976) 808–812. https://doi.org/10.1128/iai.13.3.808-812.1976.

[59] G. Isola, A. Polizzi, S. Santonocito, D. Dalessandri, M. Migliorati, F. Indelicato, New frontiers on adjuvants drug strategies and treatments in periodontitis. Scientia Pharmaceutica. 89 (2021) 46. https://doi.org/10.3390/scipharm89040046.

[60] P. Makvandi, U. Josic, M. Delfi, F. Pinelli, V. Jahed, E. Kaya, M. Ashrafizadeh, A. Zarepour, F. Rossi, A. Zarrabi, T. Agarwal, E.N. Zare, M. Ghomi, T. Kumar Maiti, L. Breschi, F.R. Tay, Drug delivery (nano)platforms for oral and dental applications: Tissue regeneration, infection control, and cancer management. Advanced Science. 8 (2021) 2004014. https://doi.org/10.1002/advs.202004014.

[61] J. Hornak, Synthesis, properties and selected technical applications of magnesium oxide nanoparticles: A review. International Journal of Molecular Sciences. 22 (2021) 12752. https://doi.org/10.3390/ijms222312752.

[62] R. Eivazzadeh-Keihan, E. Bahojb Noruzi, K. Khanmohammadi Chenab, A. Jafari, F. Radinekiyan, S.M. Hashemi, F. Ahmadpour, A. Behboudi, J. Mosafer, A. Mokhtarzadeh, A. Maleki, M.R. Hamblin, Metal-based nanoparticles for bone tissue engineering. Journal of Tissue Engineering and Regenerative Medicine. 14 (2020) 1687–1714. https://doi.org/10.1002/term.3131.

[63] S. Hayat, S. Muzammil, M.H. Rasool, Z. Nisar, S.Z. Hussain, A.N. Sabri, S. Jamil, In vitro antibiofilm and anti-adhesion effects of magnesium oxide nanoparticles against antibiotic resistant bacteria. Microbiology and Immunology. 62 (2018) 211–220. https://doi.org/10.1111/1348-0421.12580.

[64] G.K. Meenashisundaram, N. Wang, S. Maskomani, S. Lu, S.K. Anantharajan, S.T. Dheen, S.M.L. Nai, J.Y.H. Fuh, J. Wei, Fabrication of Ti + Mg composites by three-dimensional printing of porous Ti and subsequent pressureless infiltration of biodegradable Mg. Materials Science and Engineering C. 108 (2020) 110478. https://doi.org/10.1016/j.msec.2019.110478.

[65] B. Safari, S. Davaran, A. Aghanejad, Osteogenic potential of the growth factors and bioactive molecules in bone regeneration. International Journal of Biological Macromolecules. 175 (2021) 544–557. https://doi.org/10.1016/j.ijbiomac.2021.02.052.

[66] J.B. Cannata-andía, N. Carrillo-lópez, O.D. Messina, N.A.T. Hamdy, S. Panizo, S.L. Ferrari, Pathophysiology of vascular calcification and bone loss: Linked disorders of ageing? Nutrients. 13 (2021) 3835. https://doi.org/10.3390/nu13113835.

[67] M. Dang, L. Saunders, X. Niu, Y. Fan, P.X. Ma, Biomimetic delivery of signals for bone tissue engineering. Bone Research. 6 (2018) 1–12. https://doi.org/10.1038/s41413-018-0025-8.

[68] M.A. McGinnis, P. Larsen, M. Miloro, F.M. Beck, Comparison of resorbable and nonresorbable guided bone regeneration material. British Journal of Oral and Maxillofacial Surgery. 35 (1997) 445–446. https://doi.org/10.1016/s0266-4356(97)90742-7.

[69] Y.Y. Jo, J.H. Oh, New resorbable membrane materials for guided bone regeneration. Applied Sciences (Switzerland). 8 (2018) 2157. https://doi.org/10.3390/app8112157.

[70] X.N. Gu, Y.F. Zheng, A review on magnesium alloys as biodegradable materials. Frontiers of Materials Science in China. 4 (2010) 111–115. https://doi.org/10.1007/s11706-010-0024-1.

[71] M. Yazdimamaghani, M. Razavi, D. Vashaee, K. Moharamzadeh, A.R. Boccaccini, L. Tayebi, Porous magnesium-based scaffolds for tissue engineering. Materials Science and Engineering C. 71 (2017) 1253–1266. https://doi.org/10.1016/j.msec.2016.11.027.

[72] P. Bhattacharya, A. Dey, S. Neogi, An insight into the mechanism of antibacterial activity by magnesium oxide nanoparticles. Journal of Materials Chemistry B. 9 (2021) 5329–5339. https://doi.org/10.1039/d1tb00875g.

[73] J. Wang, X.Y. Ma, Y.F. Feng, Z.S. Ma, T.C. Ma, Y. Zhang, X. Li, L. Wang, W. Lei, Magnesium ions promote the biological behaviour of rat calvarial osteoblasts by activating the PI3K/Akt signalling pathway. Biological Trace Element Research. 179 (2017) 284–293. https://doi.org/10.1007/s12011-017-0948-8.

[74] E. Marukawa, M. Tamai, Y. Takahashi, I. Hatakeyama, M. Sato, Y. Higuchi, H. Kakidachi, H. Taniguchi, T. Sakamoto, J. Honda, K. Omura, H. Harada, Comparison of magnesium alloys and poly-l-lactide screws as degradable implants in a canine fracture model. Journal of Biomedical Materials Research-Part B Applied Biomaterials. 104 (2016) 1282–1289. https://doi.org/10.1002/jbm.b.33470.

[75] H. Hornberger, S. Virtanen, A.R. Boccaccini, Biomedical coatings on magnesium alloys—a review. Acta Biomaterialia. 8 (2012) 2442–2455. https://doi.org/10.1016/j.actbio.2012.04.012.

[76] C.R. Chitambar, W.G. Matthaeus, W.E. Antholine, K. Graff, W.J. O'Brien, Inhibition of leukemic HL60 cell growth by transferrin-gallium: Effects of ribonucleotide reductase and demonstration of drug synergy with hydroxyurea. Blood. 72 (1988) 1930–1936. https://doi.org/10.1182/blood.v72.6.1930.1930.

[77] D.W. Hedley, E.H. Tripp, P. Slowiaczek, G.J. Mann, Effect of gallium on DNA synthesis by human T-cell lymphoblasts. Cancer Research. 48 (1988) 3014–3018.

[78] M. Yu, Y. Wang, Y. Zhang, D. Cui, G. Gu, D. Zhao, Gallium ions promote osteoinduction of human and mouse osteoblasts via the TRPM7/Akt

signaling pathway. Molecular Medicine Reports. 22 (2020) 2741–2752. https://doi.org/10.3892/mmr.2020.11346.

CHAPTER SEVEN

SUMMARY

Implant-supported prostheses have become reliable therapies in the rehabilitation of patients with orthopedic prostheses. However, the long-term survival of implants is still challenged by lots of adverse bone abnormalities. Low bone density, periimplantitis, and large-volume bone defects are the common causes of insufficient osteointegration and finally lead to implant failure. Therefore, the development of implant materials to promote their osteogenesis and antibacterial property is urgently required. Surface modifications are flexible strategies for endowing multifunctionality on implant materials, such as antibacterial and pro-osteogenic functions.

In **Chapter 2**, we developed a novel surface coating via magnetron sputtering and anodization to enhance the bioactivity of zirconia surface. Results from our study showed that the TaNS coating can modulate MC3T3-E1 cells attachment, proliferation, osteogenic differentiation, and mineralization by up-regulating osteogenic-related gene expressions. Moreover, animal experiments also indicated that the TaNS coating can induce more bone tissue regeneration around zirconia implants. *In-vitro* and *vivo* findings in our study indicate the nanoporous Ta-coated zirconia implants can improve early osteointegration of the zirconia implant and will be a promising biomaterial for clinical application.

In **Chapter 3**, we developed a pH-dependent silver nanoparticle-releasing titanium implant to prevent peri-implant infection. Broad-spectrum antimicrobial (AgNPs) was successfully loaded in TNT via pH-sensitive AL, without affecting the physicochemical characteristics of TNT. The pH5.5, mimicking the pH level in the peri-implant surface during bacterial infection, was able to trigger AgNPs release from TNT, and released AgNPs efficiently controlled bacterial growth *in-vitro*. The cell experiments indicated that the new biomaterial was biocompatible and pro-osteogenic. Our findings suggested that low pH-triggered AgNPs releasing TNT-AL-AgNPs implant could be a potent therapeutic approach to control peri-implant infection.

In **Chapter 4**, we successfully synthesized a dual-functional nanofiber GBR membrane with antimicrobial and pro-osteogenic properties. The coaxial electrospinning procedure was used and successfully encapsulate a broad-spectrum antibacterial (MgONPs) agent in the shell layer and a pro-osteogenic drug (PTH) in the core layer of the nanofibers. The sustained release of

MgONPs and PTH significantly promoted antibacterial property, which was shown in-vitro. This indicated that the membrane could effectively eliminate the residual bacteria in periodontal tissues to assist wound healing, diminish post-operative infections, provide a friendly microenvironment for bone regeneration, and eventually improve osteogenesis. Furthermore, the results of release profiles and antibacterial assessments of the new GBR membrane indicated its exposure tolerance for the first month after implantation. This would contribute to prevent GBR failure caused by early exposure. The significant improvement of osteogenesis in bacterial-contaminated models in-vivo, especially with the presence of high dosage PTH, proved to be a promising approach to satisfy the complicated and phased requirements of the GBR process in periodontitis or periimplantitis patients with large-volume bone defects.

In **Chapter 5**, we successfully synthesized a properly biodegradable, antibacterial, and pro-osteogenic Ga-coated Mg alloy (Ga/AZ31) membrane through magnetron sputtering for GBR process. The firmly bonded dense Ga coating confirmed by the results of SEM and scratch tests indicated it can contribute to less susceptibility to corrosion and minimize the risk of peeling during trimming and bending in clinic. Furthermore, the results of antibacterial assessments of the new GBR membrane suggested that the Ga-coated AZ31 membranes bore more potent antibacterial activity than the naked AZ31, which further helps to reduce the risk of post-operative infection. Additionally, the Ga-coated membranes bore significantly higher ALP activity than the naked AZ31 membrane both on day 7 and 14. The antimicrobial and pro-osteogenic Ga/AZ31 was suggested as a promising material to satisfy the complicated and phased requirements of the GBR process in periodontitis or periimplantitis patients with large-volume bone defects.

Collectively, biomaterials with pro-osteogenic and antibacterial functionalization can be easily achieved through different surface modification technologies. The modified surface topology and chemical composition of the biomaterials increased antimicrobial efficiency and pro-osteogenic cells proliferation and differentiation and finally enhance the new bone regeneration. In-depth mechanistic studies of how these new materials function under adverse bone abnormalities still need further work.

APPENDICES

AUTHORS' CONTRIBUTIONS

Chapter 2 was published as:

Nanoporous tantalum coated zirconia implant improves osteointegration.

Authors:

Lianjun Wu*, **Yiwen Dong***, Litao Yao, Chuantong Liu, Abdullrahman M Al-Bishari, Kendrick Hii Ru Yie, Hualin Zhang, Jinsong Liu, Gang Wu.

(* Shared first authorship)

Authors' contributions:

Lianjun Wu: Searching references and selecting magnetron sputtering as the method for fabricating Ta coatings on the zirconia implants; Samples preparation for cell experiments and *in-vivo* experiments, cell experiments (the primers of target and housekeeping genes were provided by a company), *in-vivo* experiments (rabbits anaesthetization, skin preparation, sterilization, surgery assistance and implants' location confirmation via X-rays); Data processing and analysis (cell experiments); Writing-original draft preparation (title, abstract, cell experiments in the "materials and methods" and "results and discussion", conclusion, declaration of competing interest, acknowledgements); Writing-review and editing; Funding acquisition (Wenzhou Municipal Science and Technology Project for Public Welfare: 2017Y0308).

Yiwen Dong: Searching references and selecting electrochemical anodization as the method for fabricating nanoporous Ta coating (TaNS) on the zirconia implants, designing the experiments for detecting the physicochemical properties of the samples, designing the cell experiments and *in-vivo* experiments; Sputtering Ta coatings on the surface of the ZrO_2 discs with different parameters, fabricating TaNS via anodization, scratch test, surface characterization, protein adsorption, the cell experiments repeat, *in-vivo* experiment (the surgery, rabbits sacrifice, histological analysis); Data processing and analysis (bond strength of the coatings, surface characterization, protein adsorption, cell experiments, histological analysis); Writing-original draft preparation (introduction, sample preparation, bond strength of the coating, surface characterization, protein adsorption, *in-vivo* experiment in the "materials and methods" and "results and discussion"); Writing-review and editing.

Litao Yao: Sintering and cleaning of ZrO_2 discs, rabbits feeding, instruments sterilization used in cell experiments, writing-review and editing.
Chuantong Liu: Surgical instrument supply, writing-review and editing.
Abdullrahman M Al-Bishari: Rabbits feeding, writing-review and editing.
Kendrick Hii Ru Yie: Instruments sterilization used in the surgery, writing-review and editing.
Hualin Zhang: Designing the experiments for detecting the physicochemical properties of the samples, writing-review and editing.
Jinsong Liu: Proposing the idea of fabricating coatings on the surface of zirconia implants without changing the implants' color, designing the cell experiments and *in-vivo* experiments, funding acquisition, data processing and analysis, supervision, project administration, writing-review and editing.
Gang Wu: Supervision, writing-review and editing.

Chapter 3 was published as:

pH dependent silver nanoparticles releasing titanium implant: A novel therapeutic approach to control peri-implant infection.

Authors:

Yiwen Dong[*], Hui Ye[*], Yi Liu[*], Lihua Xu, Zuosu Wu, Xiaohui Hu, Jianfeng Ma, Janak L. Pathak, Jinsong Liu, Gang Wu

([*] Shared first authorship)

Authors' contributions:

Yiwen Dong: Conceptualization, funding acquisition (Technology Innovation Plan for Students in Zhejiang Province (Xinmiao Talents Program): No.2016R413065), methodology, data processing and analysis, writing-original draft preparation, writing-review and editing.
Hui Ye: Providing SEM and XPS equipments, writing-review and editing.
Yi Liu: The cell experiments repeat, writing-review and editing
Lihua Xu: Instruments sterilization used in cell experiments, writing-review and editing.
Zuosu Wu: Instruments sterilization used in antibacterial experiments, writing-review and editing.
Xiaohui Hu: Instruments sterilization used in cell experiments, writing-review and editing.

Jianfeng Ma: Writing-review and editing
Janak L. Pathak: Data analysis, writing-review and editing.
Jinsong Liu: Conceptualization, funding acquisition, data analysis, supervision, project administration, writing-review and editing.
Gang Wu: Supervision, writing-review and editing.

Chapter 4 was published as:

Antimicrobial and pro-osteogenic coaxially-electrospun magnesium oxide nanoparticles-polycaprolactone /parathyroid hormone-polycaprolactone composite barrier membrane for guided bone regeneration.

Authors:

Yiwen Dong, Litao Yao, Lei Cai, Mi Jin, Tymour Forouzanfar, Lianjun Wu, Jinsong Liu, Gang Wu

Authors' contributions:

Yiwen Dong: Conceptualization, funding acquisition (Wenzhou Municipal Science and Technology Project for Public Welfare No. Y20190107), methodology (micro-CT scanner was manipulated by technician), data processing and analysis, writing-original draft preparation, writing-review and editing.
Litao Yao: *In-vivo* experiment (rats anaesthetization, skin preparation, sterilization, surgery assistance), the cell experiments repeat, writing-review and editing.
Lei Cai: Rats feeding, Instruments sterilization used in antibacterial experiments and cell experiments, writing-review and editing.
Mi Jin: Rats feeding, Instruments sterilization used in *in-vivo* experiments, writing-review and editing.
Tymour Forouzanfar: Supervision.
Lianjun Wu: Funding acquisition, writing-review and editing.
Jinsong Liu: Conceptualization, funding acquisition, data analysis, supervision, project administration, writing-review and editing.
Gang Wu: Supervision, data analysis, writing-review and editing.

Chapter 5 was submitted as:

Antibacterial and pro-osteogenic functionalized gallium-coated magnesium alloy membrane for guided bone regeneration.

Authors:

Yiwen Dong, Litao Yao, Lei Cai, Mi Jin, Tymour Forouzanfar, Lianjun Wu, Jinsong Liu, Gang Wu

Authors' contributions:

Yiwen Dong: Conceptualization, funding acquisition (Wenzhou Municipal Science and Technology Project for Public Welfare No. Y20190107), methodology, data processing and analysis, writing-original draft preparation, writing-review and editing.

Litao Yao: The cell experiments repeat, writing-review and editing.

Lei Cai: Instruments sterilization used in antibacterial experiments, writing-review and editing.

Mi Jin: Instruments sterilization used in cell experiments, writing-review and editing.

Tymour Forouzanfar: Supervision.

Lianjun Wu: Funding acquisition, writing-review and editing.

Jinsong Liu: Conceptualization, funding acquisition, data analysis, supervision, project administration, writing-review and editing.

Gang Wu: Supervision, data analysis, writing-review and editing.

Acknowledgments

At the end of this thesis, it is really hard for me to express how grateful I am to all the people who give me support, encourage, and guide. This was one of the most challenging and confusing time in my life, fortunately, I got a lot of kind help and learned a lot on this journey. With the limitation of space, I cannot include all the names of those who have ever helped and encouraged, but I will try my best.

First and foremost, I am very grateful to my supervisor Prof. Dr. **Tymour Forouzanfar**, who kindly allowed me to perform this research. Dear Tymour, I am sincerely appreciating your full and strongly supporting to complete my research and thesis. Your guide, intellectual elegance, and amiable personality always gave me great power to keep on working. When I had problems, you were always very willing to help. I clearly remembered your comfort words and useful advice when I had some problems with my course, credits, and visa. I will not forget the experience of my PhD study in Amsterdam.

Another important person I would like to thank is my daily supervisor Dr. **Gang Wu**. Dear Gang, I am so happy to have you as my daily supervisor. You always supported, encouraged, and shared your own experience with me when I met problems and felt frustrated. Your wisdom, your optimism, and your blueprint in research always gave me the courage and guide to move on. You were so patient in helping me design my project and train my critical thinking. You spent a lot of time to correct and rephrase the sentences of my thesis and gave constructive advice to make the figures better no matter how busy you were. It is my honor to be one of your students and to have learned so many new skills from you.

I would like to express my thanks to my co-promoter and my master's supervisor, Prof. Dr. **Jinsong Liu**. Dear Jinsong, words have not been able to express my gratitude for your tireless help and encouragement. You were the first guide to lead me into the scientific world and enlightened me during my first postgraduate study with endless patience. Without your help, I would not have had the opportunity to start my PhD journey at ACTA. My project would not be complete without your excellent suggestions and financial support.

I would like to thank the doctorial committee members who spent time on reading and evaluating my thesis, Dr**. Marco N. Helder**, Prof. Dr. **Jenneke Klein-Nulend,** Prof. Dr. **Richard T. Jaspers**, Dr. **Qi Wang** and Dr. **Jeroen van den Beucken**. This is my honor!

I would also like to thank Dr. **Astrid D Bakker**. Dear Astrid, I am so grateful for your kind, patiently help and useful suggestions and information with my credits. I still remembered your comfort words and timely responded emails when I met problems. Dear Prof. Dr. **Jenneke Klein-Nulend**, thanks for your kind corrections of my spoken English and the opportunity you offered for me to present my project in our data meeting. To improve my thesis, you really gave me very excellent suggestions and comments. I am so appreciating for the time and efforts you spent. Another person I want to thank is Dr. **Yuelian Liu**. Dear Yuelian, I can clearly remember the first time we meet in ACTA. You gave a lot of useful small tips about how to quickly fit daily life in the Netherlands. You also gave me a lot of suggestions about my project in our regular data meetings.

Next, I would like to thank my dear friends, and colleagues, who gave their friendly feedback and useful suggestions to my papers. Dear **Cor**, thank you for your patience and humorous introduction of laboratory equipment for us, I still remembered your joke about the different pronunciations of the word in English and Dutch. You always called my Chinese name correctly although it was difficult to remember and speak. Dear **Jolanda**, I enjoy your laugh. During coffee time and lunchtime, you were always willing to share your travel experience and provide me a lot of useful tips. Dear **Behrouz**, you always gave useful advice and were willing to answer the questions. I cannot forget our nice talk in OCB activity. Dear **Jianfeng**, thank you so much for your consistent and kind help. You are a person with so many good characteristics and I really learned a lot from you. Dear **Ton, Inneke, Teun, Cees, Sue, Jan Harm, Kamran, Jacqueline, Tineke,** and **Victor**: I appreciate all your kindness, help, and care. Dear **Yuanyuan, Shuyi, Andi, Yan, Lei, Xumin, Gaoli, and Jiayi**, you always shared delicious Chinese food with me, invited me to your home, and celebrated Chinese festivals. We made dumplings and hotpots together. When I was frustrated, you always comforted and accompanied. I really enjoy the life in Uilenstede. I would also like to express my gratitude to my teachers and friends in China, **Congxin, Chuantong, YunYang, Yifan, Xiaohui, Litao, Lei, Mi, and Lili** for your support and encouragement.

To my family: 感谢我的父母对我的无限包容和支持，谢谢你们，我爱你们，亲爱的爸爸妈妈。

To myself: 摘抄自一本我很喜欢的小说，曾在我彷徨迷茫时无数次激励了我。亲爱的董伊雯小姐， 在这漫长而美好的一生里，如果你真找到了你想做的事情，那么无论何时你决定开始，都不算晚。人的能力有限，但有些东西，却可以无限。成为天才并不是解决一切困难的法宝，但真正的天才们永远坦然无畏，他们东西本心、忠于理想、追寻所爱、始终不渝。

Curriculum Vitae

Name: Yiwen Dong
Date of birth: October 27th, 1988
Place of birth: Wenzhou, Zhejiang province, China
Email: y.dong@actal.nl, triangle1988@126.com

Publications:

1. **Yiwen Dong,** Litao Yao*, Lei Cai, Mi Jin, Tymour Forouzanfar, Lianjun Wu, Jinsong Liu*, Gang Wu. Antimicrobial and Pro-Osteogenic Coaxially-Electrospun Magnesium Oxide Nanoparticles-Polycaprolactone /Parathyroid Hormone-Polycaprolactone Composite Barrier Membrane for Guided Bone Regeneration. International journal of nanomedicine. 18 (2023) 369–383.
2. **Yiwen Dong**†, HuiYe†, Yi Liu†, Lihua Xu, Zuosu Wu, Xiaohui Hu, Jianfeng Ma, Janak L.Pathak*, Jinsong Liu*, Gang Wu. pH dependent silver nanoparticles releasing titanium implant: A novel therapeutic approach to control peri-implant infection. Colloids and Surfaces B: Biointerfaces. 158 (2017) 127–136.
3. Lianjun Wu†, **Yiwen Dong**†, Litao Yao, Chuantong Liu, Abdullrahman M Al-Bishari, Kendrick Hii Ru Yie, Hualin Zhang*, Jinsong Liu*, Gang Wu. Nanoporous tantalum coated zirconia implant improves osteointegration. Ceramics International. 46 (2020) 17437–17448.
4. **Yiwen Dong**, Litao Yao, Lei Cai, Mi Jin, Tymour Forouzanfar*, Jinsong Liu*, Gang Wu. Antibacterial and Pro-Osteogenic Functionalized Gallium Coated Magnesium Alloy Membrane for Guided Bone Regeneration. (Submitted)
5. Weiwei Lou†, **Yiwen Dong** †, Hualin Zhang †, Yifan Jin, Xiaohui Hu, Jianfeng Ma*, Jinsong Liu *, Gang Wu. Preparation and characterization of lanthanum-incorporated hydroxyapatite coatings on titanium substrates. International Journal of Molecular Sciences. 16 (2015) 21070–21086.
6. Jinsong Liu †, Hualin Zhang†, **Yiwen Dong**, Yifan Jin, Xiaohui Hu, Kaiyong Cai *, Jianfeng Ma*, Gang Wu. Bi-directionally selective bone targeting delivery for anabolic and antiresorptive drugs: A novel combined therapy for osteoporosis? Medical Hypotheses. 83 (2014) 694–696.

Patent

1. **Yiwen Dong,** Chuantong Liu, Jinsong Liu**.** Preparation of Antibacterial and Osteogenic Dual-functional Absorbable Guided Bone Regeneration Membrane.2019, CN106492271B.

Funding

1. Wenzhou Municipal Science and Technology Project for Public Welfare: No. Y20190107.